BRANDFORSK
2018:1

Fire and explosion hazards of alternative fuel vehicles in tunnels

Ying Zhen Li

Brandforsk

PROJECT TECHNICAL PANEL

Ulf Lundström, Swedish Transport Administration (STA)
Erik Egardt, Myndigheten för Samhällsskydd & Beredskap (MSB)
Åke Persson, Brandskyddsföreningen
Markus Börjes, Scania
Anders Ek, Volvo Truck
Petter Berg, Volvo Cars
Björn Forsberg, Volvo Cars
Haukur Ingason, RISE
Peter Karlsson, RISE
Krister Palmkvist, RISE
Thomas Gell, Brandforsk

Keywords
alternative fuel vehicles, tunnel, liquid fuels, liquefied fuels, compressed gas, electric vehicles

RISE Research Institutes of Sweden
RISE Rapport 2018:20
ISBN 978-91-88695-55-0
ISSN 0284-5172

This report constitutes a final working manuscript for the headlined project.

The official project report, to which reference should be made, can be found on the RISE's website.

"Fire and explosion hazards of alternative fuel vehicles in tunnels"

www.ri.se

BRANDFORSK 2018:1

Abstract

An investigation of fire and explosion hazards of different types of alternative fuel vehicles in tunnels is presented. The different fuels are divided into four types: liquid fuels, liquefied fuels, compressed gases, and electricity, and detailed parameters are obtained. Three types of fire hazards for the alternative fuel vehicles: pool fires, jet fires and fireballs are identified and investigated in detail. From the perspective of pool fire size, the liquid fuels pose equivalent or even much lower fire hazards compared to the traditionally used fuels, but the liquefied fuels may pose higher hazards. For pressurized tanks, the fires are generally much larger in size but shorter in duration. The gas releases from pressure relief devices and the resulting jet fires are highly transient. For hydrogen vehicles, the fire sizes are significantly higher compared to CNG tanks, while flame lengths only slighter longer. Investigation of the peak overpressure in case of an explosion in a tunnel was also carried out. The results showed that, for the vehicles investigated, the peak overpressure of tank rupture and BLEVE are mostly in a range of 0.1 to 0.36 bar at 50 m away. The situations in case of cloud explosion are mostly much more severe and intolerable. These hazards need to be carefully considered in both vehicle safety design and tunnel fire safety design. Further researches on these hazards are in urgent need.

Key words: alternative fuel vehicles, tunnel, liquid fuels, liquefied fuels, compressed gas, electric vehicles

RISE Research Institutes of Sweden
RISE Rapport 2018:20
ISBN 978-91-88695-55-0
ISSN 0284-5172
Borås 2018

Table of Contents

Preface

The project is financially supported by Åforsk Foundation and the Swedish Fire Research Board (BRANDFORSK), which are greatly appreciated.

Acknowledgement to the reference group members consisting of:

- Ulf Lundström, Sweish Transport Administration (STA)
- Erik Egardt, Myndigheten för Samhällsskydd och Beredskap (MSB)
- Åke Persson, Brandskyddsföreningen
- Markus Börjes, Scania
- Anders Ek, Volvo Truck
- Petter Berg, Volvo car
- Björn Forsberg, Volvo car
- Haukur Ingason, RISE
- Peter Karlsson, RISE
- Krister Palmkvist, RISE
- Thomas Gell, BrandForsk

Summary

An investigation of fire and explosion hazards of different types of alternative fuel vehicles in tunnels is presented. According to the different fuels used, they could be divided into four types: liquid fuels, liquefied fuels, compressed gases, and electricity and detailed parameters are obtained.

From the perspective of pool fire size, the liquid fuels may pose equivalent or even much lower fire hazards compared to the traditionally used fuels, but the liquefied fuels may pose higher hazards. The pool fire hazards are related to the spillage area, which highly depends on tunnel slopes and outflow holes. For pressurized tanks, the fires are generally much larger in size but shorter in duration. The gas release from PRD and the resulting jet fires are highly transient. For hydrogen vehicles, the fire sizes are significantly higher compared to CNG tanks, while flame lengths only slighter longer.

Investigation of the peak overpressure in case of an explosion in a tunnel was also carried out. The results showed that, for the vehicles investigated, the peak overpressure of tank rupture and BLEVE are mostly in a range of 0.1 to 0.36 bar at 50 m away. The situations in case of cloud explosion are mostly much more severe and intolerable.

These hazards need to be carefully considered in both vehicle safety design and tunnel fire safety design, e.g. limiting the fuels and stringent prevention of such incidents. Further researches on these hazards, especially large scale experiments, are in urgent need.

1 Introduction

Environmental issues and scarcity of resources have stimulated the development and use of alternative fuel vehicles worldwide. In many countries, governments are encouraging the transformation from the use of internal combustion engine vehicles to alternative fuel vehicles by tax exemption or tax subsidization, and some even has planned to ban the use of internal combustion engine vehicles in the near future.

Nowadays, the use of alternative fuel vehicles has occurred in almost every type of transportation, e.g. car, bus, heavy goods vehicle, train locomotive and airplanes. For example, there have been over 600 ethanol buses running in Sweden nowadays. Another example is that Scania has developed alternative fuel powered heavy goods vehicles. According to data from US Department of Energy, the number of such vehicles in USA in 2011 was twice that in 2006. In Sweden, there are many CNG and ethanol buses running on roads, e.g. over 600 ethanol buses. In Norway, 51.4 % of new vehicle registrations in January 2017 were electric vehicles (17.6 %) and hybrid vehicles (33.8 %), according to the Norwegian Road Traffic Information Council. On 22 June of 2016, Sweden started to test the electric high way on the E16 in Sandviken. It can be foreseen that more and more such vehicles will be on roads, as well as in tunnels and other underground spaces, e.g. underground garages.

In comparison to traditional vehicles, the hazards for some alternative fuel vehicles are much higher. From the accidents occurred in the past, it can be found that the most severe consequence is related to explosions. For example, in Salerno, Italy in 2007, a LPG vehicle exploded resulting in a three-story building completely destroyed and 5 other buildings affected. Date back to 2002 in Seine-et-Marne, France, leaked gases from a LPG vehicle in a garage caused an explosion that affected 39 buildings with a radius of 200 m and blew its own roof to 150 m from the initial location [1]. For electric vehicle batteries, a thermal runaway due to overcharging or short circuits could result in explosion. Different types of explosion could de facto occur, including boiling liquid expanding vapour explosion (BLEVE), deflagration and detonation. Another hazard is the jet fires which may correspond to much higher gas temperatures compared to those in traditional vehicle fires. If the flame impinges on the tunnel structure as it would mostly be in a large fire, the tunnel structure, e.g. concrete, could even melt down after a certain exposure. This indicates a possible need for higher requirement for thermal resistance of the tunnel structure.

In the past few decades, many catastrophic fires occurred in tunnels [2]. These accidents show that the consequences of vehicle fires in tunnels are generally much higher than on the open roads. For use of alternative fuel vehicles in tunnels, special attentions need to be paid to the fire and explosion hazards. There have been very limited researches related to fire and explosion hazards of alternative fuel vehicles, much less on their hazards in tunnels. Weerheijm [3] illustrated the explosion hazards and consequences for a large LPG tanker in a tunnel. These tankers are much larger in size compared to the fuel tanks of common alternative fuel vehicles. There have also been some experimental tests on deflagrations and detonations in model scale tunnels [4], and the data were later used for an inter-comparison exercise on modelling [5]. However, only several scenarios with hydrogen were investigated. Clearly, there is a huge lack in researches on fire and explosion hazards of alternative fuel vehicles in tunnels.

Despite the lack of knowledge on fire and explosion hazards of alternative fuel vehicles, these vehicles have already been used widely to some extent as mentioned previously. This de facto put the whole society in a potentially high risk. Different rules are applied worldwide. For example, the LPG vehicles with safety valves are allowed both in tunnels and garages in France while in Italy LPG should be labeled before entering the Mont Blanc tunnel [1]. The Swedish authorities, i.e. Swedish Transport Administration and Swedish Transport Agency, propose that vehicles in tunnels should have equivalent safety level as in open areas [6]. To make such a

judgement or to achieve this goal, quantitative risk analysis is required. However, at present, there is no such knowledge of fire and explosion hazards of these different types of vehicles possibly running in the tunnels. Therefore carrying out such a quantitative risk analysis at present is impossible.

Before the wide use, the hazards related to these alternative fuel vehicles need to be identified and quantified, in comparison to the traditional vehicles. For example, where should we position the pressure release valves, e.g. facing upward or sides of a bus or truck? There have been accidents with a horizontal jet flame of over 10 m length from the release valve facing one side. If it occurs in a tunnel, the flame will impinge on the tunnel wall and then deflect to the floor level. This could significantly increase the risk for fire spread to neighbouring vehicles and also endanger the tunnel users. At a training programme for fire fighters, they were hesitated to approach the CNG bus on fire as they were uncertain about what would happen. From the perspectives of tunnel users incl. fire fighters, knowledge about the phenomena and the consequences is needed.

From every perspective, it is clear that there is a strong and urgent need to investigate and quantify the hazard related to these alternative fuel vehicles.

The objective of this work is to investigate the fire and explosion hazards of alternative fuel vehicles in tunnels. Specifically, it is to obtain detailed parameters for each type of alternative fuel vehicles, to identify the potential hazards for each type of alternative fuel vehicles in tunnels, and to quantify the consequences based on state-of-the-art knowledge.

2 State-of-the-art

2.1 Spilled liquid fires

Experimental data on burning rates for different liquid fuels are available, e.g. [7]. However, most of these tests were carried out using steel trays with high rims, which is entirely different from a spilled fire where fuel pours continuously from a tank onto a road surface or floor [8]. In such a case, the fuel thickness is much thinner and therefore the potential fire size can be much higher. Note that most road surfaces have a small slope for water drainage. In such cases, the slope plays a key role in the shape and size of the pool [8]. There is rather limited research on this issue. Recently, Ingason and Li [8] investigated the spillage and burning behaviors of spilled gasoline fires. However, at present no work is available concerning burning behaviors of spilled methanol and ethanol fires.

2.2 Jet flame behaviors

Pressure relief valves are required for both compressed gas tanks and liquefied fuel tanks to prevent tank rupture in case of an incident. The high speed fuel jets released result in jet flames if ignited. Jet fires normally correspond to longer flame lengths and higher heat fluxes compared to traditional vehicle fires. This poses high hazards for personnel injury, fire spread and structure failure.

Most research on jet fires was carried out in oil and gas industry, e.g. [9]. The behaviors of free jet flames in the open have been well studied [10, 11] but much less research on jet fires in enclosures. Virk [12] carried out small scale propane jet fire tests with flame impingement onto a vertical plate and investigated the heat fluxes on the plate. The heat flux is, however, highly dependent on jet flame size, and thus the results obtained cannot be directly used. Wu [13] simulated hydrogen jet flames with relatively low initial speeds in a tunnel, but the speeds analyzed are much lower than those from a typical hydrogen tank used in alternative fuel vehicles.

There is a strong need to investigate the behaviors of jet flames in or nearby different structures, heat radiation to surroundings and risk for fire spread for different types and configurations of alternative fuel vehicles.

2.3 Explosion hazards

Compressed gas, liquefied fuel and battery vehicles pose explosion hazards. There are mainly three types of explosion hazards, i.e. compressed gas tank rupture, Boiling Liquid Expanding Vapor Explosion (BLEVE) and vapor cloud explosion (gas explosion). For CNG vehicles, it has been found that tank rupture is the most common consequence [14, 15].

Most existing knowledge on explosion hazards comes from the research on chemical process safety [16] and mining safety [17]. Rather limited research exists on the explosion hazards concerning alternative fuel vehicles. Recently much focus has been put on explosion of hydrogen, e.g. the tests on deflagrations and detonations of hydrogen in a tunnel model [18] and the following inter-comparison exercise on modelling [5], the numerical work done by Venetsanos et al. [19] and Middha and Hansen [20], and the fire exposure test on a composite hydrogen fuel tank in the open by Zalosh and Weyandt [21]. Weerheijm [3] illustrated the possibility of explosion and possible consequences for a large LPG tanker in a tunnel but the tank size is apparently much larger than those in alternative fuel vehicles. Schoor et al [22] also

investigated the explosion hazards of LPG vehicles by computational modelling. There is still a lack of experimental data and research on explosion hazards of compressed gas and liquefied fuel vehicles.

There have been many studies on the transportation of blast waves along small smooth tubes. However, most studies focus on explosion from solid explosives such as TNT, and are also not relevant to vehicle transportation. Some authors investigated the influence of roughness on the blast wave transportation. For example, Smith et al. [23] carried out explosion tests in two small scale straight tubes roughened by means of different-sized roughness elements fixed along the sides, and their results showed that the increase in roughness can reduce the peak overpressure in the tunnel and thus can be used as passive protection measure for sensitive structures. Another possible measure is to use perforated plats as passive mitigation systems. Kumar et al.'s numerical results [24] showed that after using a perforated plate in a tunnel, the overpressure was immediately reduced by 26 % to 44 % for a plate porosity varying from 10 % to 40% . Silvestrini et al. [25] proposed a simple concept of energy concentration factor to allow the prediction of overpressure in confined space from the open space blast data. They also proposed a correlation for simple estimation of the blast wave transportation along a tunnel.

2.4 Battery electric vehicles

Fires in battery electric vehicles may not be significantly severer than traditional vehicles in terms of fire size [26-28]. The major hazard for these vehicles is the thermal runaway of the batteries due to overcharging, short circuits or external heating. After a thermal runaway, gases will be vented out of the batteries. These gases are not only toxic but also explosive. In case there is an ignition with a certain delay, a gas explosion could occur, which has not been systematically studied yet. Further, the release of some toxic gases, such as HF, poses another problem.

2.5 Summary

There is rather limited research on fire and explosion hazards of alternative fuel vehicles. Despite lack of the knowledge, these vehicles have been widely used, which de facto puts the whole society in a potentially high hazard. There is an urgent need to do research on this topic to understand the mechanisms and quantify the hazards.

3 Incidents with alternative fuel vehicles

There have been many incidents involving alternative fuel vehicles occurred especially in the past decade. Most of the incidents reported refer to CNG vehicles, LPG vehicles and electric battery vehicles.

3.1 CNG vehicles

CNG is the abbreviation of Compressed Natural Gas. A list of some CNG vehicle incidents recently occurred is given in Table 1. Note that in the table, "explosion" means a gas explosion following a tank rupture in case of a fire. The incidents occurred on the road or in the refueling station. The majority of these incidents started from a fire and ended with a rupture and even a gas explosion. In some incidents jet flames existed after the PRDs functioned, but there would still be a subsequent explosion if the venting flow was not high enough to release the pressure or the tank was locally damaged.

Table 1 A list of some CNG vehicle fires.

Year	Country	City	Vehicle	Fire location	ignition	Consequence
2002 [1]	USA		car		Fire	Rupture
2007 [29]	USA	Seattle	car	Street	Arson fire	12 cars damaged; rupture (explosion); debris 30 m away
2007 [29]	USA	California	Car (van)	Refueling station		Rupture, driver killed
2012 [30]	Nether-land	Wassenaar	Bus	Aside traffic	Fire in engine	No injury but a 15-20 m long jet flame
2015[1]	USA	Indianapolis	Refuse truck	Outside stores	fire in back	1 fireman minor injured; Windws broken; 1 tank found around 400 m away
2016[2]	USA	Hamilton, New Jersey	Refuse truck	street	Fire	Jet fire/explosion; damaged 4 homes
2016 [31]	Sweden	Gothenburg	Bus	Outside tunnel	Fire, ceiling	Rupture; two fire fighters injured.
2016[3,4]	Sweden	Kramfors	Car		Fire	Explosion; roof landed 30 m away.
2016[5,6]	Sweden	Katrineholm	Refuse truck		Fire	truck burned.

The CNG bus fire incident in Wassenaar, Netherland On 29 Oct. 2012 attracted much attention from the public. The bus was a MAN Lion's city CNG bus with 8 CNG tanks on top. The fire broke out in the engine compartment. After noticing the coming smoke, the driver continued to

[1] https://www.autoblog.com/2015/01/28/natural-gas-garbage-truck-explosion-indianapolis
[2] http://abc7ny.com/news/video-garbage-truck-explodes-in-hamilton/1175308/
[3] http://www.trailer.se/fordonsexplosioner-oroar/
[4] http://www.expressen.se/motor/bilnyheter/larm-om-gasfordon-som-exploderar/
[5] http://www.trailer.se/fordonsexplosioner-oroar/
[6] http://www.expressen.se/motor/bilnyheter/larm-om-gasfordon-som-exploderar/

drive and stop at a halt on the open road. The passengers then successfully evacuated. The fire developed rapidly and when the fire brigade arrived in the site, the whole bus was on fire. Later several PRDs were activated, resulting jet flames with a length of around 15 m - 20 m to shoot out in a horizontal and sideward direction. The resulting long jet flame may potentially cause danger to personnel and result in fire spread to neighboring buildings or vehicles. As no buildings were located nearby, no damage to structure was reported although it would be if the bus was in a street instead of on the open road.

In 2016, there were three CNG vehicle incidents reported in Sweden. The most known one may be the bus explosion in Gothenburg on 12 juli, 2016 [31]. It was a Solaris Urbino 15E CNG bus with 48 seats and a wheel chair. There were 7 composite tanks loaded on top each with a volume of 214 liters and an operating pressure of 200 bar. After the bus was found to be caught fire on the ceiling in the 712 m long Gnistäng tunnel in Gothenburg, the driver continued driving the bus out of the tunnel and stopped aside at around 100 m outside the southern portal. The passengers were safety evacuated and then the fire fighters came to extinguish the fire. When the incident commander felt that the fire was under control, representatives from the bus company went to turn off the gas to the engine compartment. When both staff from the emergency services and bus company stood next to the bus, one of the gas tanks exploded. Two firefighters were thrown to the ground by the shock wave and injured. The consequence could be much more severe if the explosion occurred during the evacuation stage or several seconds later when the firefighters were closer.

The other two incidents occurred in Kramfors and Katrineholm. During fire fighting of a gas car fire in Kramfors in 2016, a gas tank of the car exploded. The roof landed a few meters from a firefighter who was 30 meters from the car. In Katrineholm a gas-powered refuse truck after refueling exploded. Salvage staff could have suffered a nasty accident when they thought the other damaged tanks were empty. Fortunately quenched salvage after which the tanks, that could not be discharged otherwise, was depressurized by bombardment.

In 2013, U.S. Department of Transportation conducted a study on incidents with CNG vehicles, see Table 2 [14, 15]. A total of 135 incidents from 1976-2010 was analyzed [14].

Table 2 Summary of some accidents with CNG vehicles between 1976-2010 [14, 15].

Type of incident	No. of incidents	Percentage
Tank rupture	50	37 %
PRD release (no fire)	14	10 %
Vehicle fire (no rupture)	17	13 %
Accident w/another vehicle	12	9 %
Single vehicle accident	6*	4 %
Cylinder or fuel tank leak	14	10 %
other	7**	5 %
Unknown cause	15	11 %
Sum	135	

*5 of these hit overpass.**5 related to operation/maintenance.

Among the incidents considered in Table 2, 56% of them occurred in U.S. and others in Europe, Asia, and South America. The vehicles consisted of 51% trucks, 38% buses and 11% other commercial vehicles. It was found that most incidents with CNG vehicles were not caused by the CNG tank or fuel storage systems (only one in 17 vehicle fires). Instead they were started by an electrical short, brakes, or leaking fuel or hydraulic fluid impinging on a hot engine or exhaust system. Form the table, it is clear that tank rupture is the most likely consequence, followed by vehicles fires, PRD release failure, and tank leaks.

It was found that most tank rupture occurred during the refueling or a vehicle fire. In about 35 % of the reported fire incidents, the installed thermally activated PRDs did not work probably due to the localized fires. In 42 % of all the fire incidents, PRDs worked as intended, and leaking gases were ignited in more than 50 % of these. It should be noticed that although no gas explosion was included in the table, there were such incidents occurred as discussed previously.

From the above analyses, it can be concluded that rupture is a very common consequence of a CNG vehicle incident. If a fire starts at other parts of the vehicle, it could spread to the tanks unless it is suppressed. This will result in either a jet fire if the PRDs functions properly or a gas explosion following a rupture. The severity of the gas explosion depends on how much gas is released and whether the flames exist at the moment of rupture. If the flammable gases are ignited immediately after the rupture, the contribution from the gas explosion may be limited due to the small size of the flammable cloud.

3.2 LPG vehicles

LPG is the abbreviation of Liquefied Petroleum Gas. A list of some LPG vehicle incidents is given in Table 3. In most of these incidents, explosion is involved.

Table 3 A summary of LPG fire incidents.

Year	Country	City	Vehicle location	Ignition	Consequence
1999 [32]	France	Venissieux		arson	explosion, 6 fire fighters severely injured
2002 [7]	France	Seine-et-Marne	garage		explosion; one building collapsed; 39 houses damaged
2006 [1]	Italy	Collatino	street parking	arson	explosion, several cars, 2 garages, shops, fire spread to aparments
2007 [1]	Italy	Salerno	underground garage	gas leakage	explosion;3-store building destroyed; 5 others affected.
2008 [1]	Italy	Rovigno	underground garage		fire spread to nearby garage
2008[8]	UK	South Yorkshire	road	cigarette	Explosion
2008 [1]	Malaysia	Mallaca	refueling station		explosion; passengers severely injured
2008 [1]	UK	Sampford Peverell	road		car burnt out
2009 [1]	Italy	Marigliano	parking		explosion; damaged vehicles and buildings

[7] http://www.leparisien.fr/faits-divers/l-explosion-d-une-voiture-au-gpl-devaste-un-quartier-11-11-2002-2003562566.php (Retrieved 2017-01-01)
[8] http://www.telegraph.co.uk/motoring/3329109/LPG-car-explodes-as-driver-lights-cigarette.html (Retrieved 2017-01-01)

3.3 Electric battery vehicles

A summary of some electric battery vehicle incidents is given in Table 4. In most of these incidents, the vehicles hit some objects and caused mechanical failure. The subsequent fire caused no deaths except in the accident in Shenzheng causing 3 deaths. However, it was reported that the 3 deaths was caused by the incident rather than the subsequent fire.

The main consequence of these electric vehicle fires is the loss of the vehicle. No explosion was reported. However, there might be low speed explosion (deflagration) occurred but not clearly observed.

Table 4 A summary of fire incidents with electric vehicles.

Year	Country	City	Vehicle	Fire location	Ignition	Consequence
2011[9]	China	Hangzhou	Zotye M300 EV	road		no one injured
2012[10]	USA	California	Karma	parking lot	overheating of fan	no one injured
2012[11]	China	Shenzheng	BYD	road	crashed by a car and then run into a tree	3 persons killed
2013 [12]	USA	Washington	Tesla	road	fire after running over large metal objects	fire
2013 [13]	Mexico	Merida	Tesla	road	fire after hitting a tree	fire
2014 [14]	Canada	Toronto	Tesla	Garage		fire
2013[15]	USA	California	Tesla	Road	Fire after running over large metal objects	fire
2016[16]	Norway	Gjerstad	Tesla	Charge station	Might be a short circuit	burnt

[9] "Hangzhou Halts All Electric Taxis as a Zotye Langyue (Multipla) EV Catches Fire". China Auto Web. 2011-04-12. Retrieved 2013-06-25

[10] John Voelcker (2012-08-13). "Second Fisker Karma Fire Casts Fresh Doubt On Plug-In Hybrid". Green Car Reports. Retrieved 2012-08-13

[11] China Autoweb (2012-05-28). "Initial details on fiery crash involving BYD e6 that killed 3". Green Car Congress. http://www.greencarcongress.com/2012/05/bydcrash-20120528.html (Retrieved 2017-01-01)

[12] https://www.technologyreview.com/s/521976/are-electric-vehicles-a-fire-hazard (Retrieved 2017-01-01)

[13] Blanco, Sebastian. "Second Tesla Model S fire caught on video after Mexico crash". Autoblog Green. (Retrieved 2017-01-01)

[14] Linette Lopez (2014-02-13). "Another Tesla Caught On Fire While Sitting In A Toronto Garage This Month". Business Insider. (Retrieved 2017-01-01)

[15] https://www.technologyreview.com/s/521976/are-electric-vehicles-a-fire-hazard (Retrieved 2017-01-01)

[16] http://www.fvn.no/nyheter/lokalt/Tesla

4 Alternative fuel vehicles

There are many different types of alternative fuel vehicles. According to the different fuels used, they could be divided into four types: liquid fuels, liquefied fuels, compressed gases, and electricity. The liquid fuels mainly consist of ethanol, biodiesel and other alcohols. The liquefied fuels mainly consist of liquefied petroleum gases (LPG), liquefied natural gas (LNG) and liquefied hydrogen (LH_2). The compressed gases mainly consist of compressed natural gas (CNG), and compressed hydrogen (GH_2). The electric cars could be driven either by rechargeable batteries or other fuel cells such as renewable hydrogen fuel cells. In some literature, liquefied fuels are considered as one part of compressed gas, but here they are distinguished due to the different forms of conservation in the tank.

The number of alternative fuel vehicles is continuously increasing in the past decade. The number of alternative fuel stations may be used as indications of their use. Figure 1 gives a diagram of the percentage of the number of stations providing individual new fuels to the total number of stations of new fuels in USA. There might be some stations that provide more than one fuel types, which is not considered in the diagram. The data are gathered from the website of U.S. Department of Energy on 4 Oct 2016 [17]. Clearly, it shows that the most available stations in USA are for electric vehicles (14465 stations), followed by LPG (3317 stations), E85(2775 stations), and CNG (954 stations). The stations are much less for Biodiesel (178 stations), LNG (82 stations), and H2 (29 stations). The large number of electricity stations is easy to understand as the recharging takes much longer time compared to other types of fuel.
The number of LPG stations in USA, is surprisingly large in comparison to 45 in Sweden [18]. However, in some European countries a large amount of LPG stations are available, e.g. 7240 in Germany, 3363 in Italy, 1708 in Netherlands and 595 in Belgian. This could indicate a potentially wider use of LPG in Sweden.

To some extent, these numbers of stations may be correlated with the number of vehicles of specific fuel. This information indicates where the focus should be placed in the following work.

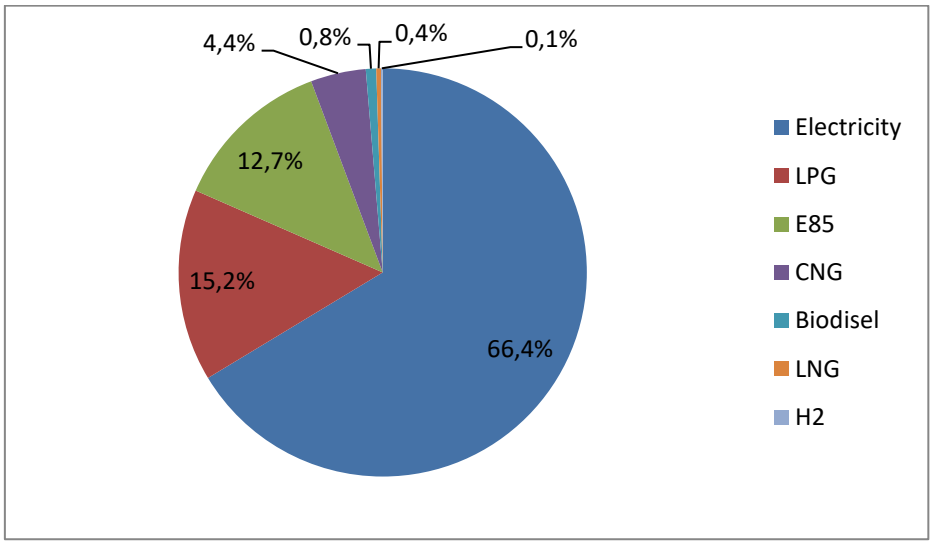

Figure 1 A diagram of the percentage of the number of stations open to public in USA, 2016.

[17] http://www.afdc.energy.gov/data_download
[18] http://www.mylpg.eu/stations/

In the following, a short description of different new fuels is presented. A summary of properties for the typical new fuels is presented in Table 8.

4.1 Liquid fuels

The liquid fuels discussed here are the fuels of liquid form at ambient pressure and temperature.

4.1.1 Ethanol

Ethanol is one renewable fuel. The chemical formula is C_2H_5OH. It has been widely used nowadays. The use of ethanol is widespread, and approximately 97% of gasoline in the U.S. contains some ethanol [19]. For example, E85 at gas station generally refers to a mixture of approximately 85 % of ethanol and 15 % of gasoline, E10 means a mixture of 10 % of ethanol and 90 % of gasoline.

Ethanol could be considered as a clean fuel as the combustion efficiency is very high and the majority of the combustion products are CO_2 and H_2O.

The fuel tanks are similar to those for traditional energy carriers but the boiling point is somewhat lower. It is 78.5 °C at atmospheric conditions from Table 8 compared to 35-210 °C for gasoline and 150-350 °C for diesel.

4.1.2 Methanol

Methanol is also a renewable fuel. It could be produced in wood industry. The chemical formula is CH_3OH. Similar to ethanol, methanol could be considered as a clean fuel.

The fuel tanks are similar to those for traditional energy carriers but the boiling point is somewhat lower. The boiling point is 64.5 °C at atmospheric conditions from Table 8.

4.1.3 Biodiesel

Biodiesel is also a renewable fuel. It can be manufactured from vegetable oils, animal fats, or recycled restaurant grease for use in diesel vehicles [20].

It consists of similar chemical compounds as diesel, and in need it could be directly used by traditional diesel engines. Therefore it has its advantage in the near future.

4.1.4 Other alcohols

There are also other alcohols that have potential to be alternative fuels for vehicles, e.g. butyl alcohol or butanol. Its chemical formula is C_4H_9OH. The boiling temperature is around 118.5 °C at atmospheric conditions, higher than ethanol and methanol.

4.1.5 Fuel tank

The size of the tank is mostly 50 to 100 liters for passenger cars, and 400 to 1000 liters for heavy duty vehicles.

[19] http://www.afdc.energy.gov/fuels/ethanol.html
[20] http://www.afdc.energy.gov/fuels/biodiesel.html

4.2 Liquefied fuels

In contrast to liquid fuels, the liquefied fuels here are the fuels that are of gas phase at atmospheric pressure and temperature. By increasing the pressure and/or decreasing the temperature, the gaseous fuels are liquefied and stored in the tanks. Note that if the liquefied fuels are exposed suddenly to atmospheric conditions, the fuels need to absorb enough heat for evaporation.

There are two types of valves existing in both liquefied gas tanks and compressed gas tanks, i.e. pressure relief valve (PRV) for normal venting and pressure relief device (PRD) for emergent venting. Under normal operations, when the pressure inside the tank rises above around a preset value, a tank normally vents via a PRV to avoid overpressure in the tank. When the pressure returns to the normal level the PRV will automatically turn off. However, excessive venting may cause a problem. To avoid rupture of a fuel tank in an emergency case, e.g. in a fire, a PRD will be activated after the tank pressure or temperature is over a certain value, which is generally much higher than preset value for PRVs.

4.2.1 Liquefied natural gas (LNG)

For vehicles with heavy duty (travelling long distances), liquefied natural gas (LNG) has been considered as a good choice as it carries more energy for a given volume compared to a CNG tank. LNG tanks are mainly used for heavy goods vehicles and city buses at present.

LNG is typically stored in a range of 4 to 10 bar. At atmospheric pressure, natural gas remains in the liquid form at a temperature below -162 °C. In a vehicle tank, the temperature is slightly higher, mostly in a range of -140 °C to -136 °C. For LNG tanks, the activation pressure of PRDs is mostly in a range of 15 to 30 bar.

The LNG tanks are only used for heavy duty vehicles, e.g. buses and trucks. As cryogenic tanks are used careful maintenance is required. Normally the tanks are well insulated.

Table A- 2 gives a summary of parameters for LNG vehicles on market. For trucks, the mass of LNG is in a range of 112 kg to 450 kg, and volume of 315 l to 1080 l. For buses, the mass of LNG is in a range of 150 kg to 214 kg, and volume of 356 l to 508 l. The number of cryogenic LNG tanks is mostly 1 or 2. The mass for a single LNG tank mostly varies between 110 kg and 220 kg.

4.2.2 Liquefied petroleum gas (LPG)

Liquefied petroleum gas is also called “Autogas”. It mainly consist of either propane (C_3H_8) or butane (C_4H_{10}), or a mixture of them.

The tank pressure is mostly in a range of 8 to 10 bar. The tank pressure in reality is a function of temperature. Therefore the exterior temperature significantly affects the tank pressure. After the pressure is over around 20 bar, the PRVs will be activated for venting the gas, and recloses or reseals after the pressure is reduced. Therefore, under normal operation, the tank pressure is a variable, between 8 to 20 bar.

PRDs for LPG tanks are generally activated when the pressure is around 32 bar, while the tank is generally supposed to sustain integrity at around 46 bar.

The fuel has density and heat of combustion similar to gasoline and diesel. Therefore the tanks are of similar size. For many vehicles, versions of different fuel types are available, e.g. gasoline, diesel or LPG.

For personal vehicles, the fuel tank size is mostly in a range of 50 to 100 liters. For trucks, the size can be as large as 400 liters.

4.2.3 Liquefied hydrogen (LH_2)

Quite limited vehicles have used liquefied hydrogen. One main reason is the low temperature of -252 °C required to keep hydrogen in liquid form. The low temperature also indicates that the tank is sensitive to ambient temperature. If a tank has been placed in ambient for a certain time, the inside temperature will increase, and the pressure relief valves will activate to release gases. The tank pressure under normal operation is below 8 bar. It may be assumed to be around 5 bar.

Table A- 4 gives a summary of parameters for LH_2 vehicles. The vehicles are all equipped with internal combustion engines. The mass of liquid hydrogen is in a range of 2.4 kg to 8 kg. These are mostly concept vehicles.

4.2.4 Liquefied dimethyl ether (LDME)

DME is primarily produced from waste, biomass or natural gas. At ambient conditions, dimethyl ether is a colorless gas. But it can be easily liquefied, similar to propane. The pressure to keep it in the liquid form is around 5 bar. There has been some vehicle demonstrations with LDME but it may be of more use in the future. The operating pressure and pressure values for PRV and PRD are expected to be similar to those for LPG.

4.3 Compressed gas

Unlike the liquefied fuels, the compressed gases are stored in gaseous form and do not need to absorb heat for evaporation.

4.3.1 Compressed natural gas (CNG)

Natural gas mainly consists of methane. It could be produced from fossil or biogas industry. CNG is typically stored in steel or composite containers at a pressure of around 200 bar. It may also be stored in an adsorbed tank at a lower pressure, which however is not the case of main interest in this work.

The tanks can be placed at various locations, see Figure 2 for example. A bus generally has several small tanks and they are mostly located on the top. A truck normally has
one or two large tanks and they are mostly placed in the vicinity of the driver cab. A passenger car may have one to three small tanks which are placed in the trunk or below the seats.

The pressure relief devices on CNG tanks are normally activated at a temperature of 110 °C. In case of a localized fire, the pressure relief devices may not be exposed to fire and thus not activated on time. Therefore, some CNG tanks also have pressure relief devices activating at a certain pressure, e.g. around 340 bar. The venting direction may either face upwards, downwards or horizontally. Long tubes may be used in order to relieve the pressure upwards.

(a) In front of body

(b) Roof mounted

(c) Back of the cab, side mounted

Figure 2 Possible locations of the CNG tanks [33].

Table A- 1 gives a summary of parameters for CNG vehicles on market. Most of the passenger cars and light commercial vehicles listed consist of both CNG tanks and petrol tanks, i.e. they are so called “hybrid vehicles”. For passenger cars, the mass of CNG is in a range of 11 to 37 kg. For light commercial vehicles, the mass of CNG is in a range of 12 to 39 kg. The number of fuel tanks mostly varies between 1 and 5. The mass of a single tank varies between 10 and 20 kg.

For buses, the mass of CNG is mostly in a range of 160 kg and 365 kg. The number of fuel tanks mostly varies between 4 and 10. The mass of a single tank varies between 20 and 50 kg.

For trucks, the mass of CNG is in a range of 81 kg and 390 kg. The number of fuel tanks mostly vary between 4 and 8. The mass of a single tank varies between 10 and 50 kg.

Table 5 Summary of total mass and mass of single tank for CNG vehicles.

Vehicle type	Total mass (kg)	Mas for single tank (kg)
Passenger car	11-37	10-20
Light commercial Vehicles	12-39	10-20
Bus	160-365	20-50
Truck	81-390	10-50

4.3.2 Compressed hydrogen (GH2)

Hydrogen fuel can be produced from natural gas, but also from wind, solar and even garbage. At present, the number of vehicles using hydrogen as fuels is rather limited. Hydrogen may be used as fuel for both internal combustion engine and for fuel cells. The fuel cell vehicles will be shortly depicted in Section 2.4.2.

Table A- 3 gives a summary of parameters for compressed hydrogen vehicles on market. For vehicles with internal combustion engines, the mass of hydrogen tank is 2.4 kg and the storage pressure is 350 bar. They are also equipped with a 60 liter gasoline tank.

For vehicles with fuel cells, the mass of hydrogen is in a range of 4 to 6 kg with a storage pressure of 350 bar or 700 bar. The number of tanks could vary from 1 to 4.

4.4 Electricity

Two types of electric vehicles are considered here: electric battery vehicles and fuel cell vehicles.

4.4.1 Battery

There are different types of rechargeable batteries on the market, e.g. lead-acid, nickel-cadmium, nickel metal hydride, and lithium-ion batteries. Among these, lithium-ion battery is the most common one used in electric vehicles. Some common Li-ions batteries include Lithium Iron Phosphate (LiFePO4), Lithium Manganese Oxide (LiMn2O4), Lithium Nickel Manganese Cobalt Oxide (LiNiMnCoO2 or NMC), Lithium Cobalt Oxide (LiCoO2), Lithium Nickel Cobalt Aluminum Oxide (LiNiCoAlO2), and Lithium-titanate (Li4Ti5O12). Note that the above names come from the materials for cathodes except Li4Ti5O12 which is the material for anode. A battery cell mainly consists of cathode, anode and electrolyte. Graphite is normally used as the anode material.

An electrolyte mainly consists of a liquid solvent and a salt which facilities transport of charge inside the battery by means of ions (such as Lithium hexafluorophosphate, LiPF6) [34]. The main liquid solvents used in lithium-ion batteries are ethyl carbonate (EC), propyl carbonate (PC), dimethyl carbonate (DMC), Ethyl-Methyl carbonate (EMC) and di-ethyl carbonate (DEC). The properties can be found in Table 6.

Table 6 . Chemical parameters for the electrolytes [34].

Solvent	Molecular Structure	CAS num.	Boling temp.	Start temp. in Air	Start temp. Argon	Flash-point	Auto ignition point	Steam-press (STP)	Explosion limits	Combustion energy
			°C	°C	°C	°C	°C	mmHg	%	MJ/kg
EC		96-49-1	238	170	140	160	465	0.02	3.6/16.1	13.24
PC	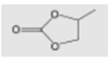	108-32-7	242	100	100*	132	435	0.03	1.8/14.3	14.21
DMC	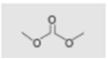	616-38-6	90	177	223	18	458	18.33	4.22/12.9	15.86
EMC	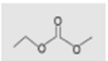	623-53-0	109		160	27				
DEC	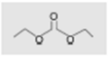	105-58-8	126	138	243	31	445	9.998	1.4/11	22.76

**Standard Temperature and Pressure (20°C and 1 atm).*

In a power optimized Li-ion battery cell, the mass percentage for the flammable solvent is around 12%, and around 12% for graphite and 5 % for plastics around the cell (the “coffee

bag") [34]. Typical heat of combustion for the solvents from a battery cell can be found in Figure 3 [34]. An average value of 16 MJ/kg could be used for typical solvents.

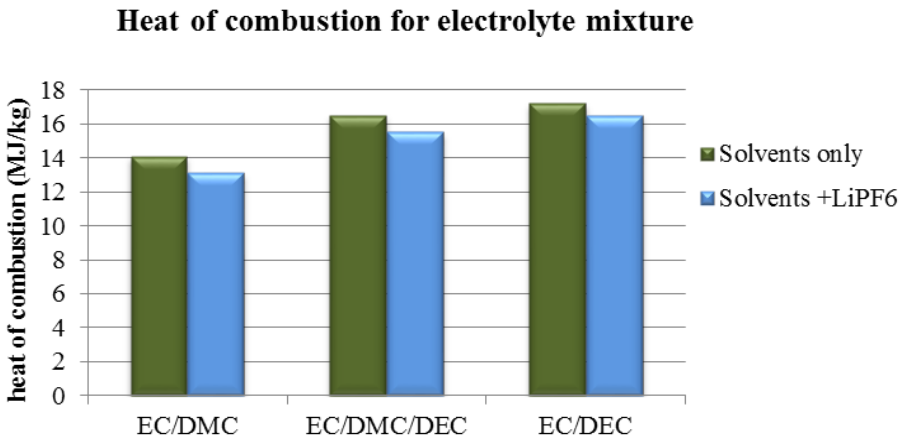

Figure 3 Heat of combustion of electrolyte mixture [34].

The battery is generally of significant size and mostly placed beneath the seats. The battery pack used in an electric vehicle mostly consists of several battery modules, each of which consists of many cells.

A serious malfunction of the batteries or the control system can potentially result in a thermal runaway. The reason may be overcharge, electrical fault, an external fire or heating source, and etc. A thermal runaway normally occurs when the temperature is in a range of 150 °C to 250 °C. In case of a thermal runaway, combustible gases are released in the surrounding compartment. Examples of the compositions of the venting gases released from battery cells with thermal runaway are shown in Table 7. The venting gases mainly consist of carbon monoxide, carbon dioxide, hydrogen and other combustible gases. Despite the fact that the mass percentage for hydrogen is small, the volume percentage is as high as around 30 %. Further, carbon dioxide and some other gases such as hydrogen fluoride are toxic, which endanger personnel nearby. It is known from Table 7 that the main combustible gases consist of hydrogen, carbon monoxide and some hydrocarbon fuels.

Table 7 Composition of the venting gases from Li-ion batteries (percentage in weight, kg/kg).

Gas	Corvus NMC 18650 cell, test conducted by Sandia [35]	NMC 18650 cell [36] *	LCO/NMC 18650 cell [36] *	LFP 18650 cell [36] *	Li-ion batteries in general, RECHARGE [37] *
	%	%	%	%	%
H2	5.1	2.4	2.6	2.2	2.7
CO	15.1	14.1	33.3	4.8	50.1
CO2	61.4	70.4	47.3	83.4	39.4
CH4	-	4.2	5.9	2.3	5.0
C2H4	8.7	8.9	9.3	6.8	3.8
C2H6	1.9	-	1.6	0.3	1.3
C3H6	0.3	-	-	-	1.9
HF	-	-	-	-	0.3

* These values are mass percentage, estimated based on volume ratios from literature.

The amount of venting gases may vary with other parameters, e.g. state of overcharge. In an electric battery vehicle incident, the fire spread between cells/modules takes time, depending on the configurations of the battery pack and the battery type. To be on the safe side, all the flammable solvents are assumed to be released into surroundings after an incident, while considering the explosion hazards.

The venting gas may auto-ignite, or be ignited by an external fire or heating source. The consequence may be a fire or an explosion, depending on how the venting gases are distributed and how the combustion starts. The venting of the gases is generally similar to a jet with a high initial velocity. In some cases, it seems to be a jet fire during a certain period.

There are mainly three types of Li-Ion batteries used, i.e. Lithium Manganese Oxide (LiMn2O4), Lithium Iron Phosphate (LiFePO4) and Lithium Nickel Cobalt Aluminum Oxide (LiNiCoAlO2). The corresponding energy density is 120 Wh/kg, 130 Wh/kg and 130 Wh/kg, respectively [37]. The value calculated based on data from the table is 80-110 Wh/kg for LiMn2O4 and LiFePO4, and 167 Wh/kg for LiNiCoAlO2. These values correlate relatively well with each other. However, the energy density for Lithium-titanate (Li4Ti5O12) batteries is around 80 Wh/kg. For the common Li-Ion batteries except Lithium-titanate (Li4Ti5O12), an average value of 125 Wh/kg could be used for the energy density.

The properties for the batteries in electric vehicles are shown in Table A- 5, Table A- 6 and Table A- 7.

For passenger cars, the capacity is mostly in a range of 16 kWh to 100 kWh, and the mass in a range of 200 to 540 kg. More information on the electric passenger cars can be found in the literature [38].

For electric buses, the capacity is mostly in a range of 150 kWh to 660 kWh. The mass is estimated to be 929 kg to 7800 kg. Excluding Proterra with Lithium-titanate batteries, the mass is mostly in a range of 1200 kg and 2500 kg.

For electric trucks, the capacity is mostly in a range of 80 kWh to 350 kWh. The mass is around 615 kg to 3300 kg.

4.4.2 Fuel cell

The fuel cell vehicles mainly use hydrogen as fuels. At present, there have been many fuel cell vehicles under development. However, in reality there are only several vehicle models available on the market. The main reason may be that the fuel cell vehicles are considered to be less efficient than the battery electric vehicles.

The hydrogen tanks are mostly placed beneath the back seats or between the seats and the trunk. In some cases, hydrogen tanks may also be placed in trunks.

The parameters for compressed hydrogen tanks in fuel cell vehicles are given in Table A- 3. They have been discussed in Section 2.3.2.

Table 8 A summary of fuel properties.

Fuel	Chemical formula	M	$\rho_{air,1atm}$	ρ_{liquid}	T_b	T_c	P_c	T_{ig}	L_v	ΔH_c	Stoichio volume fraction	Max laminar flame speed	Min ignition energy	Flammability	
														low	high
		g/mol	kg/m^3	kg/m^3	°C	°C	bar	°C	kJ/kg	MJ/kg		m/s	mJ		
Ethanol	C_2H_5OH	46.1	–	789	78.5			392	836.8	26.8	0.065	–	0.65	0.033	0.19
Methanol	CH_3OH	32	–	793	64.5	239	81	470	1101	19.8	0.1224	0.52	0.14	0.067	0.37
Dimethyl ether	C_2H_6O	46	1.99	735	-24			350	461.6*	31.6	–	0.45**	0.29	0.034	0.27
Propane	C_3H_8	44.1	1.90	580	-42.2	97	42.5	504	425.5	46.3	0.0402	0.43	0.31	0.022	0.095
Butane	C_4H_{10}	58.1	2.54	601	-0.5	153	36.5	431	385.8	45.7	0.0312	0.42	0.26	0.019	0.084
Methane	CH_4	16	0.68	422	-161.7	-83	46	632	509.2	50	0.0947	0.37	0.29	0.053	0.15
Hydrogen	H_2	2	0.085	70.8	-252.7	-240	13	571	451.0	141.8	0.295	2.91	0.015	0.040	0.75

* http://encyclopedia.airliquide.com/
** from reference [39, 40].

5 Qualitative analysis of fire and explosion hazards

5.1 Fire hazards

There are four types of fire hazards for the alternative fuel vehicles: pool fires, jet fires, fireballs and flash fires.

After an incident, the liquid fuels may leak and form a pool on the floor. If an ignition source exists, a pool fire will occur. Note that a pool fire may also occur for a liquefied fuel vehicle. If a liquefied tank leaks, a two-phase jet may form and meanwhile some liquid may spill to floor and form a pool. This mostly occurs when the pressure valve is located at the low level of the tank (below the liquid surface). If a liquefied tank ruptures, a pool may also form. The main reason is that generally there is not enough heat to evaporate all the fuels instantaneously. Therefore, a fire incident with the liquefied fuels may involve a pool fire together with a jet fire. The burning of the pool fires is similar to a gasoline pool fire but the burning intensities for liquefied fuels, e.g. mass burning rates, are normally much higher.

For a compressed gas vehicle, the most common fire hazard is a jet fire. A jet fire may also occur for a liquefied fuel vehicle. Much of the liquefied fuel may change in phase instantaneously when it is released to the ambient. In both cases, the jet fire occurs when the pressure valve is operating properly and the tank does not rupture. If there are several tanks in the vehicle, several pressure valves may be activated and several jets or one combined jets may be formed. For an electric battery vehicle, jet fires are also common consequence. After a thermal runaway, the gases vent out in the form of a jet. This phenomenon is obvious mostly during the initial stage of venting of a cell or a module. The venting gases at this stage mainly consist of electrolyte. But the flame length is not expected to be as long as for a jet fire from a compressed gas tank.

At the beginning of a jet fire or immediately after a tank ruptures, a fireball may form. A fire ball refers to immediate ignition after a flammable gas is suddenly released, and therefore the mixing of flammable gas with air is rather limited and a flame ball will form. Normally the concentration of flammable gas is high in the center of the cloud due to lack of mixing. A fireball mostly occurs immediately after a tank ruptures.

For all the fuels in the open, a flash fire may occur. A flash fire results from the ignition of a released flammable cloud in which there is essentially no increase in combustion rate [16] and pressure. The flame spread is similar to that in a laminar flow with a typical flame spread velocity of around 10 m/s. The physical meaning is a very low speed combustion that results in no blast wave. The main hazards of a flash fire are the convective heat (by direct flame contact) and radiation heat. As the way that a flash fire influences the personnel and surrounding structure is more similar to that in a fire rather than an explosion, it is therefore considered to be one type of fire hazard. The phenomenon mostly occurs in a quiescent open area or a large space without obstruction on the way of flame spread. Note that a tunnel or an enclosure is partly or completely enclosed. Further, there could be many vehicles and the tunnel walls are relatively rough. Therefore, a more probable scenario in a tunnel is that a low speed deflagration may develop to a high speed deflagration. In other words, a flash fire may seldom occur in a tunnel.

Note that when liquid fuels in tanks are heated, e.g. to the superheat temperature, they pose same hazards as liquefied fuels. In other words, liquid fuels can pose hazards of pool fires, jet fires, fireballs and flash fires. However, preheating of a certain period is required, e.g. from a

fire. But it is not a precondition for compressed gases and liquefied fuels, although liquefied fuels also needs heating to produce longer jet flames or larger fireballs. Therefore, from this point of view, liquefied fuels pose higher hazards than liquid fuels.

In summary, the four fire hazards may occur for any type of alternative fuel vehicles with the exception of no pool fires for compressed gas tanks and electric battery vehicles. Although a flash fire may occur for any type of the fuels discussed, but the likelihood in a confined space or a tunnel is small. Further, preheating of a certain period is required for a liquid tank to produce a jet fire, fireball or flash fire, and thus the likelihood is considered to be lower compared to the liquefied fuels. Therefore, the most probable fire incidents involving alternative fuel vehicles in a tunnel are considered to be:

(1) a pool fire for liquid fuels,
(2) a pool fire with a jet fire, or a fireball for liquefied fuels,
(3) a jet fire, or a fireball for compressed gas vehicles, and
(4) a normal fire with a small jet fire for electric battery vehicles.

5.2 Explosion hazards

There are three types of explosion hazards for the alternative fuel vehicles: gas cloud explosion (combustion), gas tank rupture and boiling liquid expanding vapour explosion (BLEVE). A BLEVE is a special type of tank rupture but in this work it is considered separately due to its uniqueness.

Gas cloud explosion refers to chemical reactions of premixed combustible gases. There are two types of gas cloud explosion, i.e. deflagration and detonation. A deflagration refers to combustion flows of subsonic flame propagation speed. A detonation refers to combustion flows of supersonic flame speed. Note that common fires refer to diffusion flames, and they are not called deflagration in this work. Unless a huge ignition source exists, all the gas cloud explosion starts form a deflagration with low flame speed. But the flame speed of a deflagration could in some cases increase continuously up to supersonic flow and suddenly transits to a detonation. The Deflagration to Detonation Transition is commonly written as DDT. In the open, a DDT seldom occurs. However in a tunnel with enough fuels, the flame speed may increase continuously with the travelling distance from ignition until a DDT occurs. It has been found that local turbulence caused by obstructions or blockages (wrinkled or distorted flames with larger flame surfaces) plays a key role in determining whether a DDT occurs or not. In tunnels, existence of large vehicles and other equipment may significantly reduce the distance from ignition to DDT. Above all, the type, amount, concentration and distribution of fuels, and the physical geometry are the key parameters. Ventilation is also important as it could have a major influence on the ignitability. The precondition for an explosion is the existence of flammable gas cloud. Therefore, gas cloud explosion may occur for all types of fuels discussed, especially for compressed gas vehicles, liquefied fuel vehicles and the electric battery vehicles. The possibility of a gas cloud explosion in an incident with liquid fuel vehicles is considered to be less due to the fact that preheating the liquid fuels of a certain period is required. The venting gas from a battery pack consists of a large portion of hydrogen, and therefore the electric battery vehicles also pose a high hazard for gas cloud explosion.

A compressed gas tank may burst and result in a blast wave. This phenomenon may be called gas tank rupture or gas expansion explosion. In such a case, the gas of a significantly higher pressure above ambient will be instantaneously released into the site, forming a blast wave.

BLEVE is the abbreviation of boiling liquid expanding vapour explosion (BLEVE). When liquefied fuels are suddenly exposed to atmospheric pressure due to an activated PRD or other

openings, one portion of the liquefied fuels will evaporate instantaneously by absorbing the heat contained in the liquefied fuels. This percentage of evaporated liquefied fuels is called flash fraction. Similar to a gas tank rupture, a BLEVE can cause significant pressure rise and form a blast wave. The instantaneous evaporation throughout the bulk of the liquid is generally considered to occur mostly when the temperature exceeds the superheat temperature, which is around 0.895 times the critical temperature for a given fluid according to Reid [41], although there are some recent studies again this statement. It should be kept in mind that the liquid fuels also have the hazard of BLEVE after being exposed to fire for a certain time. However, compared to liquid fuels, liquefied fuels have much lower boiling temperature, indicating that they pose high hazard of BLEVE.

When a PRD valve of a pressurized tank is operating, the released gases may be ignited, which results in a gas cloud explosion but the resulting overpressure is generally insignificant. Stock et al. [42] investigated the explosion after jet release of propane, hydrogen and natural gas with a nozzle diameter of 10 mm to 100 mm. Their results showed that the optimum location for ignition was near the center of the jet axis at a downstream distance of 70 to 100 times the nozzle diameter, and ignition outside the region either failed or led to much lower pressures. The maximum explosion pressure was found inside the jet profile and increase with the nozzle diameter. For a nozzle diameter of 10 mm, the maximum overpressure is around 0.011 bar but it can be 3 times higher in case there are obstacles and confinement. Overall, the explosion hazards in such cases are mostly rather limited due to the limited amount of dispersed fuels that are within the flammability limits. Therefore, severe gas cloud explosion is generally not expected while immediately igniting a gas jet after a PRD opens.

When a tank rupture or a BLEVE occurs, the released gases may probably be ignited, resulting in a fireball. The fireballs are mostly considered to be low speed deflagration. The contribution of this explosion to the first peak overpressure at a given distance from the tank is generally considered to be low. But for some explosive gases, e.g. hydrogen with a high laminar flame speed, the immediate combustion followed by the tank rupture may have some influence on the blast wave. In most cases, the main hazard to be considered in such a case is the fire ball that radiates heat towards surroundings and the possible fire spread to surrounding fuels.

Although, in the above analyses, the fire hazards and explosion hazards are separately discussed, an incident may involve in both fire and explosion hazards. For example, a jet fire may cause rupture of a tank and/or ignition of a combustible gas cloud (gas cloud explosion).

It has to be pointed out that in case of a failure of a pressurized tank, some fragments can be thrown away for a significant distance, e.g. several hundreds meters from the site. These flying fragments may cause significant damages to surrounding personnel and structure. The fragments are generally divided into two groups: primary fragments (tank structure and contents inside) and secondary fragments (objects near the tank). The number of primary fragments depends on not only the pressure at the moment of rupture but also the structure and material of the tank and the vehicle. But they mostly consist of only one or several large fragments. After many incidents, composite CNG tanks were found with a large hole on one side, but their locations can vary significantly, which can be up to several hundred meters away. The number of secondary fragments depends on the objects nearby. The longest throwing length occurs when the initial velocity of a fragment from a free-standing tank is at an angle of 45 °C. For an incident in the open, if a tank is located within or under a vehicle, much of the kinetic energy may be acted to the vehicle itself, and thus the throwing length should be rather limited. However, if a tank is placed on top of a vehicle or directly exposed on one side of the vehicle, the throwing range can be large. For such an incident in a tunnel, the fragments may mostly hit the tunnel walls within a short range, even when the fuel tank is placed on top of the vehicle. The probability of the primary fragments directly thrown towards a vehicle far behind without hitting the tunnel structure is rather low. Instead, the secondary fragments, e.g. pieces of windows broken by a blast wave can be a problem.

In summary, gas cloud explosion may occur in an incident with any type of the fuels discussed, although the possibility is low for liquid fuel vehicles. Besides, an incident may be a rupture for compressed gases and a BLEVE for liquefied fuels.

Therefore, the most probable explosion incidents involving alternative fuel vehicles in a tunnel are considered to be:

(1) a BLEVE or a gas cloud explosion for liquefied fuels,
(2) a gas tank rupture or a gas cloud explosion for compressed gas vehicles, and
(3) a gas cloud explosion for electric battery vehicles.

5.3 Event trees

In incidents, physical damage to the vehicle fuel storage systems and fire impacts are the two key factors that may initiate the problems that have been discussed above. For example, a collision may result in a small or large hole on fuel tanks, or initiate a failure of a battery.

The event tree for liquid fuel vehicle incidents is shown in Figure 4. In case of an incident, if there is no external fire, a failure of a liquid fuel tank normally will not cause any blast wave or fire. However, if there is an external fire, the scenarios will be completely different. In a case with an external fire, if the incident results in a small hole on the tank or an existing PRD opens, the fuel will be released and form a pool fire. Further, if the fuel has been overheated by the external fire, some liquid fuels will evaporate and thus a jet fire may form. If the evaporated fuels are not ignited immediately after the release, the fuel gases may mix with air and an ignition can cause an explosion. As a direct initiated detonation seldom occurs in such an incident, the most probably case is a low speed deflagration but it may develop to a detonation after a certain travelling distance, especially along the path with a large amount of blockages. In the open with no significant obstruction, the deflagration process may be so low that no blast wave is formed, i.e. a flash fire. In the case with an external fire, if the PRD malfunctions, the fuel will be overheated until the tank bursts and a BLEVE occurs. The external fire probably ignites the released fuels in gas form (forming a fireball) while ignites the fuels in liquid form (forming a pool fire). If the released fuels are not ignited immediately after the BLEVE, they may be premixed with air and a late ignition may produce a deflagration or a DDT. Note that this event tree also applies to gasoline and diesel fuel vehicles.

The event tree for liquefied fuels is very similar to those for liquid fuels, see Figure 5. There are two main differences between them. Firstly, under normal operation temperature, a liquefied fuel tank incident may result in a jet fire or a BLEVE due to the low boiling temperatures, but this is mostly not the case for a liquid fuel tank. Secondly, liquefied fuel tanks generally correspond to more sever hazards of jet fires, BLEVE and gas cloud explosion, as more fuels normally evaporate after a tank burst compared to liquid fuels.

The event tree for compressed gas vehicle incidents is shown in Figure 6. Clearly, it is highly similar to the event tree for liquefied fuels in Figure 5. The main differences are that for compressed gas vehicles, there is no pool fire (accompanied with jet fires) and also no BLEVE after a gas tank rupture.

It should be clearly pointed out that even if the PRD opens as designed, a BLEVE or a tank rupture may still occur, in case that the release capacity is limited compared to the fire intensity. This case should be classified as “PRD malfunction”.

The event tree for electric battery vehicle incidents is shown in Figure 7. If the venting gas ignites immediately or quite early, a jet fire and a subsequent common solid fire will occur. But if not, there may be a gas explosion.

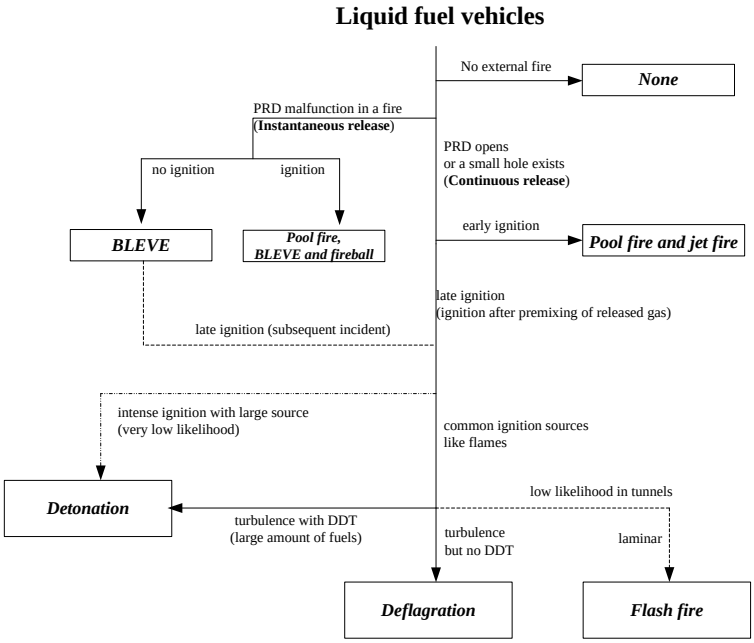

Figure 4 Event tree for liquid fuel vehicle incidents.

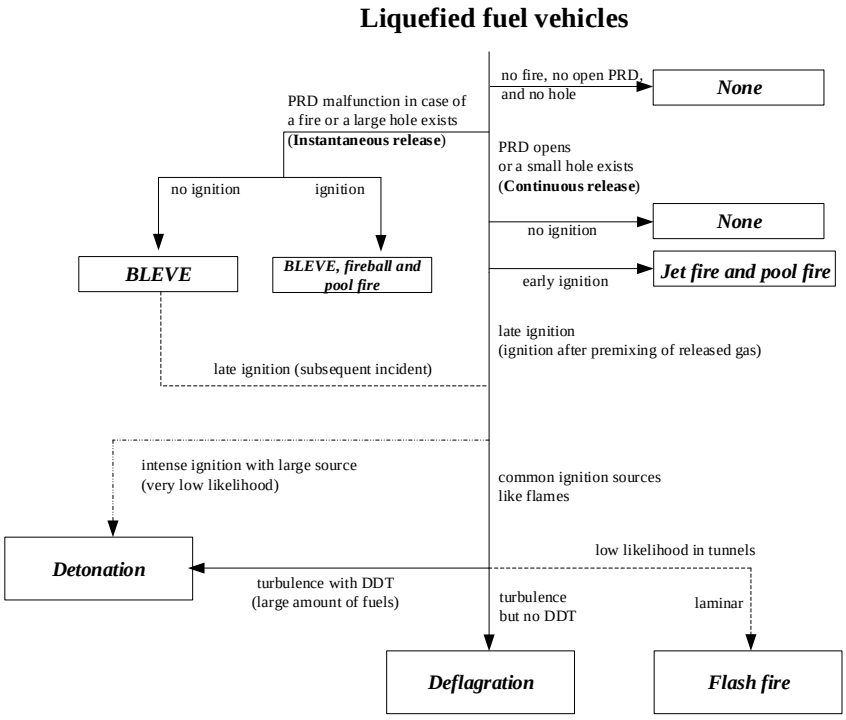

Figure 5 Event tree for liquefied fuel vehicle incidents.

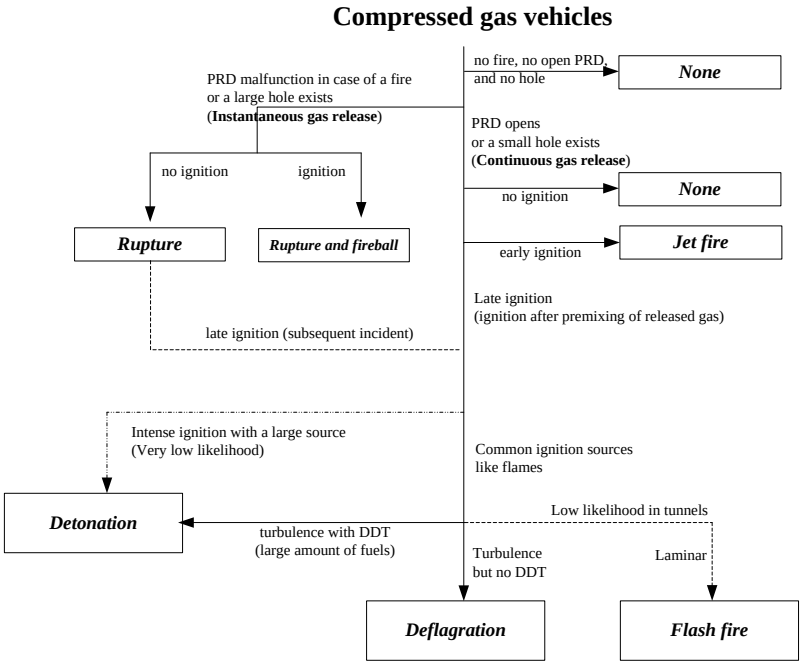

Figure 6 Event tree for compressed gas vehicle incidents.

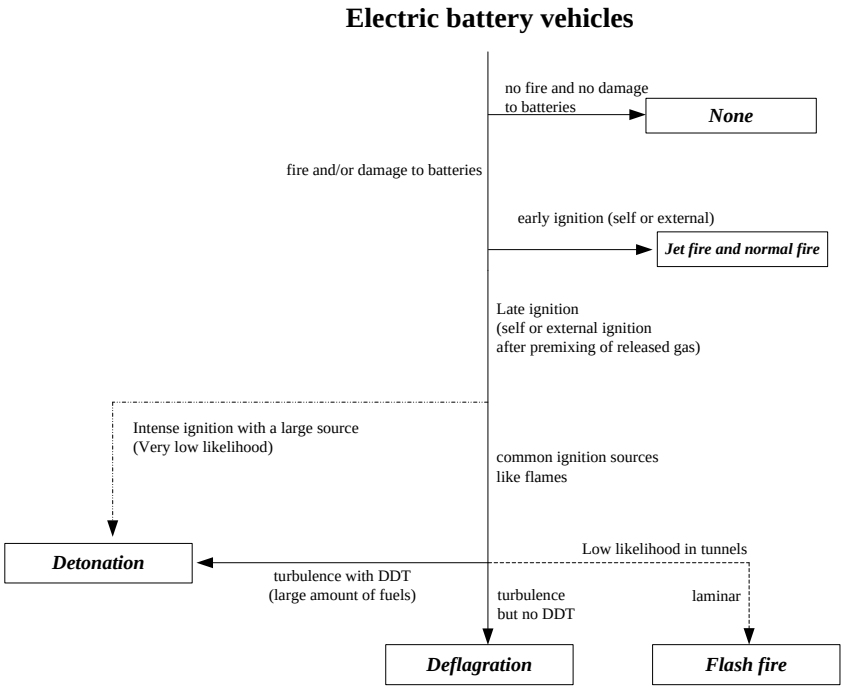

Figure 7 Event tree for electric battery vehicle incidents.

5.4 Summary

In summary, a flash fire and a gas explosion may occur for all types of the fuels. However, for a tunnel section (or an enclosure) with a large portion of the space filled with the flammable gas,

the combustion occurred is most likely a gas explosion, rather than a flash fire with closely no overpressure.

After considering both the fire hazards and explosion hazards, the most probable incidents involving alternative fuel vehicles in a tunnel are considered to be:

(1) Liquid fuel vehicles: pool fires
(2) Liquefied fuel vehicles: jet fires with pool fires; BLEVE with fireballs; gas cloud explosion
(3) Compressed gas vehicles: jet fires; Gas tank rupture with fireballs; gas cloud explosion
(4) Electric battery vehicles: Normal fires with small jet flames; Gas cloud explosion.

It may be expected that the explosion hazards, i.e. rupture, BLEVE and gas explosion, are more severe than the fire hazards. If fuels are releasing (or leaking) from a tank but not burning, it indicates that there is a flammable vapor cloud that can potentially cause an explosion. If the fuels in tanks are not releasing (or leaking), it may indicate a tank rupture or a BLEVE may occur.

6 Numerical model for explosion flow

A one dimensional CFD program is developed to simulate compressible flows in tunnels in case of a tank rupture, a BLEVE and a gas cloud explosion.

6.1 Controlling equations

The controlling equations are listed in the following.

Mass:

$$\frac{\partial \rho A}{\partial t} + \frac{\partial (\rho u A)}{\partial x} = \dot{m}_f''' \tag{1}$$

and for ith species:

$$\frac{\partial \rho A Y_i}{\partial t} + \frac{\partial (\rho u A Y_i)}{\partial x} = D_i \frac{\partial^2 Y_i}{\partial x^2} + \dot{m}_f''' Y_i \tag{2}$$

Momentum:

$$\frac{\partial (\rho u)}{\partial t} + \frac{\partial (\rho u u)}{\partial x} = \frac{\partial}{\partial x}(\mu \frac{\partial u}{\partial x}) - \frac{\partial p}{\partial x} - \frac{\partial p_{fr}}{\partial x} + S_M \tag{3}$$

Energy:

$$\frac{\partial (\rho A h)}{\partial t} + \frac{\partial (\rho u A h)}{\partial x} = \frac{\partial}{\partial x}(kA \frac{\partial T}{\partial x}) + \frac{\partial p}{\partial t} + u \frac{\partial p}{\partial x} + \dot{Q}''' - \dot{Q}_{loss}''' \tag{4}$$

Thermodynamic equilibrium can be assumed for an ideal gas. The state equation for pressure can be expressed as:

$$p = \rho \bar{R} T \sum_i \frac{Y_i}{M_i} \tag{5}$$

In the above equations, ρ is density (kg/m^3), t is time (s), x is the cartesian axis (m), u is velocity (m/s), μ is air viscosity (m^2/s), k is heat conductivity (kW/(m K)), p is pressure (Pa), g is gravitational acceleration(m^2/s), $\bar{R}$ is universal gas constant (8.314 kJ/(kmol K)), M is lumped molecular weight (kg/kmol), T is gas temperature in Kelvin (K), e is specific internal energy (kJ/kg), h is enthalpy (kJ/kg), Y is the species mass fraction, ΔH_{O2} is heat released per kg oxygen (kJ/kg), $\dot{Q}$ is heat release rate (kW), X_r is radiation fraction, A is wall surface area, h_c is convective heat transfer coefficient, ε is emissivity, τ is wall stress (friction loss). Subscripts e is exit vent, O_2 is oxygen, r is radiation, w is wall, fr is friction loss and $loss$ is heat loss. Superscript (·) indicates per unit time and (') per unit length.

The Finite volume method is applied for discretization. All the transient flow properties are solved by the modified PISO and SIMPLE algorithms for compressible flows. Godnov upwind scheme and TVD schemes are available.

6.2 Boundary conditions

Two types of flow boundaries are available: fixed values and zero gradient. An inlet or outlet may be a velocity boundary, a flow rate boundary or a zero gradient total pressure boundary. A boundary may also be a symmetrical boundary with zero gradient.

The wall is assumed to be cold as the process is quite short compared to the time required for temperature change in solid phase. Therefore the heat conduction inside the wall is not simulated.

6.3 Convective heat transfer

The convective heat transfer at the boundaries can be expressed as:

$$h_c = \frac{k}{l}\mathrm{Nu} \tag{6}$$

The Nusselt number for a wall with a rough surface is well correlated by the following relationship [43]:

$$\mathrm{Nu}_D = \frac{(f/8)\,\mathrm{Re}_D\,\mathrm{Pr}}{1+(4.5\,\mathrm{Re}_\varepsilon^{0.2}\,\mathrm{Pr}^{0.5}-8.48)\sqrt{f/8}} \tag{7}$$

and the Prandtl number, Pr, :

$$\mathrm{Pr} = \frac{v}{a}$$

The relationship applies for the following ranges of Re and the relative roughness of the surface ε/D:

$$\mathrm{Re}_D > 10^4 \text{ and } 0.002 \le \varepsilon/D \le 0.05$$

The Reynolds number depends on the relative roughness of the surface and is defined as:

$$\mathrm{Re}_\varepsilon = \mathrm{Re}_D \frac{\varepsilon}{D}\sqrt{\frac{f}{8}} \tag{8}$$

In the above equations, f is the Darcy-Weisbach friction factor, ε is the root mean square roughness of the surface (m), and ε/D is relative roughness of the surface. Note that for fully developed turbulent flows, the Darcy-Weisbach friction factor is not sensitive to the Reynolds number.

In the above equations, all properties are estimated at the flow temperature. This makes the above equations easy to use.

Generally the tunnel diameter can be used as the characteristic length in the heat transfer analysis of the whole system. Also the hydraulic diameter can be used in the analysis of heat

loss to walls surrounding the hot gases where clear stratification exists. The hydraulic diameter can be calculated by:

$$D = \frac{4A}{P} \tag{9}$$

where A is the flow area (m^2), and P is wet perimeter of the flow (m).
Note that the convective heat transfer is not very sensitive to the characteristic length scale in a tunnel. Therefore, the error introduced by slight differences in choosing the characteristic length scale should be quite limited in most cases.

6.4 Radiative heat transfer

The radiative heat transfer is simplified in such cases. Grey gas is assumed for the smoke flow. The emissivity is estimated using:

$$\varepsilon_g = 1 - e^{-\kappa_s L_m} \tag{10}$$

where the mean beam length, L_m (m), is defined as:

$$L_m = 3.6 \frac{V_m}{A_m} \tag{11}$$

and the absorption coefficient for soot, κ_s, [44]:

$$\kappa_s = 3.75 \frac{C_o}{C_2} X_s T \tag{12}$$

In the above equations, c_p is heat capacity (kJ/kgK), ρ is density (kg/m^3), t is time (s), x is the cartesian axis (m), u is velocity (m/s), k is heat conductivity (kW/(m K)), p is pressure (Pa), Pr is Prandtl number, g is gravitational acceleration(m^2/s), $\bar{R}$ is universal gas constant (8.314 kJ/(kmol K)), M is molecular weight (kg/kmol), T is gas temperature in Kelvin (K), e is specific internal energy (kJ/kg), h is enthalpy (kJ/kg), Y is the species mass fraction, ΔH_{O2} is heat released by consuming 1 kg oxygen (kJ/kg), $\dot{Q}$ is heat release rate (kW), X_r is radiation fraction, A is wall surface area, V is room volume, h_c is convective heat transfer coefficient, ε is emissivity, Xs is the soot volume fraction, Co is a constant varying between 2 and 6, dependent on the refractive index (a value of 4 is applied in PRS), C_2 is the Planck's second constant, 1.4388×10^{-2}m·K. Subscripts e is exit vent, O_2 is oxygen, r is radiation, w is wall. Superscript (·) indicates per unit time and ("") per unit volume. Subscript s indicates solid.

6.5 Tank rupture model

In case of a gas tank rupture, a simulation starts at time zero with the initial tank properties (tank pressure, temperature and fuel properties), and afterwards the tank gases are immediately exposed to the air in the tunnel. Note that the tank needs to be considered as part of tunnel section.

In case of a BLEVE, the explosive evaporation process is modelled as a vapor release from a source area covering the initial liquid volume and the vapor pressure of the superheated liquid in the source area drives the gas dynamics of the vapor release, as proposed by van den Berg [45].

Note that the flash fraction (fraction of instantaneous evaporation) of the liquefied fuel can be predetermined by use of analytical models. In the model, the tank gases release into the tunnel section instantaneously. This method may tend to be conservative.

The gas dynamics play an important role in the tank rupture. Therefore the species equation needs to be well resolved:

$$\frac{\partial \rho A Y_g}{\partial t} + \frac{\partial (\rho u A Y_g)}{\partial x} = D_g \frac{\partial^2 Y_g}{\partial x^2} + \dot{m} Y_g \tag{13}$$

6.6 Gas cloud explosion model

In the cases of main concern in this work, direct initiated detonation is not practical. Mostly a possible detonation is transited from a deflagration. However, modelling of deflagration to detonation is extremely difficult due to the complex physics, i.e. combustion, turbulence and gas dynamics. At present, most CFD models are calibrated for either deflagration flows or detonation flows, but not for both. Modeling of this phenomenon is even more difficult for a one dimensional numerical model. Therefore, assumptions are made here, following van den Berg and Weerheijm's work [46].

In the gas cloud explosion model, the flame propagation velocity is predetermined based on experimental data and calibration process. The flame speed is assumed to increase linearly with distance from the ignition center to a value of 800 m/s. After this value, the explosion is assumed to transit to detonation immediately, which correlates well with the experimental data by Zipf Jr et al [17] and Lowesmith et al. [47]. After detonation occurs, the C-J velocity is applied.

The deflagration to detonation transition (DDT) is a very complex phenomenon. It depends on not only the geometry, size of the vapor cloud, reactivity of the mixture, ignition location, ignition method, but also the local obstacles which can enhance turbulence, and thus results in earlier transition from laminar to turbulent flames. The distance for deflagration to detonation transition (DDT) was reviewed by Thomas et al [48]. For most of the experiments with duct diameters less than 0.4 m, the ratio of DDT distance to duct diameter varies between 50 and 300. The DDT distance is less for highly explosive fuel, e.g. hydrogen, compared to propane and methane.

Test data with tunnel explosion were mostly obtained from model scale tests. It is know that generally the flame velocity in model scale is lower than that in full scale. This indicates that the DDT distance is normally greater in model scale. To extrapolate the model scale results to full scale, this scale effect needs to be considered. In such cases, the Karlovitz number similarity (scaling) may be applied here. The Karlovitz number characterizes the ratio of the chemical time scale to the turbulent time scale. Catlin and Johnson [49] carried out model scale tests following the Karlovitz scaling by raising the reactivity of the mixture to compensate the scale effects in the acceleration phase of an explosion, e.g. oxygen enrichment for increasing the laminar flame speed. They found that the combination of oxygen enrichment to raise the laminar flame speed by a factor of 1/5 power of the length scale and obstacle roughening provided conservative predictions at 1/5 scale irrespective of the ignition strength and the ultimate flame speeds reached, and the scaling method provides a way of predicting an upper bound on the full scale overpressures in general explosion scenarios. If the combustible mixtures are the same in both scales, the flame speed is proportional to 1/3 power of the length scale according to the Karlovitz scaling. This indicates a lower flame speed at the corresponding

location (the location of the same dimensionless distance) in model scale. As mentioned previously, the flame speed in a one dimensional system can be assumed to increase linearly with distance from the ignition point. Therefore, to achieve the same velocity of 800 m/s in both scales, the dimensionless DDT distances follow such a scaling law:

$$\frac{x_{DDT,\mathrm{Full}} / d_{\mathrm{Full}}}{x_{DDT,\mathrm{Model}} / d_{\mathrm{Model}}} \propto \left(\frac{d_{\mathrm{Full}}}{d_{\mathrm{Model}}}\right)^{-1/3} \tag{14}$$

Or the scaling law for the DDT distance is:

$$\frac{x_{DDT,\mathrm{Full}}}{x_{DDT,\mathrm{Model}}} \propto \left(\frac{d_{\mathrm{Full}}}{d_{\mathrm{Model}}}\right)^{2/3} \tag{15}$$

This indicates that the dimensionless DDT distances scales as -1/3 power of the length scale (duct diameter). Ciccarelli and Dorofeev [50] proposed a correlation for the dimensionless DDT distance based on the boundary layer theory, and by analyzing their correlation and the results presented it can be found that the dimensionless DDT distances approximately scales as -0.19 power of the duct diameter [50]. Note that the latter corresponds to a longer DDT distance in full scale while extrapolating results from model scale. Therefore, to be on the safe side, the dimensionless DDT distances is assumed to scale as -1/3 power of the length scale.

A comparison of data for the dimensionless DDT distance is shown in Figure 8. The data for methane come from the NIOSH tests [17], the TNO tests and estimation [46], and Hendersen's work [48, 51]. For methane explosion in tunnels, the best experimental data could be the ones reported by Zipf Jr et al [17]. Their test data for methane showed that the ratio of distance to DDT to duct diameter is 19 to 23 for a blockage ratio of 0.13, 16 to 23 for a blockage ratio 0.25, and 16 to 23 for a blockage ratio of 0.50. Van den berg et al. [46] carried out methane explosion tests in a 0.25 m high and 0.5 m wide tunnel with vehicle models inside, and the dimensionless DDT distance could be estimated to around 27. According to the Karlovitz scaling, the dimensionless DDT distance can be estimated to be 9.5 using the data by Zipf Jr et al [17] and 11.6 using the data by Van den berg et al. [46].

The data summarized by Thomas et al [48] are also used for comparison although in most of the experiments the duct diameters less than 0.4 m. Clearly, the results for dimensionless DDT distance summarized by Thomas et al [48] are much greater than the others.

For methane, the correlation that fits the mediate scale test data is expressed as follows:

$$\frac{x_{DDT}}{d} = 16.3 d^{-1/3} \tag{16}$$

The correlation was obtained in a conservative way according to the Karlovitz scaling. The correlation refers to the scenarios with certain vehicle obstacles, i.e. the blockage ratio ranges between 0.13 and 0.5 for the key test data.

Test data for propane are also plotted in Figure 8 (hollow points), including the data reported by Steen and Schampel [52], Capp and Seebold [40], and Ginsburgh and Bulkley [53]. Due to the similarity in the fuel properties, including laminar flame speed and expansion ratio, the same correlation as for methane may be applied. Clearly, all test data are above the proposed correlation. The reason for this may be that in general no obstacles were considered in these tests.

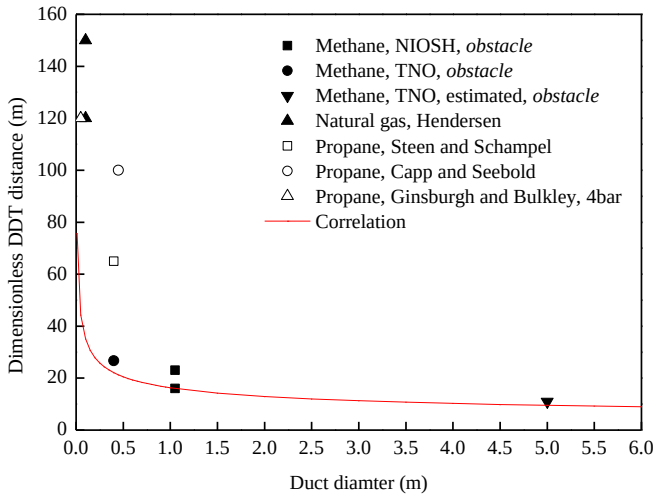

Figure 8 Test data on the DDT distance for methane and propane.

Hydrogen is well known for its susceptibility to detonate [47]. Test data for hydrogen or hydrogen/methane mixture are plotted in Figure 9, including the data reported by Lowesmith et al. [47], Ginsburgh and Bulkley [53] and Bollinger [54]. A data point estimated from the hydrogen tunnel tests by Groethea et al. [18] is also given. The estimation was based on comparison of test data and numerical results presented in Section 6.7.2.

It is clearly shown in Figure 9 that large scale test data correlate with the correlation line well, and all small scale test data are above the proposed correlation. This indicates that the correlation provides reasonable results for large scale but tends to be conservative for small scale. It should be kept in mind that in the large scales tests, there were obstacles simulating vehicle blockage while not in the small scale tests with smooth tubes.

In Lowesmith et al.'s tests [47], the test rig comprised of a long congested region measuring 3m × 3m × 18m following an chamber measuring 3m × 3m × 8.25m. The enclosure had a closed end [55] and another end connected to the congested region. The number of the 3 m long obstacles of a diameter of 0.18 m in the chamber varies from 0 to 21, while the congested region was formed from 12 racks spaced 1.5 m apart supporting either 7 or 6 horizontal pipes of 3 m length and 0.18 m diameter. The blockage ratio in the congested region can be estimated as 42 % at some racks. The hydrogen and methane mixture was used as the fuel.

For hydrogen, the correlation that fits the mediate scale test data is expressed as follows:

$$\frac{x_{DDT}}{d} = 11.2 d^{-1/3} \tag{17}$$

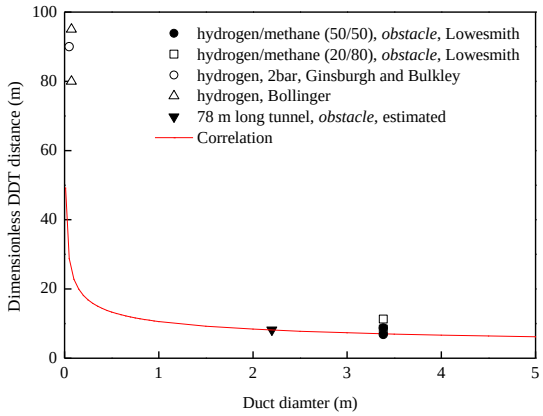

Figure 9 Test data on the DDT distance for hydrogen and hydrogen/methane mixture.

For battery, the combustible mixture consists of several fuels. The interaction between the fuels needs to be considered. Lowesmith et al. [47] investigated the effect of combined combustibles in explosion in a long congested region. The hydrogen content in the methane/hydrogen mixture was varied from 0 to 50 % by volume in the combined combustible mixture. They concluded that for low flame speed initiated in the congestion region, hydrogen concentration less than 30 % is likely to be similar to methane, and the value is 20 % for high speed flame being generated in a connected enclosure. For a higher concentration of hydrogen, the risk of DDT and high overpressures is significantly increased. For battery, the hydrogen volumetric concentration is generally over 30 % in the venting gases and the other combustibles are much less. Therefore, the DDT distance for hydrogen is used for battery explosion in the following analysis.

In the above analysis, the ignition was assumed to be in the middle of the gas cloud, while the DDT distance refers to the distance between the DDT location and the ignition location. If the ignition is at one edge of the cloud, the DDT distance will be longer, e.g. Van den Berg et al. [46] considered the DDT distance for edge ignition to be twice that for center ignition.

The combustion intensity also depends on the local mixture concentration, i.e. the fuel concentration and the oxygen concentration. The species concentration was modelled by the following:

$$\frac{\partial \rho A Y_i}{\partial t} + \frac{\partial (\rho u A Y_i)}{\partial x} = D_i \frac{\partial^2 Y_i}{\partial x^2} - \dot{m}_f''' Y_i \tag{18}$$

where heat addition:

$$\dot{Q}_i''' = \dot{m}_f''' \min(Y_f, Y_{O_2} / s)$$

Note that at the early stage, the fuels are pushed away from the ignition source as the flame front is behind the fuel-air interface. This results in a larger combustion zone in reality, compared to the initial fuel zone.

6.7 Verification of modelling

Three tests were used for verification of modelling of the explosion sub model. These tests include the CO2 BLEVE tests by van der Voort et al. [56], the tunnel tests with hydrogen cloud explosion by , and the tunnel tests with methane cloud explosion by TNO.

6.7.1 CO2 BLEVE tests

The TNO tests with a liquefied CO2 tank in a test bunker with an internal volume of 6 m × 12 m × 4 m [56] was simulated for verification. The tank had a diameter of 0.23 m and a height of 1.37 m. It was placed vertically on the floor in the center of the room. The rupture was initiated by cutting charges with a length of 1 m installed at two opposite sides of the tank. Pressure transducers were installed at 0.7 m above floor and 1m, 2 m and 3 m away from the tank. The flash fraction is estimated to be 0.4 [56]. In the tests, two tests, i.e. test 1 and test 2, were carried out but test 2 was a repeat of test 1. To simulate the overpressure in the vicinity of the tank, the scenario is assumed to be cylindrical in the numerical modelling.

The comparison between test data and numerical results for overpressure at 1 m, 2 m and 3 m from the tank is shown in Figure 10, Figure 11 and Figure 12, respectively.

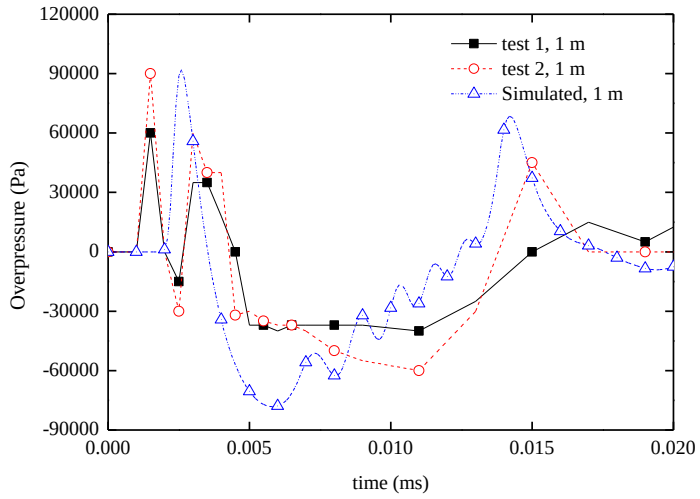

Figure 10 The overpressure at three different locations in the tunnel fully filled with stoichiometric methane air mixture [46].

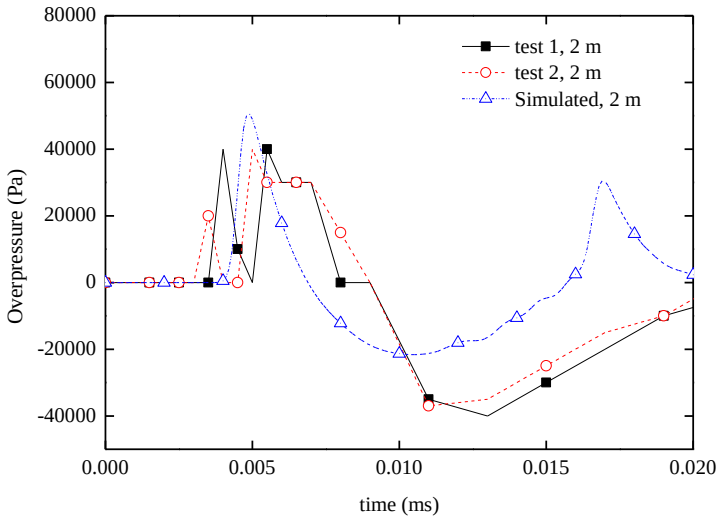

Figure 11 The overpressure at three different locations in the tunnel fully filled with stoichiometric methane air mixture [46].

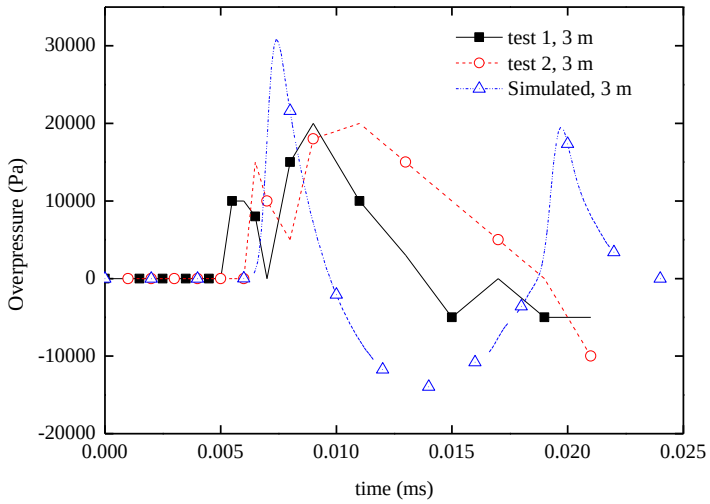

Figure 12 The overpressure at three different locations in the tunnel fully filled with stoichiometric methane air mixture [46].

6.7.2 Tunnel tests with hydrogen cloud explosion

Three series of tests was carried out by Groethea et al. [18] in a 78.5 m long tunnel with a cross sectional area of 3.74 m^2 and two open portals. The arcuate tunnel is 1.84 m high. In some tests, vehicle models with dimensions of 0.94 m (L)×0.362m (W) ×0.343m (H) were placed on the floor with an interval of 0.94 m along the centerline of the tunnel. The blockage ratio is 3.32 %. The scale ratio is 1:5.

In the first series of tests, homogeneous mixtures of hydrogen and air were contained within a 37 m^3 volume at the center of the tunnel with plastic film barriers which were cut before ignition. The hydrogen volume concentrations tested were 9.5 %, 20 % and 30 %. The fuels were ignited at the bottom center of the fuel volume. The corresponding fuel masses were 0.32 kg, 0.67 kg and 1 kg. Test data showed that for hydrogen mixture of 9.5 %, the pressure was too low for the sensors. The maximum overpressure was around 35 kPa throughout the length of the tunnel for hydrogen mixture of 20 %, and 150 kPa for hydrogen mixture of 30 %. The presence of the vehicle models of blockage ratio of 3.32 % has nearly no influence on the results.

In the 2nd series of tests, the hydrogen was released from a nozzle into the tunnel and then ignited at certain time. In two tests, the hydrogen was continuously released for 20 seconds into the center of the tunnel (1 kg hydrogen in total) and then ignited at different time. There was no ventilation during the tests. No data for pressure were recorded in these two tests as the resulting pressures were probably below the measurement range of the equipment. The volume fraction in the vicinity of the release point was however registered, which showed that the concentration is close to the lower flammability limit at around 6 m from the release point in one test and at around 3 m in another test. It was mentioned that these concentration was registered before the ignition. The results indicate that the hydrogen concentration decreases rather rapidly with distance from the release point due to entrainment similar to a ceiling jet.

In the 3rd series of tests [57], the hydrogen was released into a ventilated tunnel at the inflow portal. The ventilation flow rate is 1.6 m^3/s. In one test, the hydrogen was continuously released for 20 seconds with a flow rate of 0.005 kg/s (1 kg in total). In another test, the release lasted for around 420 seconds (2.2 kg in total). The measured volume concentration of hydrogen was below 5 % downstream of the release point. No ignition took place due to the low

concentration. This should be attributed to the longitudinal ventilation which dilutes the hydrogen concentration. However, it should be kept in mind that in the tests the hydrogen was continuously released at a low flow rate to simulate the emergency release of a pressure relief device. This flow rate is much lower compared to the value in case of tank burst or BLEVE. In such cases, the volume fraction of hydrogen could be high enough to support ignition and sustain flame spread.

The test from the first series of tests with homogeneous mixtures of hydrogen and air contained within a 37 m^3 volume at the center of the tunnel are simulated and compared with the test results, see Figure 13.

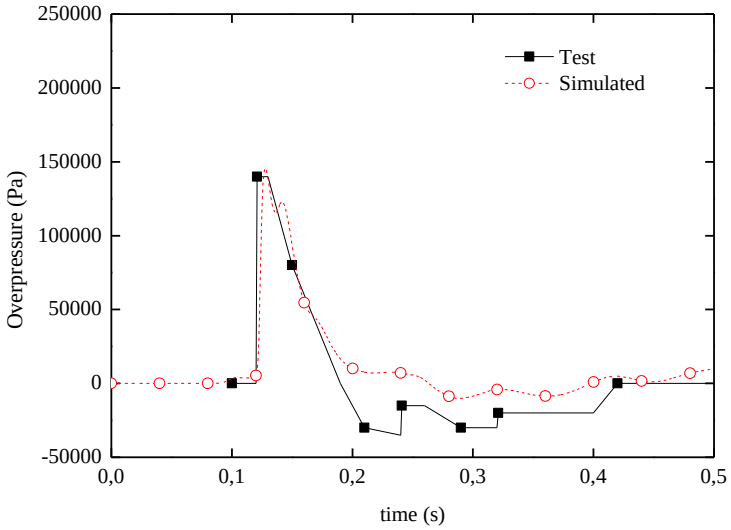

Figure 13 The overpressure close to the tunnel portal.

6.7.3 Tunnel tests with methane cloud explosion

The TNO-Prins Maurits Laboratory performed an extensive experimental programme [46]. To this end a steel channel of 0.25 m x 0.5 m cross-section and 8 m long was used. This small-scale model (1:20) of a traffic tunnel was provided with a configuration of steel obstacles to simulate a standing traffic jam (Figure 14). The channel was filled with a flammable gas-air cloud and ignited at a closed end, simulating central ignition in a two-sided open channel twice as long. The cloud length was varied as being: 25 %, 50 %, 75 % and 100 % of the channel length. The fuels used were methane and propane at three different compositions.

The results showed that for the cloud length of 25 % of tunnel length, the flame after having passed the 25 % of channel length gradually propagated into leaner and leaner mixture and the explosion has shorter length to develop. In contrast, in all cases with cloud length over 25 % of tunnel length, the flame hardly consumed leaner mixture before it met the open end and the cloud length nearly has no influence on the overpressure.

The cloud compositions also have influence on pressure development. The stoichiometric mixture generally produced highest overpressure in the tests. However, in the test with cloud

length of 25 % of tunnel length, the test with rich fuel results in higher pressure than the fuel lean and stoichiometric cases as the additional fuel was pushed forward and consumed later.

The results with ignition at one closed end are shown in Figure 15. The tunnel was full filled with stoichiometric methane air mixture. The pressures were registered at the closed end, in the middle and at the open portal respectively, see Figure 14. There is a sudden increase in the pressure at one position for a very short period and the reason is unknown. However, the maximum overpressures at different locations are approximately at the same level. This is one behavior of the one dimensional combustion.

Figure 14 TNO model scale tunnel explosion tests [46].

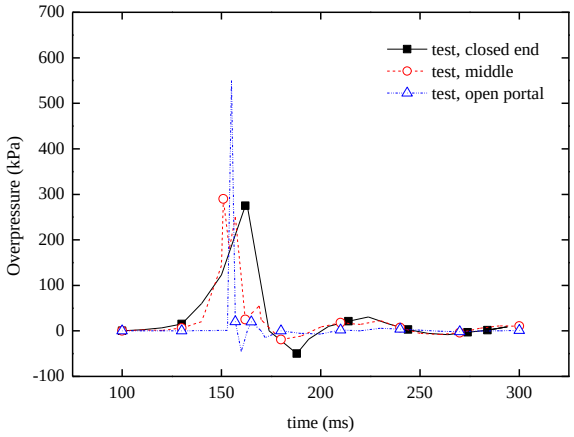

(a) Test results, obtained from the report [46]

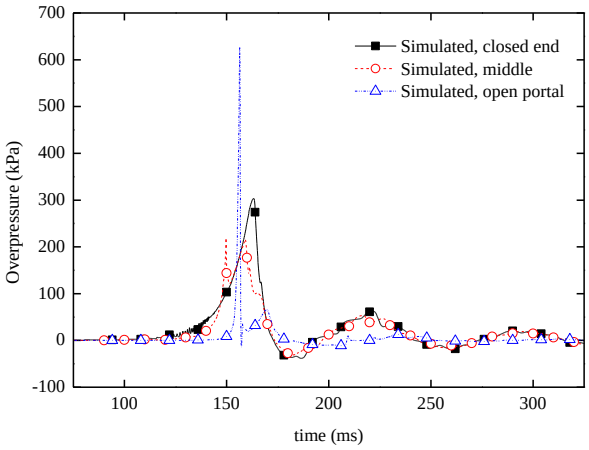

(b) Simulation results

Figure 15 The overpressure at three different locations in the tunnel fully filled with stoichiometric methane air mixture.

7 Quantitative analysis of fire hazards

There are three types of fire hazards concerning the alternative fuel vehicles, i.e. common fires, jet fires and flash fires.

For all the fires, the heat release rate can be estimated by:

$$\dot{Q} = \chi \dot{m} \Delta H_c \tag{19}$$

where the mass burning rate, $\dot{m}$ (kg/m^{2}s), is:

$$\dot{m} = \rho \dot{V} \tag{20}$$

In the above equation, χ is combustion efficiency, which can be considered as 1 in most cases.

7.1 Spilled pool fires

7.1.1 Leakage rate

Liquefied fuel - pressurized tank

In case of a hole at the bottom of a pressurized liquid fuel tank, e.g. a LPG tank, the volume flow rate can be estimated by:

$$\dot{V} = C_d A_d \sqrt{\frac{2(P_{\text{tank}} - P_o)}{\rho} + 2gh} \tag{21}$$

Normally the term related to static pressure difference is much higher than the potential energy term. Further, if the process occurs during a significantly long period, the tank pressure may probably be close to the equilibrium pressure, dependent on the liquid temperature. Therefore a constant volume flow rate could be expected.

For superheated liquid, a large portion of the leaked flow may evaporate instantaneously and thus only the unevaporated fraction will temporarily form a pool on the ground. Details on flash fraction will be given in Chapter 8.

Liquid tank – No overpressure in the tank
For a tank with a hole of cross sectional area, A_d (m^2), and liquid surface at the level h (m) above a hole, the outflow, $\dot{V}$ (m^3/s), as a function of time, can be obtained based on the Bernoulli equation:

$$\dot{V} = C_d A_d \sqrt{2gh} \tag{22}$$

For gasoline tank, assuming the tank has a constant cross sectional area along the height, A_{tank} (m^2), the transient volume flow, $\dot{V}$ (l/s), can be estimated by:

$$\dot{V} = 2000 A_{tank} K(\sqrt{h_{initial}} - Kt) \tag{23}$$

where g is the gravitational acceleration in m/s^2, and C_d is a flow coefficient for the opening at which the water flows out. The ideal value is 0.7 but it can also be determined experimentally. The parameter K is calculated according to Eq. (5),

$$K = \frac{\sqrt{2g}C_d A_d}{2A_{tank}} \tag{24}$$

The equation for the outflow can be used to estimate the initial flow rate for tanks of various shapes after setting t equals zero. But the transient flow rate is highly dependent on the tank shapes and thus no uniform equation is proposed.

7.1.2 Burning rate

The burning of the liquid fuels listed in Section 4.1 is similar to a common pool fire, although some differences indeed exist. For an ethanol or a methanol fire, the flame is much less luminous and the smoke is less dense. Therefore, it is difficult to visually notice such a fire. A hydrogen flame has similar behaviors, while it may be more noticeable due to the noise affiliated with the high speed hydrogen jet release.

For the liquefied fuels, a pool may also form if the fuel leaks from the liquid side of the tank. The reason is that generally the heat containing in the liquid is not great enough to support complete evaporation and thus a portion of the fuel will remain in liquid form and form a pool.

Note that most data on burning rate come from tests with deep pools. The burning of spilled fires is different but it has been found that there are correlations between them. Therefore, the burning rate of deep pools is discussed first in the following.

For small and deep pools, the burning rate generally increases with the increasing area, but it approaches constant when the pool diameter exceeds a certain value, generally 1 m or 2 m in the diameter for deep pools.

The burning rate for a deep pool could be expressed as a function of the pool diameter in such a form [58]:

$$\dot{m}'' = \dot{m}''_{\infty}(1 - e^{-k\beta D}) \tag{25}$$

where $k\beta$ is a flame emittance parameter that is considered as a constant for a given fuel. The parameters for common fuels are listed in Table 9.

Table 9 A list of burning properties for different fuels in deep pools.

Fuel	density	L_v	ΔH_c	$\dot{m}''_{\infty}$	$k\beta$
	kg/m^3	kJ/kg	MJ/kg	kg/(m^2·s)	1/m
Ethanol	794	1000	26.8	0.015	-
Biodisel	800	-	43.4	0.035	1.7
Methanol	796	1230	20	0.023	-
Gasoline	740	330	43.7	0.055	2.1
LH2	70.8	442	120	0.169	6.1
LNG	415	619	50	0.078/0.15*	1.1
LPG	585	426	46	0.099	1.4

*refer to reference [59].

The mass burning rate for deep pools is:

$$\dot{m} = \dot{m}'' A \tag{26}$$

For spilled fires, the mass burning rate is much less. For the spilled gasoline fires tested, the average heat release rate per unit area is about 1/3 to 2/5 of that for a deep pool fire [60], that is, the mass burning rate for a spilled pool is:

$$\dot{m} = \varphi \dot{m}'' A \tag{27}$$

where φ is a correlation coefficient which is around 0.37 [60]. It may be expected that such a reduction also applies to other liquid fuels such as ethanol and diesel. However, from

7.1.3 Spilled area

The liquid fuels can be released in different ways: small leakages from fuel tanks or fuel hoses, ruptured tanks, leakage from a tanker carrying a flammable liquid, etc.

The spillage area is mainly affected by the amount, release rate, and type of the fuel, the configuration (e.g. flat or sloping) and the material of the floor.

For flat floor, the following correlation for thickness of the spill was proposed by Gottuk and White [61]:

$$A_s = \begin{cases} 1.4V_s, & V_s < 95 \\ 0.36V_s, & V_s \geq 95 \end{cases} \tag{28}$$

where A_s is the spillage area (m^2) and V_s is the volume of the spill (L). For flat floor, the minimum depths δ (mm), may be expressed as follows [61]:

$$\delta = \begin{cases} 0.7 \text{ mm}, & V_s < 95 \\ 2.8 \text{ mm}, & V_s \geq 95 \end{cases} \tag{29}$$

It has been found for fuels on the flat floor, the area of unconfined spill increases after being ignited and the increased area, A, can be estimated by the following [61]:

$$A = 1.55 A_s \tag{30}$$

However, tunnels mostly have both longitudinal slopes and transverse slopes (across the section). The reason for the transverse slopes is mainly for drainage. However, it aids to reduce the spillage area and the fire size in case of a liquid spilled fire.

For slopping tunnels, Ingason and Li [60] proposed correlations for estimating the spillage area and also the flow rate from a hole (or nozzle) of a tank. A sketch of a fire incident with leakage of continuous flow from a tank is shown in Figure 16. The spillage area on the road surface is shown in the same figure. Two dimensions are shown, namely the width, B (m), and length, L (m), of the spillage. In order to calculate B, the following equation was developed [60, 62]:

$$B = 2\dot{V}^{0.46}$$

where $\dot{V}$ is the outflow in l/s. The relation $\dot{V}^{0.46}$ is based on tests conducted on a painted plywood board; the coefficient 2 was determined from tests on an asphalt surface.

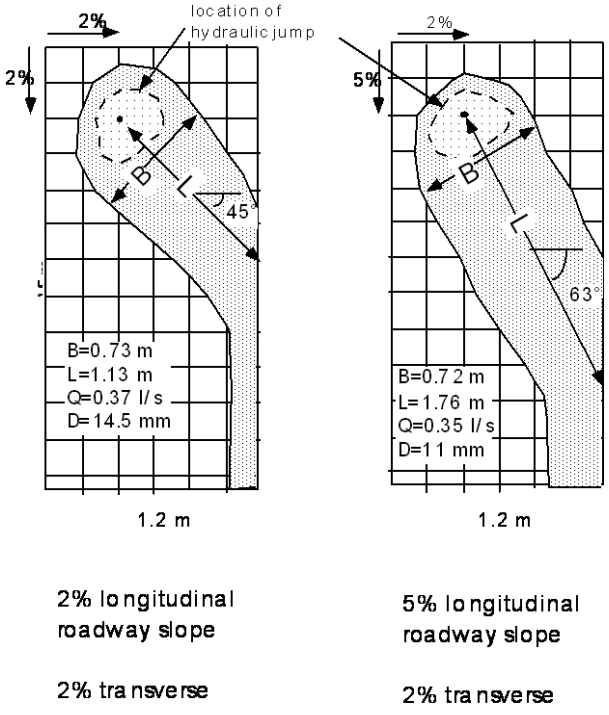

Figure 16 A sketch of a fire incident with leakage of continuous flow from a tank on a painted particleboard with different slopes [62].

The total area of the spillage up to the side of the road, A (m^2), is [62]:

$$A = BL \tag{31}$$

For which L can be calculated, dependent on the inclination of the road surface. If the inclination across the direction of traffic (transverse) is x% and in the direction of the traffic (longitudinal) is y%, the road surface is b metres wide, and the transverse distance from the release point to the opposite side of the road is c metres, L, can be calculated according to the following equation:

$$L = \frac{(b-c)}{\cos(\alpha)} \tag{32}$$

where the deflection angle $\alpha = \arctan(y\% / x\%)$.

If a tank has a hole of its whole cross section, the liquid will release instantaneously. Tests on a road tunnel with a 2.5 % longitudinal slope and a 1 % transverse slope [60] showed that the spillage area caused by an instantaneous release of 2 m^3 liquid varied between 138 m^2 and 163 m^2, with an average value of around 150 m^2. This indicates the fuel thickness is around 12 mm to 15 mm. While lacking of information, these values may be used for estimation of the spill area of an instantaneous release.

Note that if there is no drainage system nearby the fire site, the spill fuels will continue to flow downwards in the direction of the traffic. In such cases, the fire size will be much larger. In practice, some ditches have been found in tunnels as the vehicle tires especially winter tires wear asphalt down. In such cases, a pool of a significant depth can form in case of a fuel leakage. This may also need to be accounted for while analyzing the hazards of spilled pool fires.

7.1.4 Flame length

Heskestad [10] proposed a well-known correlation for the flame length for buoyant diffusion flames in the open, L_B, which is expressed as follows:

$$L_B = -1.02D + 0.235\dot{Q}^{2/5} \tag{33}$$

where D is the diameter of fuel outlet.

7.1.5 Heat flux

For all the fires, the point source method may be used in estimation of the heat flux received from flames. The view factor method could also be used. However, the view factor method requires the emissive power and flame shape, which could vary significantly in different cases. In comparison, the point source method is much simpler and robust for estimation of heat flux.

A schematic drawing of the radiation from flames to an object is shown in Figure 17. The flame can be simplified to a point source at 1/4 of the flame length with a radiation fraction. This model has been validated by Ingason et al [2].

For jet flames, the radiation fraction generally increases with the carbon number of the fuel. Beyler [63] summarized results for jet flames from literature and showed that, the radiation fraction is 0.17-0.2 for hydrogen, 0.19-0.23 for methane, 0.25-0.36 for propane, 0.3-0.37 for butane and 0.4 for fuels with carbon number greater than 4. Lowesmith et al. [9] showed that the radiation fraction is 0.13 for natural gas, 0.24 for propane, 0.32 for butane and 0.5 for crude oil. Beyler [63] also showed the trend that the radiation fraction decreases with the increasing jet velocity. For example, the radiation fraction decreases from 0.2 at 5 m/s to 0.12 at 50 m/s for methane, and from 0.35 at 5 m/s to 0.15 at 50 m/s. The results presented by Lowesmith et al. [9] appears to fit these results at high velocity better and therefore used for natural gas and propane. The radiation fraction for hydrogen should be close to that for methane, and thus the same value is assumed. In summary, in the calculation, the radiation fraction is 0.13 for hydrogen, 0.13 for natural gas, and 0.24 for propane.

For both pool fires and flash fires, the radiation fraction is mostly in a range of 0.1 and 0.4 [16, 64]. For both types of fires, a value of 0.35 may be used. For hydrocarbon pool fires, a large amount of data are analyzed and a correlation was proposed [64]. However, the correlation predicts average value. To be on the safe side, a new correlation could be proposed for estimation of the radiation fraction for common hydrocarbon fires (pool flames):

$$\chi_r = 0.35 - 0.006D \tag{34}$$

Therefore, the incident heat flux at an object on the tunnel wall can be calculated using the following equation:

$$\dot{q}'' = \frac{\chi_r \dot{Q}}{4\pi R^2} \tag{35}$$

where χ_r is the fraction of the total HRR that is lost by flame radiation, and R is the distance between the flame centre and the object (m).

Note that the heat flux received by a surface is related to the surface orientation. The incident heat flux received by the surface must be multiplied by a factor of cosβ (the angle between the incident radiation and the object surface), that is, the above equation must be corrected by:

$$\dot{q}'' = \frac{\chi_r \dot{Q}}{4\pi R^2} \cos\beta \tag{36}$$

where β (°) is the angle between the incident radiation and a line normal to the object surface, see Figure 17. Note that when the object surface can see part of the flame the angle will be close to 0.

Further, note that the equation can only be used to roughly estimate the flame radiation. It is not valid when the object is too close to the fire, e.g. when the target is surrounded by flames. More specifically, the validity can be checked after the calculation, considering that the heat flux from a fire is generally not greater than 400 kW/m^2, which corresponds to a gas temperature of about 1360 ^{o}C.

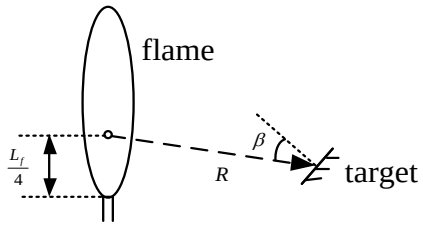

Figure 17 A sketch of radiation from the flame to an object.

7.1.6 Analysis results

The heat release rate per unit fuel area (HRRPUA) for different fuels is given in Table 10. The values presented here are for spilled fuels around 1 mm thick. Apparently, the values for ethanol and methanol are much less than those for gasoline and diesel (biodiesel). However, the liquefied fuels have much higher values for HRRPUA. Especially for LH2 the value is as high as 8.9 MW/m^2, which is around 60 times that for ethanol and methanol.

The heat release rate depends on the spill area. Here a typical road tunnel is considered where the 9 m wide tunnel has a 2% longitudinal slope and a 1% transverse slope. The tank for all the liquid fuels is assumed to be 0.2 m high (passenger cars) and has a hole of 1 cm diameter at bottom. The volumetric flow rate is estimated to be around 0.1 liter/s for all the liquid fuels but much higher for the liquefied fuel tanks. The largest spill area and the highest heat release rate are shown in Table 10. As the spill area is mainly affected by the tunnel slopes, location of the tank, and the spillage flow rate, the spill area is considered to be the same, i.e. the calculated value is 15 m^2 for a 2 % longitudinal slope and 65 m^2 for a 10 % longitudinal slope, but a larger hole or a larger slope will produce a larger area. For the 2 % longitudinal slope, the estimated highest heat release rate is around 2 MW for ethanol and methanol, compared to 13 MW for

gasoline and 8 MW for diesel. For the 10 % longitudinal slope, the estimated highest heat release rate is around 10-11 MW for ethanol and methanol, compared to 58 MW for gasoline and 37 MW for diesel. Clearly, the fire sizes for alcohol fuels are much lower.

As the knowledge on spillage area for liquefied fuels is not clearly known, it is assumed here that all leaked fuels are burnt. The HRR is in a range of 43 to 49 MW.

If a tank has a hole of its whole cross section, the liquid will release instantaneously. Tests on a road tunnel [60] showed that the spillage area caused by an instantaneous release of 2 m^3 liquid varied between 138 m^2 and 163 m^2, with an average value of around 150 m^2. This corresponding to a heat release rate of 144 MW for gasoline, 91 MW for biodiesel, 24 MW for ethanol and 27 MW for methanol. The maximum heat release rate value is considered to be high, but it would be reasonably short-lived in terms of duration.

Therefore, it can be concluded that, from the perspective of fire size, the liquid fuels pose equivalent or even lower fire hazards compared to the traditional fuels (gasoline and diesel). However, the liquefied fuels may pose higher hazards compared to the traditional fuels.

Table 10 Heat release rates for different fuels spilled on the floor in a tunnel with 1 % transverse slope (A hole of 10 mm diameter at the bottom of the 0.2 m high fuel tank).

Fuel	HRRPUA (MW/m^2)	Spillage rate (l/s)	Spill area (m^2)		Peak HRR** (MW)	
			2 % slope*	10 % slope*	2 % slope*	10 % slope*
Ethanol	0.15	0.11	15	65	2	10
Methanol	0.17	0.11	15	65	2	11
Diesel	0.56	0.11	15	65	8	37
Gasoline	0.89	0.11	15	65	13	58
LPG	1.7	1.6			43	43
LNG	1.4	2.3			49	49
LH2	8.9	4.5			45	45

* longitudinal slope. ** Assuming all leaked fuels are burnt.

7.2 Jet fires

A fuel jet could be formed if there is a small hole or open nozzle on a tank containing compressed gas or liquefied fuels. A jet fire differs from a common fire as its initial momentum (due to high velocity) has significant influence on the flame characteristics.

7.2.1 Burning rate

The fuel mass flow rate for pressurized gases through a nozzle is:

$$\dot{m} = C_d \frac{\pi d^2}{4} \rho u \tag{37}$$

In practice, the fuel flows from the nozzles are mostly critical flow. The calculation of the jet velocity at the nozzle exit, *u*, can be found in Appendix C.

For superheated liquid, a large portion of the leaked flow may evaporate instantaneously and thus only the unevaporated fraction will temporarily form a pool on the ground. Details on flash fraction will be given in Chapter 8.

7.2.2 Flame length

Different models to estimate the jet flame length will be depicted in the following.

7.2.2.1 Heskestad's model [10]

Heskestad [10] correlated the flame length for buoyant diffusions flames with that for jet flames with small outlets. He used a momentum parameter, R_M, to distinct the buoyant flames from the momentum dominated flames. The momentum parameter is defined as the ratio of gas release momentum to the momentum generated by a purely buoyant diffusion flame:

$$R_M = 1.36 \frac{T_o}{T_L} \left(\frac{c_p \Delta T_L}{\Delta H_c / r}\right)^{4/5} \frac{\rho_o}{\rho_e r^2} N^{2/5} \tag{38}$$

where r is the mass stoichiometric ratio of air to volatiles, ρ_e is the fuel density at the nozzle exit. Subscripts M is momentum, L is flame tip, e is exit and o is ambient.

The excess temperature at the flame tip ΔT_L is set to 500 K by Heskestad [10]. The non-dimensional parameter, N, is defined as:

$$N = \frac{c_p T_o}{g \rho_o^2 (\Delta H_c / r)^3} \frac{Q^2}{D^5} \tag{39}$$

Heskestad [10] found that when the momentum parameter, R_M, is less than 0.1, the flame length is very close to that for buoyant diffusion flames, but slightly higher when the momentum parameter is close to 0.1. The proposed equation is:

$$L_F = 1.2 L_B \tag{40}$$

For momentum parameter greater than 0.1, the flame is found to be momentum dominated and the flame length can be expressed as follows:

$$L_M = 5.42 D \left(\frac{T_L}{T_o}\right)^{1/2} \left(\frac{\Delta H_c / r}{c_p \Delta T_L}\right)^{2/5} \left(\frac{\rho_e}{\rho_o}\right)^{1/2} r \tag{41}$$

For most hydrocarbon fuels with $\Delta H_c / r$ =3100 kJ/kg, it may be simplified into:

$$\frac{L_M}{D} = 18.5 \left(\frac{\rho_e}{\rho_o}\right)^{1/2} r \tag{42}$$

The above equation should not be used, however, for fuels with different values for $\Delta H_c / r$.

7.2.2.2 Delichatsios' model [11]

Delichatsios [11] defined a Froude number as:

$$Fr_f = \frac{u_e}{(\frac{\rho_e}{\rho_o})^{1/4}(\frac{\Delta T_f gD}{T_o})^{1/2}(1+r)^{3/2}} \tag{43}$$

where the modified mean flame temperature rise is:

$$\Delta T_f = \frac{\Delta H_c(\chi - \chi_R)}{(1+r)c_p}$$

where χ is combustion efficiency, and χ_R is the radiation loss fraction.

The following equation was proposed for the flame heights [11] :

$$L^* = \frac{L_f}{(1+r)D(\frac{\rho_e}{\rho_o})^{1/2}} = \begin{cases} \frac{13.5Fr_f^{2/5}}{(1+0.07Fr_f^2)^{1/5}} & Fr_f \le 5 \\ 23 & Fr_f > 5 \end{cases} \tag{44}$$

It was pointed out that the transition point could be a value of 3 to 5 for the Froude number. In applications, a value of 5 is generally used.

Similarly, two regions are identified: a buoyant flame region and a momentum dominated region. By comparing the equation for the momentum dominated region with Heskestad's equation, it can be found that the differences are limited.

7.2.2.3 Lowesmith et al's model [11]

Lowesmith et al. proposed the following correlation for jet flame length based on test data for various fuels including mixed fuels:

$$L(\mathrm{m}) = 2.8893\dot{Q}(\mathrm{MW})^{0.3728} \tag{45}$$

This model will be used in estimation of jet flame lengths for liquid fuel spray/aerosols for superheated liquid.

7.2.3 Analysis results

After a PRD opens, the fuel releases as a function of time. The CNG tank is 20 kg with initial tank pressure of 200 bar and diameter of the PRD varies between 2.5 mm and 10 mm. The transient pressure as a function of time is shown in Figure 18. The transient fuel mass in the tank is shown in Figure 19. The transient mass flow rate is shown in Figure 20. The jet flame length is shown in Figure 21. Clearly, the majority of the fuel is released within 1 min.

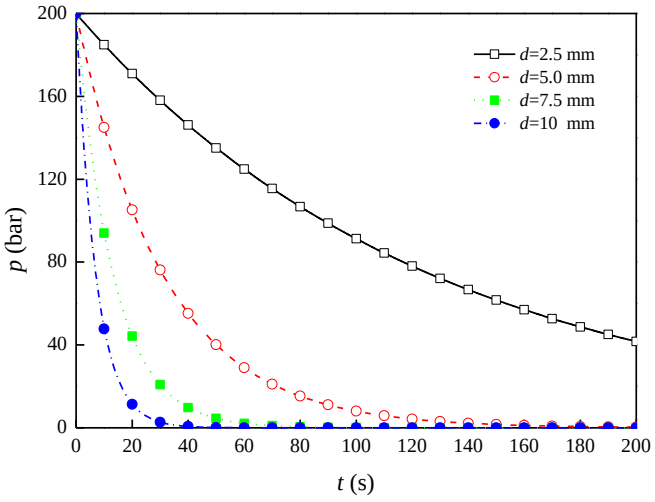

Figure 18 Tank pressure as a function of time after the nozzle opens in a 20 kg CNG tank.

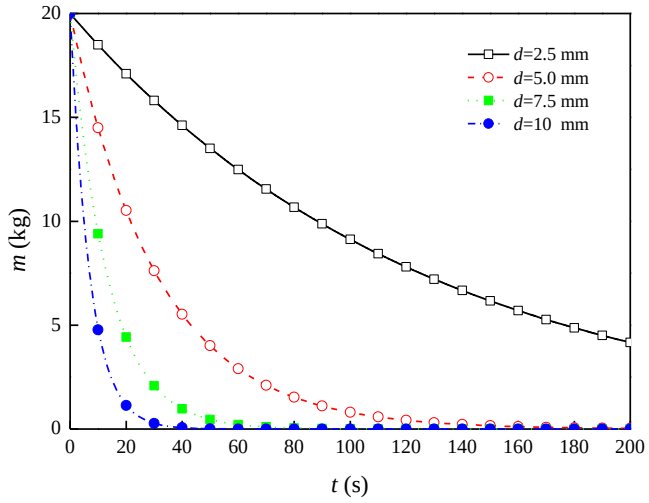

Figure 19 Tank fuel mass as a function of time after the nozzle opens in a 20 kg CNG tank.

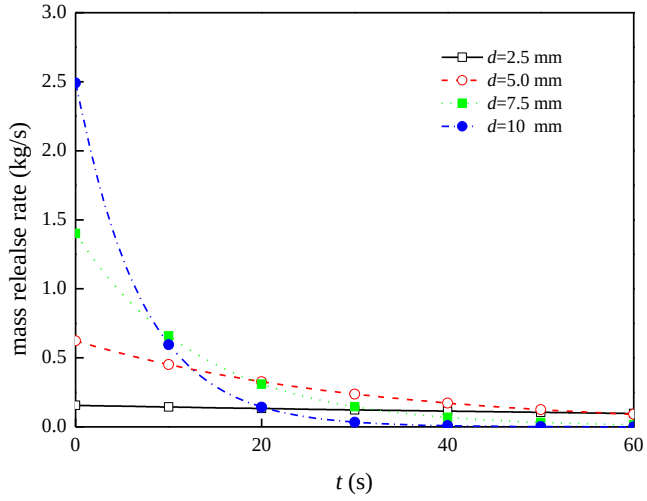

Figure 20 Fuel release rate as a function of time after the nozzle opens in a 20 kg CNG tank.

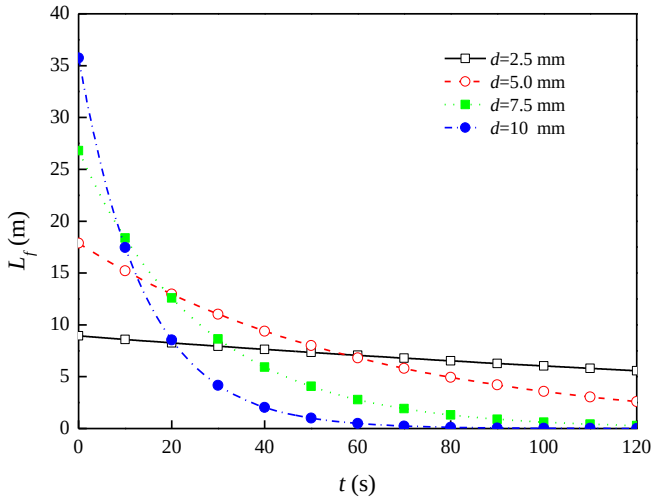

Figure 21 Jet flame length as a function of time after the nozzle opens in a 20 kg CNG tank.

The time required for pressure decreasing to 10 % initial pressure after the nozzle opens in a 20 kg 200 bar CNG tank can be found in Figure 22. It can be seen that the time required for the pressure drop decreases dramatically with the increasing nozzle diameter.

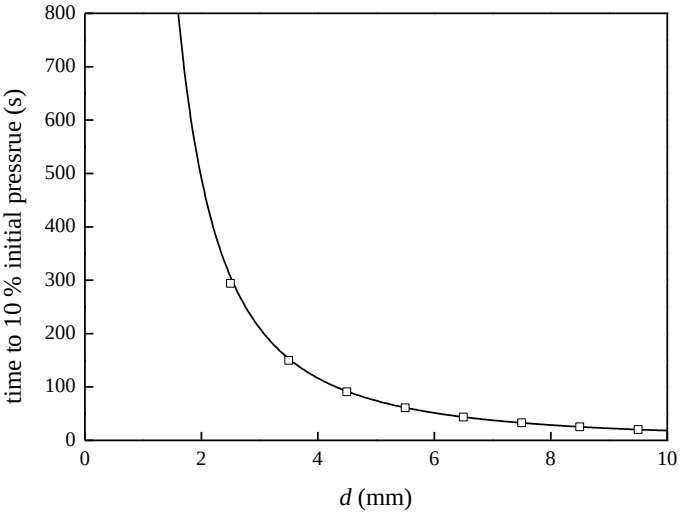

Figure 22 Time for pressure decreasing to 10 % after the nozzle opens in a 20 kg CNG tank.

As the release rate is highly transient, the initial release rate will be the focus in the following. Table 11 gives the initial release rate for varying compressed gas fuels. It is assumed that the PRDs activate due to a sudden temperature rise and the internal pressure is close to the tank operation pressure. It can be seen that for hydrogen vehicles, the heat release rates are significantly higher than those for the CNG tanks mainly due to the high value for heat of combustion. In contrast, the flame lengths for hydrogen fuels are only slighter greater than those for CNG tanks. The flame length increases with the increasing diameter of the PRDs. The flame length can be as long as 40 m. The heat flux can be up to 14 kW/m^2 for CNG and 45 kW/m^2 for GH2 at 10 m from the fire. This indicates that the possibility for fire spread is high.

In the following, results for a 8 kg hydrogen tank is presented for comparison, noting that it has approximately the same amount of combustion energy as for the 20 kg CNG tank. The initial tank pressure is 350 bar and the diameter of the PRD varies between 2.5 mm and 10 mm. The transient pressure as a function of time is shown in Figure 23. The transient fuel mass in the

tank is shown in Figure 24. The transient mass flow rate is shown in Figure 25. The jet flame length is shown in Figure 26. Clearly, the majority of the fuel is released within 1 min.

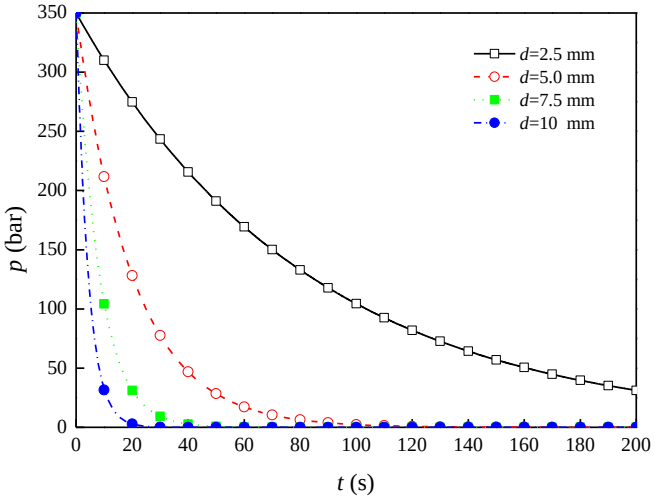

Figure 23 Tank pressure as a function of time after the nozzle opens in a 20 kg CNG tank.

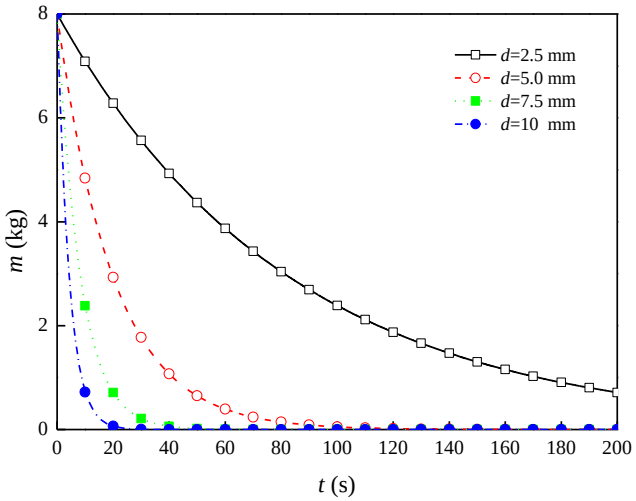

Figure 24 Tank fuel mass as a function of time after the nozzle opens in a 20 kg CNG tank.

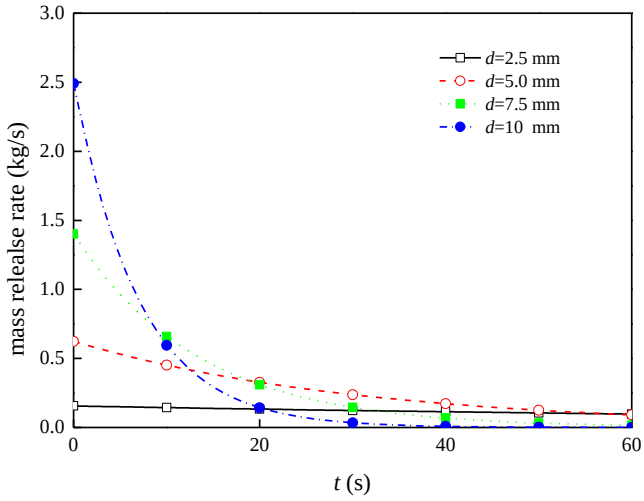

Figure 25 Fuel release rate as a function of time after the nozzle opens in a 20 kg CNG tank.

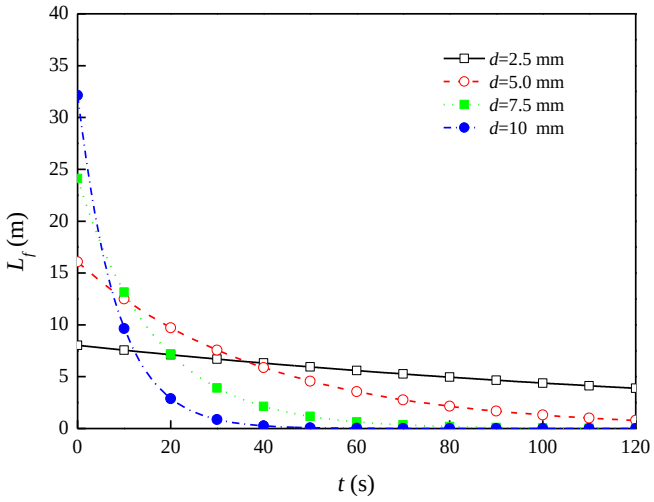

Figure 26 Jet flame length as a function of time after the nozzle opens in a 20 kg CNG tank.

Table 11 Jet fire characteristics for different compressed gas fuels under operation pressure.

Fuel	Diameter of PRD/hole	Release rate	HRR	Lf, Heskestad	Lf, Delichatsios	Lf, Lowesmith	Heat flux*
	mm	kg/s	MW	m	m	m	kW/m^2
CNG 200 bar	2.5	0.13	7	5.6	7.3	6.0	1
	5	0.62	34	13.6	17.9	10.8	4
	10	2.49	137	27.2	35.7	18.1	14
GH2 350 bar	2.5	0.10	14	7.0	8.0	7.6	1
	5	0.38	54	13.9	16.1	12.8	6
	10	1.53	217	27.8	32.1	21.5	22
GH2 700 bar	2.5	0.19	27	9.8	11.4	9.9	3
	5	0.76	108	19.7	22.7	16.6	11
	10	3.06	434	39.3	45.4	27.8	45

* received at 10 m away from the flame.

Table 12 gives the initial release rate for varying liquefied fuels assuming that the outlets are on the gas phase side of the tank. It is assumed that the PRDs activate after the tank pressure exceeds the preset value. It can be seen that all the results are significantly lower than those for the compressed gas tanks. This indicates the duration of the release will be much longer than compressed gas tanks. It may also suggest that the hazard for a BLEVE is higher than that for a gaseous tank rupture when being exposed to a fire. The heat release rate and the heat flux are much lower but the flame length can still be as long as 10 to 20 m.

If the outlets are on the liquid phase side of the tank, e.g. a car turnover, the behavior of a jet will be very different. Table 13 gives the initial release rate for varying liquefied fuels. It is also assumed that the PRDs activate after the tank pressure exceeds the preset value. It can be seen that the results are significantly higher than those with PRDs on the gas side. For heat release rates and heat flux, the ratio between them is around 3:1. Comparing the results with those for gaseous tanks shows that the heat release rates are generally lower, especially for LH2. However, the heat flux for LPG falls on the same level as the CNG tanks since the radiation fraction for LPG is higher.

Table 12 Jet fire characteristics for different liquefied fuels with PRDs on gas side.

Fuel	Diameter of PRD/hole	Release rate	HRR	Lf, Heskestad	Lf, Delichatsios	Lf, Lowesmith	Heat flux*
	mm	kg/s	MW	m	m	m	kW/m^2
LPG 32 bar	2.5	0.041	1.9	4.0	5.4	3.7	0.36
	5	0.165	7.6	7.9	10.8	6.2	1.45
	10	0.661	30	15.9	21.7	10.3	5.81
LNG 25 bar	2.5	0.019	1.0	2.4	3.1	2.9	0.11
	5	0.076	4.2	4.8	6.3	4.9	0.43
	10	0.305	16.8	9.5	12.5	8.3	1.74
LH2 10 bar	2.5	0.003	0.4	1.2	1.4	2.0	0.04
	5	0.011	1.5	2.4	2.7	3.4	0.16
	10	0.044	6.2	4.7	5.4	5.7	0.64

* received at 10 m away from the flame.

Table 13 Jet fire characteristics for different liquefied fuels with PRDs on liquid side.

Fuel	Diameter of PRD/hole	Release rate	HRR	Lf, Lowesmith	Heat flux*
	mm	kg/s	MW	m	kW/m^2
LPG 32 bar	2.5	0.10	4.5	5.1	0.9
	5	0.40	18.2	8.5	3.5
	10	1.58	72.8	14.3	13.9
LNG 25 bar	2.5	0.055	3.0	4.4	0.3
	5	0.22	12.1	7.3	1.3
	10	0.88	48.5	12.3	5.0
LH2 10 bar	2.5	0.009	1.3	3.2	0.1
	5	0.036	5.1	5.3	0.5
	10	0.14	20.2	8.9	2.1

* received at 10 m away from the flame.

Note that the initial parameters discussed above are not dependent of the size of the fuel tank. But the size of a tank indeed affects the duration of a release.

If there are external flames continuously heating up the fuel tank, the heat absorbed will raise the tank pressure or slow down the decrease in tank pressure, and the corresponding results will be somewhat different.

For a tank jet fire in a tunnel, the initial jet flame length will probably be longer than the tunnel height or width, and impingement to tunnel structure is possible. The distribution of flames around the tank is highly dependent on the positioning of the tank valve. For a valve with outlet facing upwards, the flames will probably behave in a similar way as in a normal vehicle fire, i.e. there exist upstream and downstream ceiling flames under low ventilation while only downstream ceiling flame under high ventilation. For a valve facing downwards, significant flames will exist on floor and fire spread may occur easily. For a valve facing sidewalls, the scenario is more complicated, depending on how far it is from the side wall.

7.3 Fireballs

7.3.1 In the open

There have been many empirical correlations proposed for the diameter of the fire ball and the duration of combustion in the open. An approximate correlation for the fire ball diameter could be expressed as follows:

$$D_{\max} = 5.8 m_f^{1/3} \tag{46}$$

Zalosh and Weyandt [21] carried out a bonfire test with a hydrogen fuel tank in the field. The fuel mass is 1.64 kg and the resulting fireball diameter is around 7 m. From the above equation, it is easily known that the calculated fireball diameter is 6.8 m, which comply very well with the experimental value of 7 m.

Approximate correlations for the duration of combustion have been proposed. For momentum dominated jets (normally for fuel mass less than 30000 kg), the duration is:

$$t_{\max} = 0.45 m_f^{1/3} \tag{47}$$

For buoyancy dominated jets (normally for fuel mass greater than 30000 kg), the duration is:

$$t_{\max} = 2.6 m_f^{1/6} \tag{48}$$

Even for momentum dominated jets, if the release is greater than 30000 kg, the duration should be estimated using the equation for the momentum dominated jets.

In most cases related to alternative fuel vehicles, the fireballs followed by a rupture could be considered to be buoyancy dominated. Therefore, the latter equation could mostly apply.

The average burning rate could be estimated by:

$$\dot{m}_f = \frac{m_f}{t_{\max}} \tag{49}$$

7.3.2 In tunnel

The model for the fireball diameter in the open can be interpreted as the volume produced in case of a stoichiometric combustion in the open. Assuming the same relation between the fuel mass and flame volume, the following correlation for the longitudinal fireball length, L_{max}, can be proposed:

$$L_{\max} = 102 \frac{m_f}{A} \tag{50}$$

where A is tunnel area (m^2).

A fireball in the open refers to a low flame speed and a negligible overpressure. In contrast, the scenario in a tunnel is different to a large extent due to the confinement of the tunnel structure. In a tunnel, the flame speed may continuously increase with distance from the ignition center,

which may cause significant overpressure, i.e. a deflagration. Therefore, there may not be any typical fireball in a tunnel, i.e. an initial fireball may result in a deflagration in the tunnel. The average burning rate may be significantly increased, in combination of reduction in flame length and duration. Therefore, the above equation may tend to be conservative.

7.3.3 Analysis results

A comparison of the fireball diameter in the open and the fireball length in a 50 m^2 tunnel is shown in Figure 27. Clearly, the fireball length in a tunnel is much longer than the fireball diameter when the fuel mass exceeds around 5 kg.

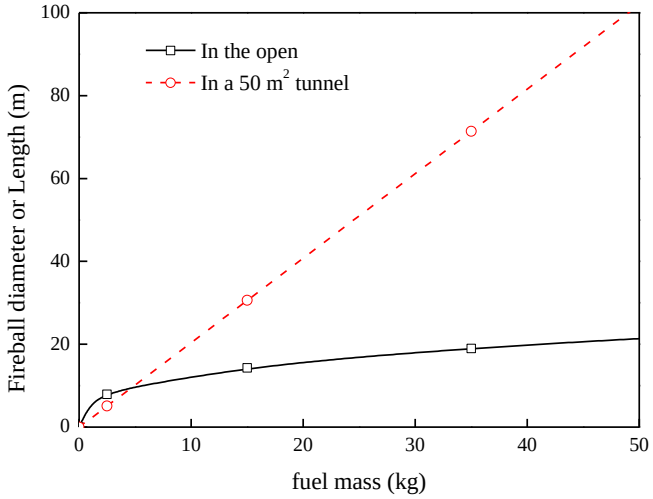

Figure 27 Comparison of fireball diameter in the open and fireball length in a 50 m^2 tunnel.

7.4 Comparison of vehicle fires

7.4.1 Traditional fuel vehicles

For comparison, the measured HRRs are summarized in the following for various traditional fuel vehicles.

For passenger cars, the measured or estimated HRRs from some fire tests are given in Figure 28. The medium and fast t-squared curves are also plotted. These tests include the Fiat 127 test by Ingason [65], the Renault test in Eureka programme by Steinert [66], the Citroen test by Steinert [67], the Trabant test by Steinert [67], the Citroen test by Shipp and Spearpoint [68], the test Car2 by Mangs and Keski-Rahkonen [69, 70], and the tests Car1 and Car 2 by Lecocq et al. [71]. It can be seen in Figure 28 that the maximum HRRs are below 6 MW for a single passenger car, and mostly below 5 MW. At the early stages, the fire development is slower than the medium curve. However, it should be kept in mind that the initial fire size can be larger if the ignition source is large, e.g. a spilled liquid pool fire.

For buses, the measured or estimated HRRs from some fire tests are also given in Figure 28. These tests include the EUREKA test 7 reported by Ingason et al. [72] and Steinert [66], SP Bus fire test by Axelsson et al. [73] and Shimizu bus tests by Kunikane et al. [74]. It can be seen in Figure 28 that the maximum HRRs are around 30 MW. At the early stages, the fire development is mostly not more rapid than the ultra fast curve. Alternatively, the typical HRR curve may be

considered as a fast curve before around 3 min and a linear curve to the maximum value of 30 MW with the slope of 5.7 MW/min. The closely linear slope could be attributed to the flame spread process along the carriage, similar to that in a train carriage fire [75, 76].

For trucks, the measured or estimated HRRs for heavy goods vehicles (HGV) are also given in Figure 28. These HGV tests include the EUREKA HGV fire test in 1992 [77], four HGV tests conducted in the Runehamar tunnel in 2003 by Ingason et al [78] and the LTA HGV test by Cheong et al [79, 80]. Most HGV tests that have been carried out in tunnels use a mock-up simulating the cargo of a HGV trailer. It can be seen in Figure 28 that the maximum HRRs are in a range of 60 to 200 MW. At the early stages, the fire developed even more rapidly than the ultra fast curve. The typical HRR curve may be considered as an ultra fast curve before around 3 min and then a linear curve to the maximum value with a certain slope (fire growth rate). Clearly, the fire size for a HGV is typically much greater than that for a car fire or a bus fire.

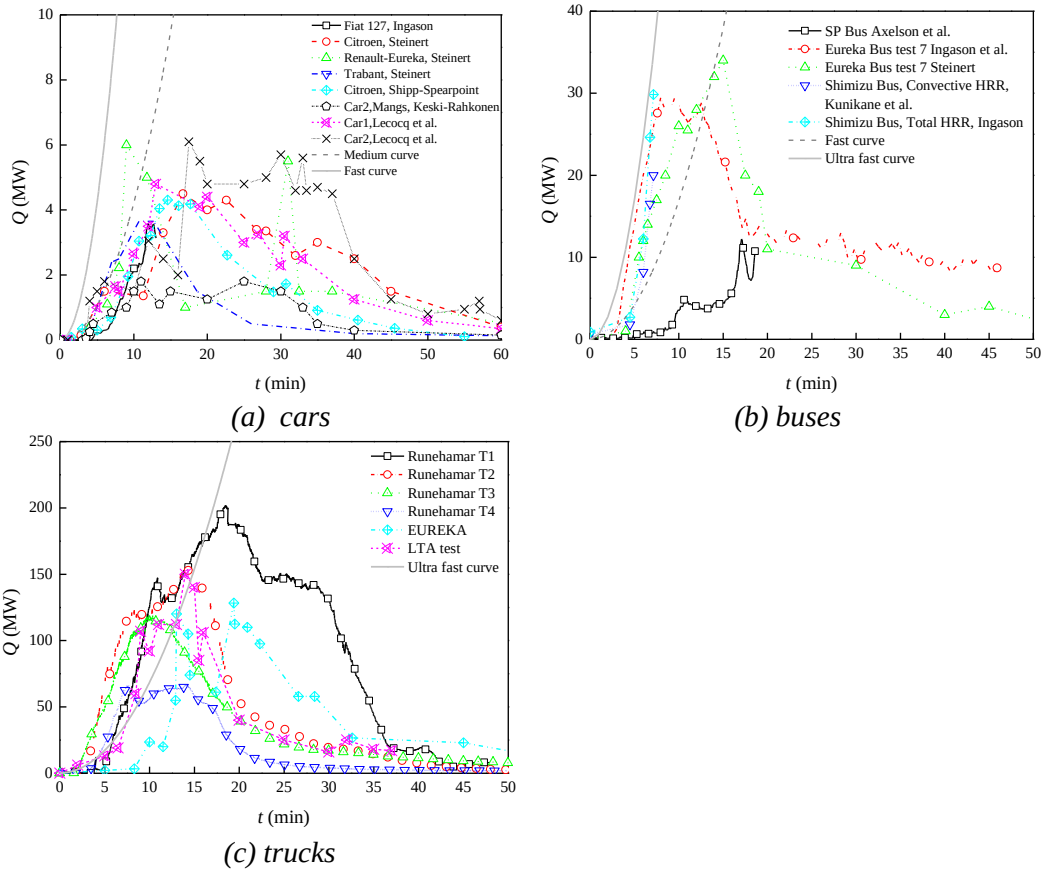

Figure 28 Summary of experimentally determined HRR for cars, buses and trucks.

7.4.2 Alternative fuel vehicles

In reality, fires in vehicles with the alternative fuels are not so different with those in traditional vehicles. The fire load mainly consists of internal combustibles, which is closely the same. The main difference may be in the fuel systems, power supply systems and engine compartments, dependent on what types of alternative vehicles are discussed.

Comparing alternative fuel vehicles with liquid fuels with traditional vehicles, the main difference is in the pool fire hazards. From the perspective of pool fire size, the liquid fuels may pose equivalent or even much lower fire hazards compared to the traditionally used fuels.

Comparing alternative fuel vehicles with liquefied fuels with traditional vehicles, the main differences are in the hazards of pool fires, jet fires, and fireball. The liquefied fuels may pose a higher pool fire hazard due to the large burning rate. In case of a PRD opened and a hole available, jet flames may form with a significant length. In such a case, location of the opening relative to the liquid surface plays a key role. The values for fire size and flame length are much larger if the opening is located on the liquid side. The potential fire size solely from the jet flame can be significantly higher than a traditional car or bus fire, despite the shorter duration. The fireball is also a common phenomenon for a fire initiated liquefied tank rupture.

Comparing alternative fuel vehicles with compressed gas with traditional vehicles, the main differences are in the hazards of jet fires and fireball. For compressed gas, the fire size generally is significantly larger than a traditional car or bus fire. The jet flame length can be much longer than for liquefied fuels. The fireball is also a common phenomenon for a fire initiated compressed gas tank rupture.

Comparing electric battery vehicles with traditional vehicles, the main difference is in explosion and toxic gas release. Data concerning HRR for electric vehicles are rather limited. Lecocq et al. [71] carried out four tests to compare the difference between internal combustion engine cars and electric battery cars. The HRR results are plotted in Figure 29. The fire was ignited inside the vehicle. It can be seen that the difference between traditional cars (car 1 and car 2) and the EV cars (EV Car 1 and Car2) is not significant. The maximum fire sizes for EVs are even lower. It can be noticed that after around 40 minutes, the fire sizes for EV vehicles are slightly higher than for traditional vehicles. The reason is that the battery modules started to involve in combustion at this moment. The productions of HF were also reported by the authors and they found significant amounts of HF production after the battery pack starts to burn. This should be attributed to the existence of LiPF6 in the electrolyte. However, it was reported that the measured HF concentrations after the batteries started to burn was much lower than those at early stage of the fire. The authors explained that that was probably due to burning of the liquids from air conditioning system. It should be noticed that in these tests, the fire was not initiated from the battery packs. If a vehicle fire occurs due to a battery thermal runaway, the fire development may be very rapid due to the rapid release of gas and the resulting jet flame, and thus the scenario would be very different.

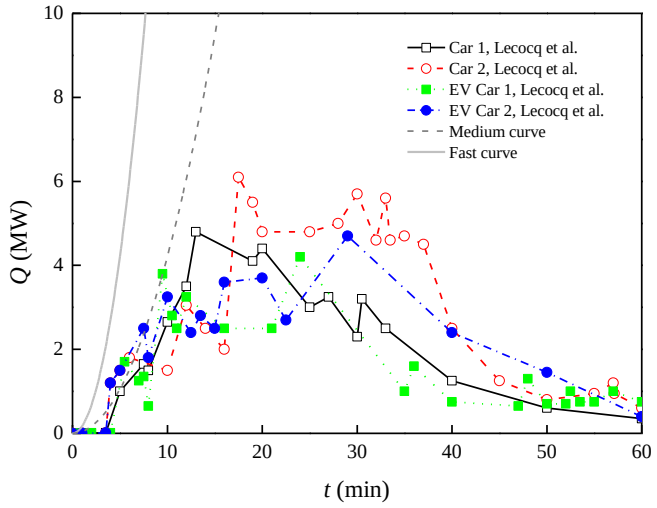

Figure 29 Summary of measured HRR for electric battery cars.

In summary, compared to traditional fuel vehicles, different alternative fuel vehicles pose some new fire hazards. From the perspective of pool fire size, the liquid fuels may pose equivalent or even much lower fire hazards compared to the traditionally used fuels, but the liquefied fuels

may pose higher hazards. The pool fire hazards are related to the spillage area, which highly depends on tunnel slopes and outflow holes. For pressurized tanks, i.e. liquefied fuel and compressed gas tanks, the fires are generally much larger in size than traditional car or bus fires, but shorter in duration. The gas release from PRD and the resulting jet fires are highly transient. For hydrogen vehicles, the fire sizes are significantly higher compared to CNG tanks, while flame lengths only slighter longer. A fire induced tank rupture mostly also produces a fireball with flame length increasing linearly with the fuel mass. For electric battery vehicles, a fire not initiated from the battery pack may be rather similar to a traditional vehicle. However, a fire initiated from a battery thermal runaway may be different. Overall, the differences in fire development between traditional fuel vehicles and different alternative fuel vehicles are generally not significant if the fire has not spread to the fuel tanks or battery packs. But if it is, additional fire hazards need to be carefully considered.

8 Quantitative analysis of explosion in the open

8.1 Gas cloud explosion in the open

8.1.1 TNT Equivalency method

There have been many models proposed in the past few decades for estimation of gas cloud explosion hazards in the open, such as the TNT equivalency model and the Multi-energy method. The TNT equivalency model is widely used for simple estimation of overpressure arising from a gas explosion. The pressure is simply correlated with the Hopkinson-scaled distance, Z (m/kg$^{1/3}$), :

$$Z = r / m_{TNT}^{1/3} \tag{51}$$

The equivalent TNT mass is estimated by

$$m_{TNT} = \eta \frac{m_f \Delta H_f}{\Delta H_{TNT}} \tag{52}$$

where the empirical yield factor η is estimated to be within 3 % to 5 %, but mostly 3 % is used. The value for ΔH_{TNT} is 4.68 MJ/kg.

For a gas cloud explosion close to the ground surface, the correlation between the side-on overpressure and the Hopkinson-scaled distance is shown in Figure 30.

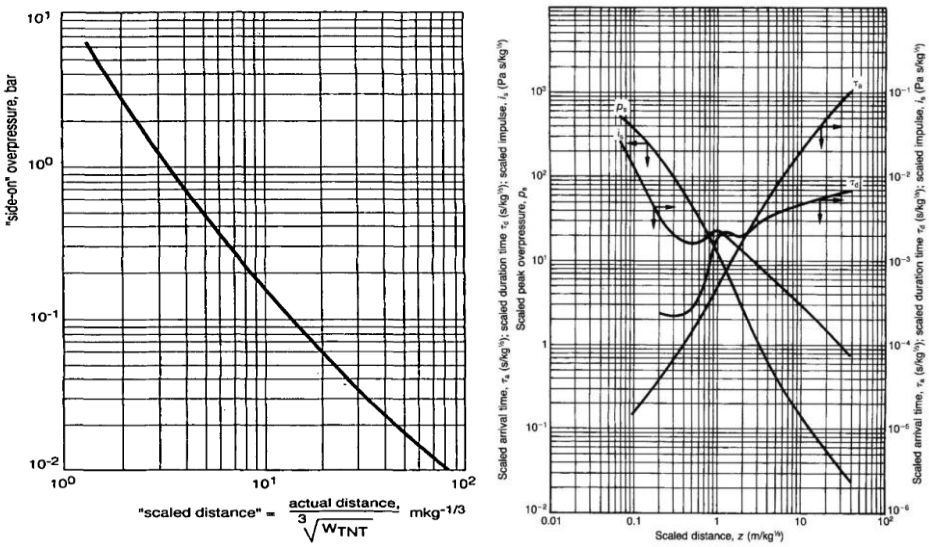

Figure 30 The pressure with Hopkinson-scaled distance for a TNT hemispherical surface burst [16]. The y axis on left figure is overpressure in Pa. But on the right figure the pressure means the ratio of overpressure to ambient pressure.

The TNT equivalency method can only be used for estimation of overpressure and impulse in the free field but the model is simple and logical.
To be on the safe side, three assumptions are made in the following analysis:

(1) stoichiometric mixture is assumed and thus all fuels contribute to the blast wave, in the following analysis.
(2) In case of an incident, all the fuel tanks of the incident vehicle are assumed to fail and contribute to the gas cloud explosion.
(3) The fuel tanks are full.

In the following, the TNT equivalency method is applied to estimate the explosion hazards of various alternative fuel vehicles.

8.1.2 Compressed gases in the open

The compressed gases may be released by pressure relief valves or by sudden rupture followed by a tank failure or vehicle incident. The release gases distribute around the tank or blown by wind. Figure 31 and Figure 32 give the peak overpressure of the blast wave as a function of distance from the fuel tanks of various quantities for CNG and GH2, respectively.

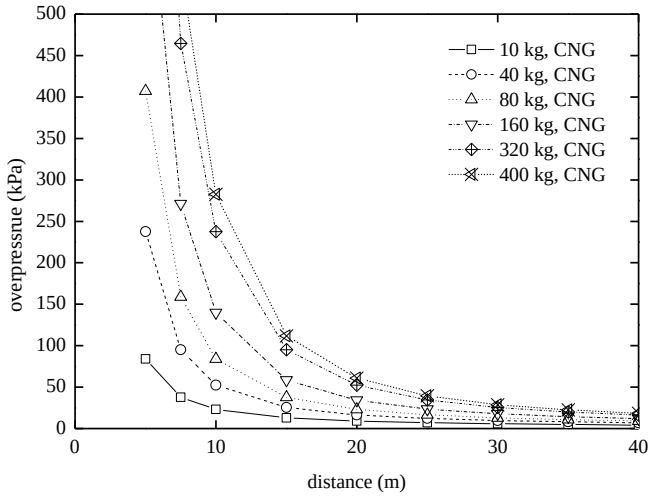

Figure 31 The overpressure vs. distance for CNG tanks of various quantities.

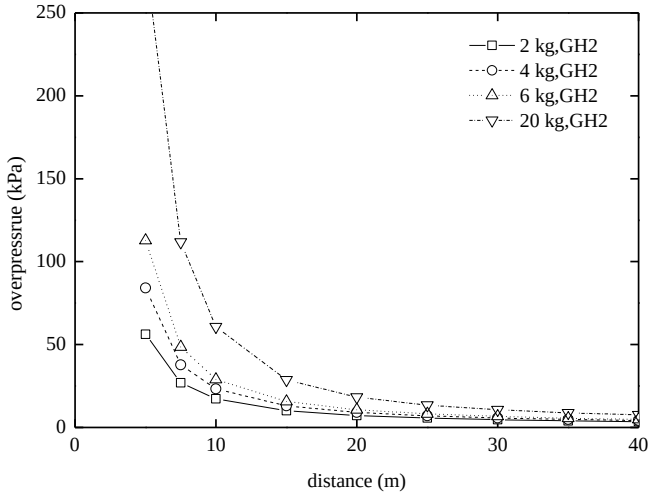

Figure 32 The overpressure vs. distance for GH2 tanks of various quantities.

8.1.3 Liquefied fuels in the open

For liquefied fuels such as LNG, the locations of nozzles or holes play an important role in the release. The main release will be in the form of gas for a hole in the gas side, while main release is in the form of liquid spray and aerosol for a hole in the liquid side.

The total fuels involved in a gas cloud explosion should include not only the flashed fuels, but also the sprays, aerosols, and the part of the fuels that evaporate by absorbing external heat before the explosion. In such case, the total amount of the fuel is generally considered to be twice the flashed fuels. The flashed fuels by instantaneous phase change can be estimated by use of the flash fraction. If the fuel temperatures in the tanks at the moment of rupture are assumed to be the superheat limit temperatures, the flash fraction is mostly in a range of 25 % and 50 %. By multiplying it with a factor of 2, the value is in a range of 50 % and 100 %. In reality, the initial temperature at the moment of rupture is not clearly known. For simplicity, in the following, it is assumed here that all the fuels are involved in the cloud explosion, which can be considered as the worst case.

Figure 33, Figure 34, Figure 35 and Figure 36 give the peak overpressure of the blast wave as a function of distance from the fuel tanks of various quantities for LNG, LH2, LPG and LDME, respectively.

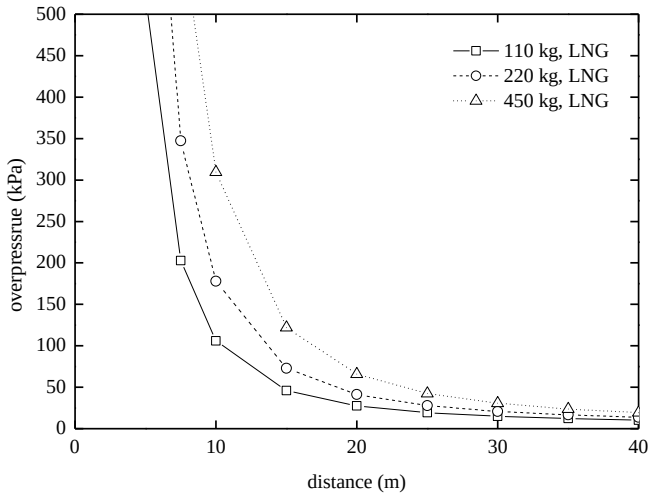

Figure 33 The overpressure vs. distance for LNG tanks of various quantities.

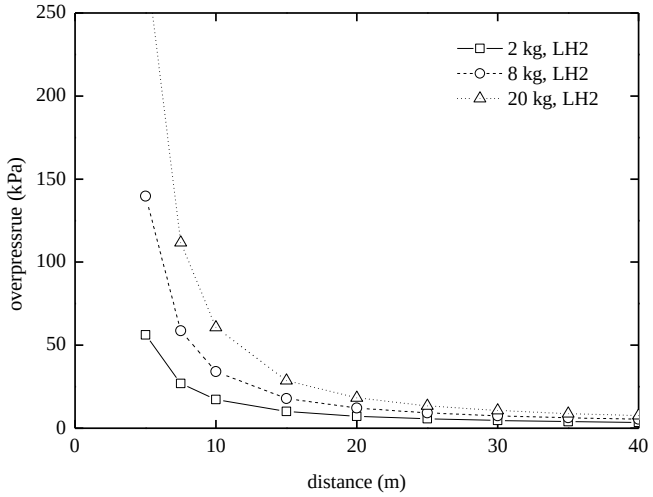

Figure 34 The overpressure vs. distance for LH2 tanks of various quantities.

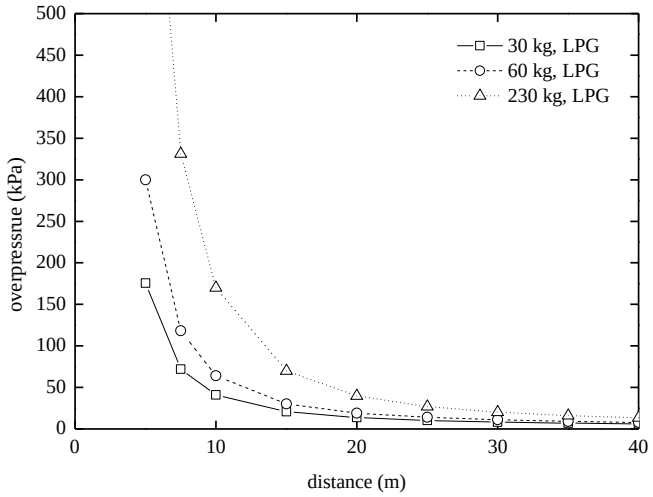

Figure 35 The overpressure vs. distance for LPG tanks of various quantities.

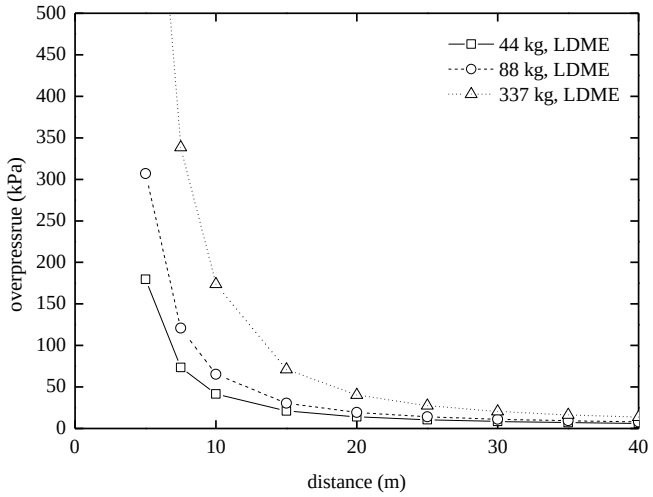

Figure 36 The overpressure vs. distance for LDME tanks of various quantities.

8.1.4 Battery in the open

Figure 37 give the peak overpressure of the blast wave as a function of distance from the fuel tanks of various quantities for battery vehicles.

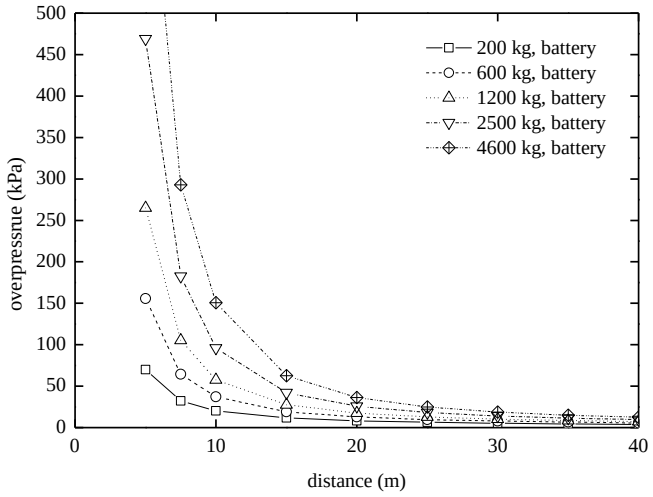

Figure 37 The overpressure vs. distance for batteries of various quantities.

8.1.5 Comparison for gas cloud explosion in the open

A summary of the peak overpressures and explosion energies for gas cloud explosion with various fuels in existing vehicles is summarized in Table 14. The explosion energy is in a range of 0.2 – 23 GJ. The peak overpressure is in a range of 0.17 – 3 bar at 10 m from the ignition center. The overpressures for GH2 and LH2 are relatively low as the fuel mass or the explosion energy is small in comparison to others. This does not mean that they are safer than the others. It only means that the hydrogen tank sizes presently used in vehicles are relatively small.

Table 14 Comparison of energy and overpressure for various vehicle types.

Vehicle type	Energy	Overpressure at 10 m
	GJ	kPa
CNG	0.5 - 20	23 - 280
GH2	0.2 - 0.7	17 - 30
LNG	5.5 - 23	100 - 300
LH2	0.2 - 1	17 - 35
LPG	1.4 - 11	40 - 170
LDME	1.4 - 11	40 - 170
Battery	0.4 - 9	20 - 150

8.2 Gas tank burst and BLEVE in the open

8.2.1 Calculation model

For gas tank rupture and BLEVE, the overpressure is generally calculated by use of the Sachs-scaled distance:

$$R = r p_o^{1/3} / (2E)^{1/3} \tag{53}$$

where E is expansion energy (J). The factor of 2 is to consider the ground reflection.

The non-dimensional maximum overpressure is defined as follows:

$$\bar{P} = \frac{\Delta P}{P_o} = \frac{P - P_o}{P_o} \tag{54}$$

The Sachs scaled impulse, i, is defined as:

$$i = I \cdot a_o / (E^{1/3} p_o^{2/3}) \tag{55}$$

where a_o is ambient air speed, i.e. 340 m/s, and I is impulse (Pa·s).

The non-dimensional maximum overpressure as a function of the Sachs scaled distance for tank rupture is shown in Figure 38. In the near filed, e.g. when the Sachs scale distance is lower than 1, the predicted pressure may be too low. In such cases, some other blast curves that were designed specifically for tank rupture can be used, e.g. the blast curves proposed by Tang, Cao and Baker [81].

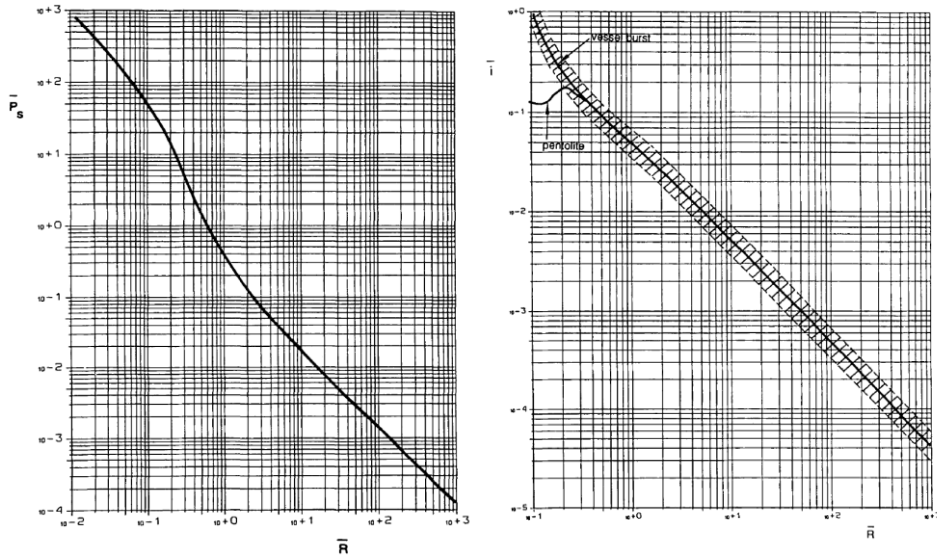

Figure 38 The pressure and impulse with Sachs scaled distance [16].

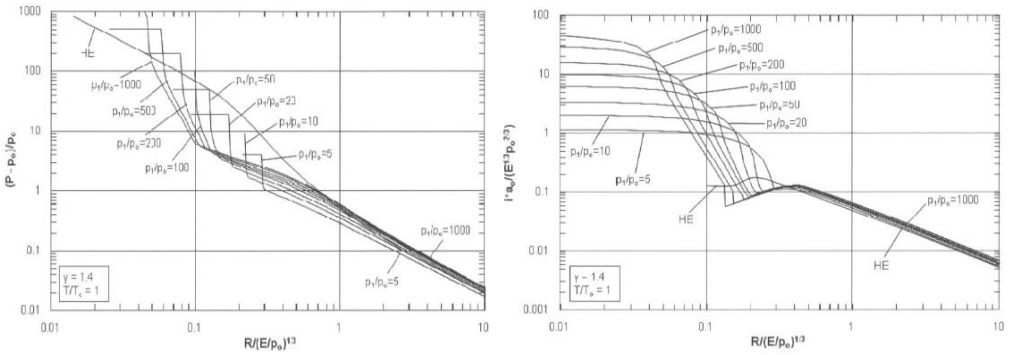

Figure 39 The pressure and impulse with Sachs scaled distance [81]. Note that E in the figure is the total energy in spherical coordinate, i.e. 2E in this work.

However, generally the TNT equivalence method is not recommended for tank rupture, as it may overestimate PVB overpressure close in, and underestimate it in the far field [16]. But due to its simplicity, it is a good method as reference especially in the near field of the tank.

During a gas tank burst, most energy of the compressed gas is lost to the environment by performing work on surrounding gases. This energy is similar to the heat released by combustion of a combustible gas cloud. The TNT equivalence method may still be used although some work shows that it overestimates the pressure in the near field while underestimate the pressure in the far field.

The energy of a compressed gas tank could be estimated by the method proposed by Brode [82]:

$$E = \frac{(p - p_o)V}{\gamma - 1} \tag{56}$$

Besides the Brode's equation, the isentropic method can also be used for calculation of the energy from a gas tank burst, which is expressed as follows:

$$E = \frac{pV}{\gamma - 1}[1 - (\frac{p_o}{p})^{(\gamma-1)/\gamma}] \tag{57}$$

The isentropic model appears to be more reasonable. However, the Brode's equation was used while plotting the blast curves, and thus also used in the analysis.

In estimation of energy released in a BLEVE, a different method to that for compressed gas tank burst is used. Different to a compressed gas tank burst, the liquid evaporation absorbs a large amount of heat during a BLEVE. The heat could come from the liquid itself or from tank boundaries. But for rapid expansion that may cause a blast wave, the heat from boundaries is rather limited. In other words, most of heat for the instantaneous phase change comes from the liquid itself.

Generally the state of liquid and vapor right before the rupture is assumed to be saturated (equilibrium). After depressurization, part of saturated liquid evaporates, and also part of gas may condense. For both liquid and vapor, the energy released can be calculated by the following equation:

$$e = e_{f,ini} - (1 - X)e_f - Xe_g \tag{58}$$

where X is mass percentage of fuels in the vapor form:

$$X = \frac{s_{f,ini} - s_l}{s_g - s_l} \tag{59}$$

where m is total mass and s is entropy. Subscript g is vapor, l is liquid, f is fuel (liquid or vapor), and *ini* is the initial value. Note that the mass percentage of fuels in the vapor form calculated based on the initial condition of the liquid fuel, X_f, in reality is the flash fraction of the liquid fuel, F.

The total expansion energy is the sum of liquid and vapor:

$$E = Y_f me_f + (1 - Y_f)me_g \tag{60}$$

The Brode's model or the isentropic model may also be used to estimate the explosion energy but the volume, *V*, needs to be replaced by a modified volume, V', according to the following correlation [83]:

$$V' = V + m_l\left(\frac{F}{\rho_g} - \frac{1}{\rho_l}\right) \tag{61}$$

A simple correlation may also be used to roughly estimate the flash fraction for liquefied fuels in case of a BLEVE [83]:

$$F = 1 - \mathrm{e}^{2.63 c_{p,liq}\left\{1-[(T_c - T_{ini})/(T_c - T_b)]^{0.38}\right\}(T_c - T_b)/L_v} \tag{62}$$

where T_b is the boiling temperature at ambient pressure, T_c is the critical temperature, and c_p is mean heat capacity of liquid fuel.

The TNT equivalency method could also be used for tank rupture. The equivalent mass can be calculated as follows:

$$m_{TNT} = \frac{E}{\Delta H_{TNT}} \tag{63}$$

Clearly, the initial liquid temperature is an important parameter. This simple correlation, however, may produce large error as the parameters such as specific heat may significantly vary with temperatures.

During a rupture of a high pressure gas tank, the instantaneous energy released normally causes a blast wave. Generally, it should be reasonable to assume that:

- only one tank ruptures in an incident,
- or even if more than one tank ruptures the blast waves can be separately considered from the perspectives of explosion safety.

Therefore, the scenarios considered here significantly differ from those for gas cloud explosion. Further, it is aslo assumed that the tank is full before rupture.

In the following, the calculation model based on the Sachs scaled distance is applied to estimate the tank rupture and BLEVE hazards for various alternative fuel vehicles.

8.2.2 Compressed gases in the open

The rupture pressure of a compared gas tank may vary from case to case. In the following analysis, the rupture pressure is assumed to be the normal operation pressure. The value is set to be 200 bar for CNG and 350 bar for GH2 tanks.

Figure 40 and Figure 41 give the peak overpressure of the blast wave as a function of distance from the fuel tanks of various quantities for CNG and GH2, respectively.

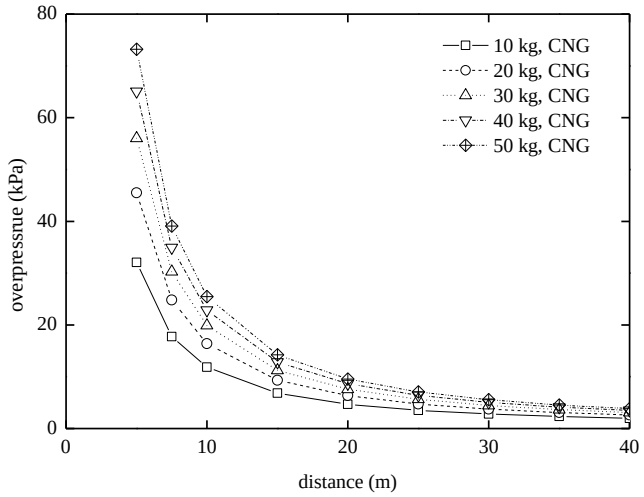

Figure 40 The overpressure vs. distance for CNG tanks of various quantities.

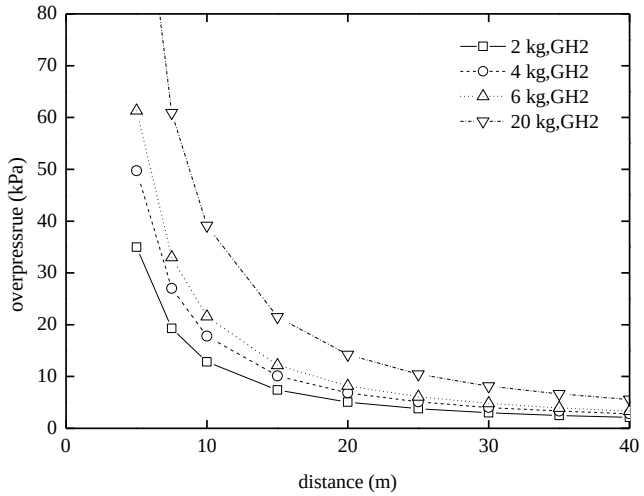

Figure 41 The overpressure vs. distance for GH2 tanks of various quantities (350 bar tank under normal condition).

8.2.3 Liquefied fuels in the open

The fuel tanks are assumed to be fully filled with liquid as the explosion energy is greater than that in a partly filled tank. The liquid in the tank is assumed to be at superheat temperature and thus an instantaneous evaporation occurs after a tank failure.

Figure 42, Figure 43, Figure 44 and Figure 45 give the peak overpressure of the blast wave as a function of distance from the fuel tanks of various quantities for LNG, LH2, LPG and LDME, respectively.

Due to lack of detailed state data for LDME, the data for LPG are used for reference. According to the simple model for flash fraction, the flash fractions for LPG nad LDME are approximately the same. It is also assumed that the energy released per kg of LDME equals that for LPG.

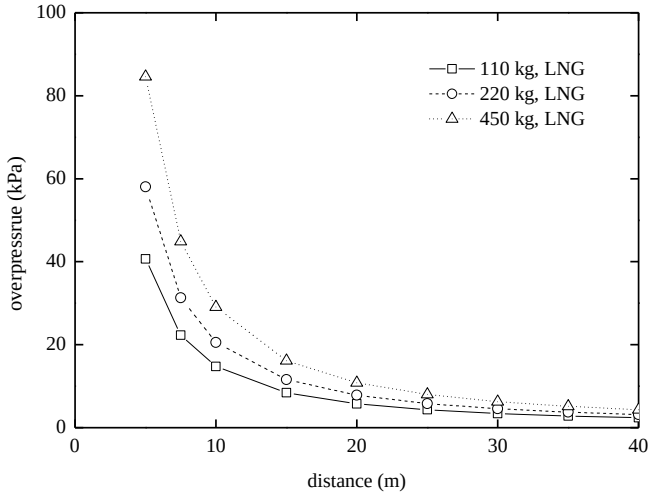

Figure 42 The overpressure vs. distance for LNG tanks of various quantities.

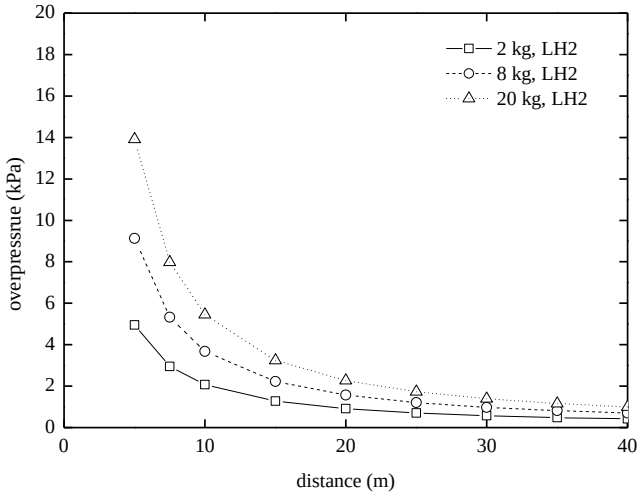

Figure 43 The overpressure vs. distance for LH2 tanks of various quantities.

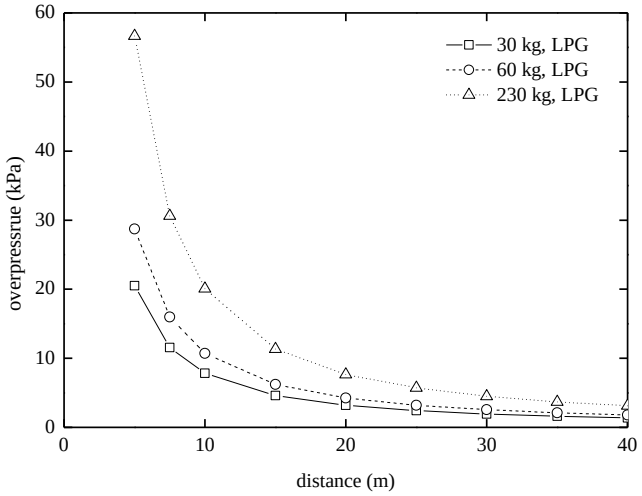

Figure 44 The overpressure vs. distance for LPG tanks of various quantities.

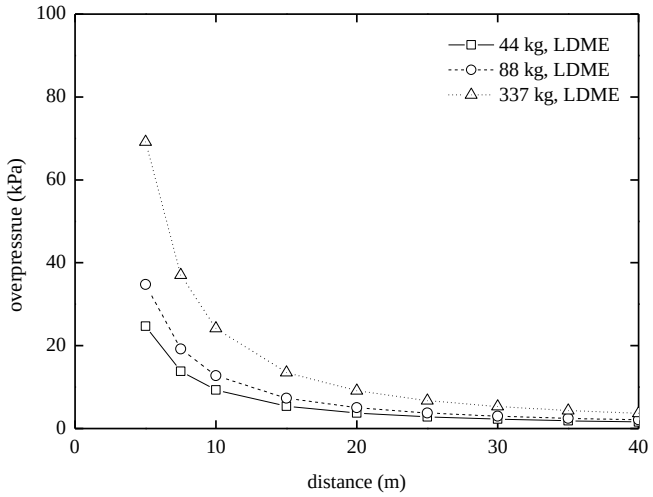

Figure 45 The overpressure vs. distance for LDME tanks of various quantities.

8.2.4 Comparison for gas tank burst and BLEVE in the open

A summary of the peak overpressures and explosion energies for tanks with various gaseous and liquefied fuels in existing vehicles is summarized in Table 15. The explosion energy is mostly in a range of 2 – 50 MJ. The peak overpressure is in a range of 0.02 –0.4 bar at 10 m from the ignition center.

Table 15 Comparison of energy and overpressure for various vehicle types.

Vehicle type	Energy	Overpressure at 10 m
	MJ	kPa
CNG	5 - 26	12 - 25
GH2	6 - 55	13 - 40
LNG	7 - 30	15 - 30
LH2	0.08 – 0.8	2 - 5
LPG	2 - 14	8 - 20
LDME	3 - 20	9 - 24

9 Quantitative analysis of explosion in tunnels

Two methods may be applied to quantitative analysis of explosion hazards in tunnels: the empirical model and the numerical model developed in Chapter 6. The empirical model called Energy concentration factor (ECF) method was developed by Silvestrini et al. [25] based on the classical explosion models. However, only some limited test data for explosion with solid explosives were used for validation of the model. There is a need to further check whether it provides reasonable results in the scenarios considered in this work, which will be presented in Section 9.1.

Note that the results presented except in Section 9.1 are calculated using the numerical model developed in Chapter 6. The reasons will be given later.

9.1 Possible use of empirical explosion models

9.1.1 Energy concentration factor (ECF)

Silvestrini et al. [25] proposed a simple concept of energy concentration factor (ECF) to allow the prediction of overpressure in confined space from the open space blast data. They modified the scaled distance by adding an effective factor:

$$R = r / (F_{EC} m_{TNT})^{1/3} \tag{64}$$

Or the Sachs-scaled distance:

$$R = r p_o^{1/3} / (2F_{EC} \cdot E)^{1/3} \tag{65}$$

where for normal tunnel, the energy concentration factor, E_{CF}, is defined as:

$$F_{EC} = \frac{V_{sphere}}{V_{tunnel}} = \frac{2/3\pi r^3}{2Ar} = \frac{\pi r^2}{3A} \tag{66}$$

And for one closed end tunnel, the factor ECF is defined as:

$$F_{EC} = \frac{V_{sphere}}{V_{tunnel}} = \frac{2/3\pi r^3}{Ar} = \frac{2\pi r^2}{3A} \tag{67}$$

In the near field, the model may predict a lower pressure than that in free field due to the assumption that the pressure is evenly distributed at any tunnel cross section. To avoid this, the modified energy concentration factor, $F_{EC,mod}$, is proposed here as follows:

$$F_{EC,\mathrm{mod}} = \max(F_{EC}, 1)$$

9.1.2 Comparison of the model with experimental and numerical results

The hydrogen explosion tests in a tunnel by Groethea et al. [18] and the TNO methane tunnel tests [46] are simulated and compared with the ECF model. Further, numerical results for a 20 kg CNG BLEVE in a 50 m2 tunnel simulated by the numerical model developed in this work are also used for comparison.

The comparison of ECF predictions with test data and numerical results in tunnels is shown in Table 16. Clearly, the estimated overpressures by the ECF model is normally much lower than the measured values but can be much higher close to the initial location. Compared to the numerical results for the CNG tank, the estimated overpressures by the ECF model is systematically lower.

Table 16 Comparison of ECF predictions with test data and numerical results in tunnels.

Test series	Tunnel diameter (m)	Location	Measured data or numerical results for overpressure (kPa)	ECF model predictions for overpressure (kPa)
Hydrogen tunnel	2.2	*x*=39 m	140	32
TNO Methane	0.6	*x*=0.5 m	270	1060
		x=4 m	300	215
		x=8 m	540	127
Numerical results for CNG tank	6.7	*x*=25 m	28	16
		x=50 m	20	11
		x=100 m	14	8

Therefore, the ECF model cannot be applied to predict the peak overpressures arising from tank rupture or cloud explosion in tunnels.

9.2 Gas tank burst and BLEVE in a tunnel

In the following, the numerical model is thus used for predictions of overpressures in tunnels. The tunnel geometry also affects the results. Generally a smaller cross section indicates a higher overpressure. In the following simulations, a tunnel cross section of 5 m (H) × 10 m (W) is assumed by default.

9.2.1 Compressed gases in a tunnel

The rupture pressure of a compared gas tank may vary from case to case. Tank rupture due to physical failure is one typical scenario, which is assumed by default.

Figure 46 and Figure 47 shows the peak overpressure as a function of distance from tanks of various quantities for CNG (200 bar) and GH2 (350 bar) vehicles in a tunnel, respectively. Clearly, the peak overpressure decreases rapidly within the first 50 m.

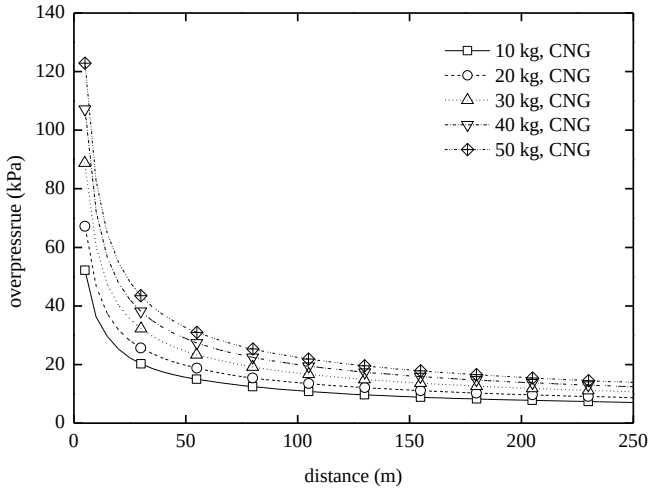

Figure 46 The overpressure vs. distance for rupture of CNG tanks of various quantities.

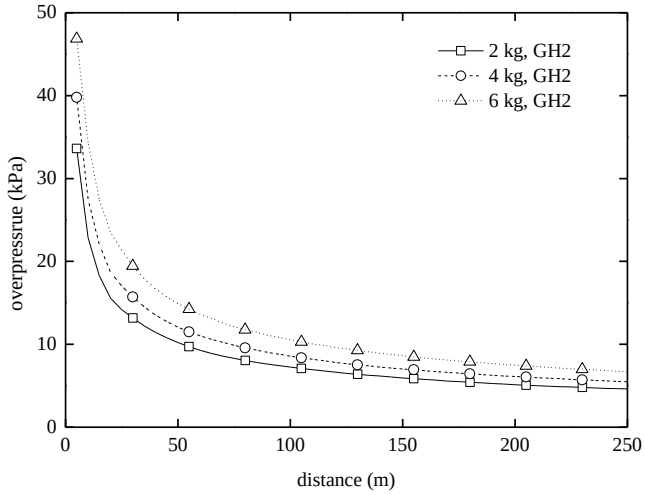

Figure 47 The overpressure vs. distance for GH2 tanks of various quantities (350 bar tank under normal condition).

9.2.2 Liquefied fuels in a tunnel

Note that the fuel tanks are assumed to be fully filled with liquid as the explosion energy is greater than that in a partly filled tank. The liquid in the tank is assumed to be at superheat temperature and thus an instantaneous evaporation occurs after a tank failure.

Figure 48 shows the peak overpressure as a function of distance for BLEVE of LNG tanks of various quantities in a tunnel. Similar trend can be found as in Figure 46. By comparing the two figures, it can be found that the overpressure for 110 kg LNG is similar to that for 50 kg CNG. This indicates that the explosion energy for LNG is much lower than that for CNG of the same amount of fuels. This is mainly related to the initial high tank pressure in the CNG tank.

Figure 49, Figure 50 and Figure 51 shows the peak overpressure as a function of distance for BLEVE of LNG tanks of various quantities for LH2, LPG and LDME vehicles in a tunnel, respectively.

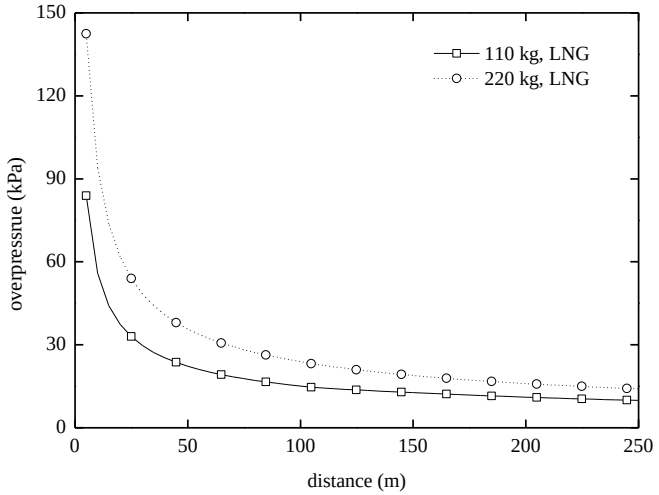

Figure 48 The overpressure vs. distance for BLEVE of LNG tanks of various quantities.

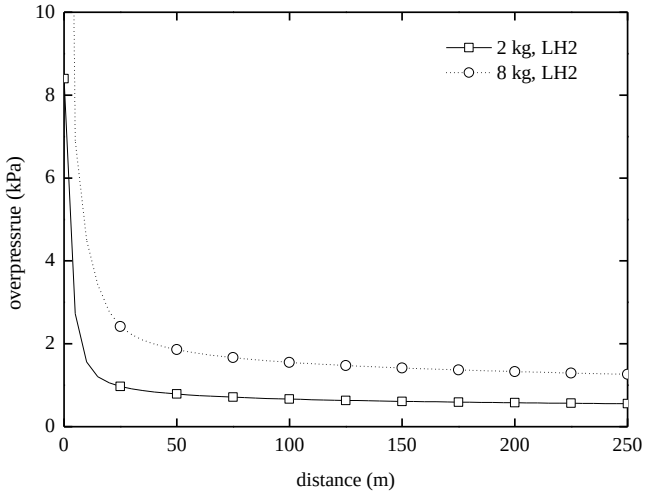

Figure 49 The overpressure vs. distance for LH2 tanks of various quantities.

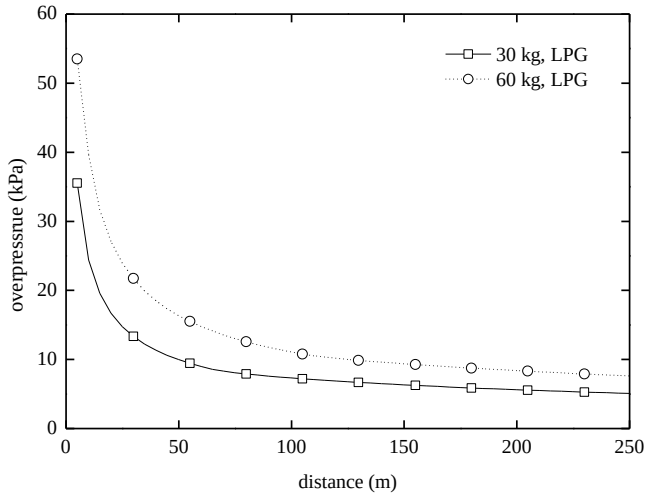

Figure 50 The overpressure vs. distance for LPG tanks of various quantities.

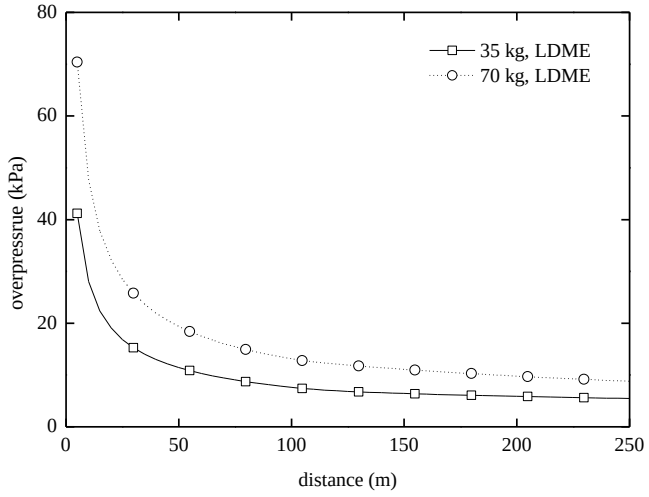

Figure 51 The overpressure vs. distance for LDME tanks of various quantities.

9.2.3 Comparison for gas tank burst and BLEVE

A summary of the peak overpressures and explosion energies for tanks with various gaseous and liquefied fuels in existing vehicles is summarized in Table 17. The explosion energy is mostly in a range of 2 – 30 MJ. The peak overpressure is mostly in a range of 0.1 –0.36 bar at 50 m, and 0.07-0.24 bar at 100 m from the tank. The overpressures for GH2 and LH2 are relatively lower as the fuel mass or the explosion energy is less in comparison to others. This does not mean that they are safer than the others. It only means that the hydrogen tank sizes presently used in vehicles are relatively small.

Table 17 Comparison of energy and overpressure for various vehicle types in tunnels.

Vehicle type	Energy	Overpressure at 50 m	Overpressure at 100 m
	MJ	kPa	kPa
CNG	5 - 26	15 - 29	10 - 20
GH2	5 - 18	10 - 15	7 - 11
LNG	7 - 30	22 - 36	15 - 24
LH2	0.08 – 0.8	1 - 2	0.7 - 1.5
LPG	2 - 14	10 - 16	7 - 11
LDME	3 - 20	11 - 19	7 - 13

9.3 Gas cloud explosion in a tunnel

To be on the safe side, three assumptions are made in the following analysis: (1) stoichiometric mixture is assumed and thus all fuels contribute to the blast wave, in the following analysis; (2) In case of an incident, all the fuel tanks of the incident vehicle are assumed to fail and contribute to the gas cloud explosion; (3) the fuel tanks are full. The ignition source is located at the center of the gas cloud.

9.3.1 Compressed gases in a tunnel

The compressed gases may be released by pressure relief valves or by sudden rupture followed by a tank failure or vehicle incident. The release gases may distribute around the tank or be blown by wind.

Figure 52 shows peak overpressure vs. distance for cloud explosion of CNG tanks of various quantities in a tunnel. The peak overpressure for CNG tanks with fuels over 320 kg is over 24 bar. In such cases, deflagration to detonation has occurred, and there exists a rather sharp decrease in peak overpressure at around 80 m from the ignition center, after which the decay is much slower. To express the results more clearly, results for 10 kg to 80 kg CNG are also plotted. For 10 kg CNG, the pressure decay over the distance is rather slow, in contrast to that for a tank rupture or BLEVE. For 10 kg CNG, the overpressure is mostly less than 20 kPa.

Note that the assumption that all tanks fail simultaneously before ignition may not be likely to occur. Instead, a single tank or small portions of the gas tanks contribute to the gas cloud explosion is more realistic. Therefore, the results can be interpreted in a different way.

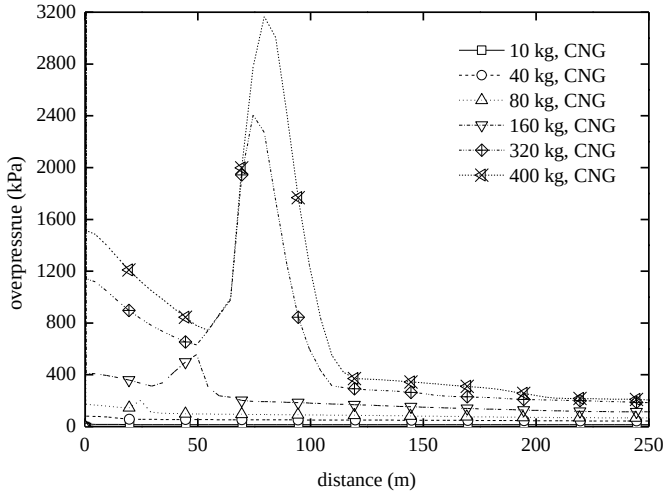

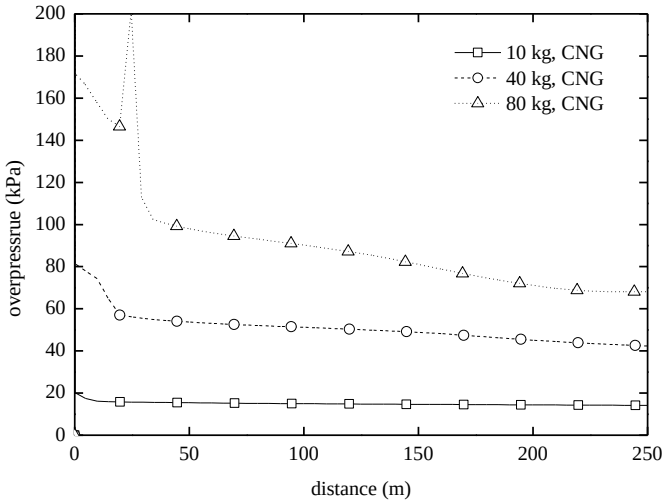

Figure 52 The overpressure vs. distance for cloud explosion of CNG tanks in tunnel.

Figure 53 give the peak overpressure of the blast wave as a function of distance from the fuel tanks of various quantities for GH2.

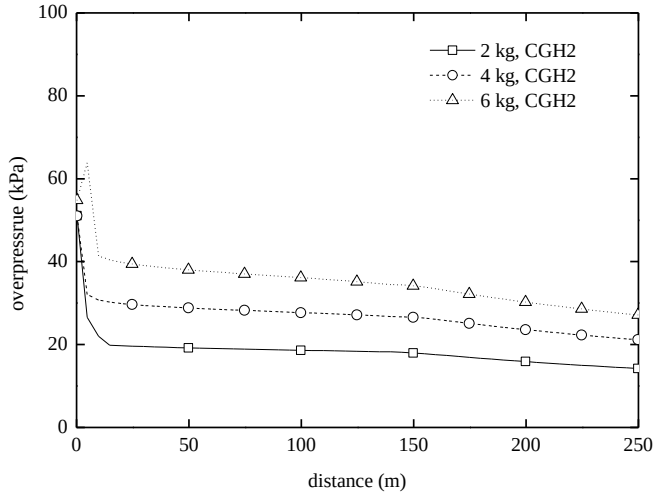

Figure 53 The overpressure vs. distance for GH2 tanks of various quantities.

9.3.2 Liquefied fuels in a tunnel

Figure 54, Figure 55, Figure 56 and Figure 57 shows the peak overpressure as a function of distance for gas cloud explosion of LNG, LH2, LPG and LDME tanks of various quantities in a tunnel, respectively.

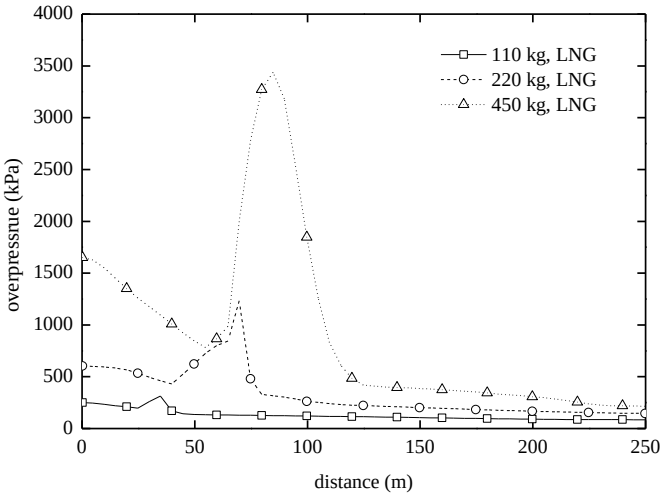

Figure 54 The overpressure vs. distance for LNG tanks of various quantities.

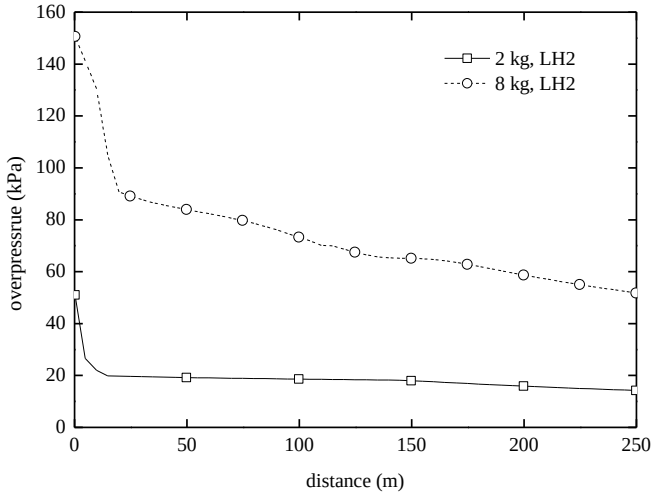

Figure 55 The overpressure vs. distance for LH2 tanks of various quantities.

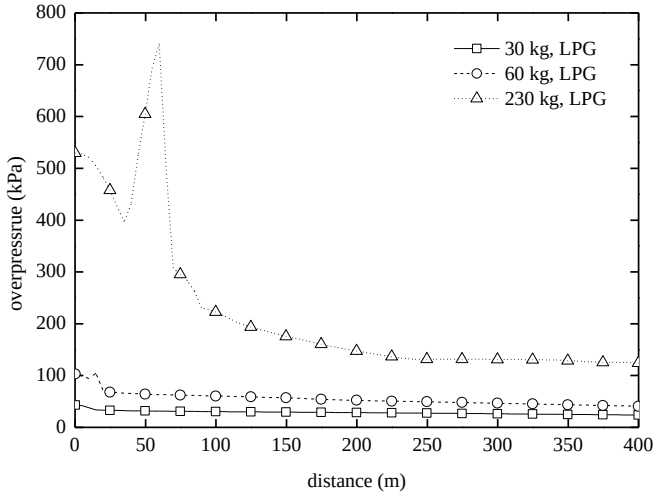

Figure 56 The overpressure vs. distance for LPG tanks of various quantities.

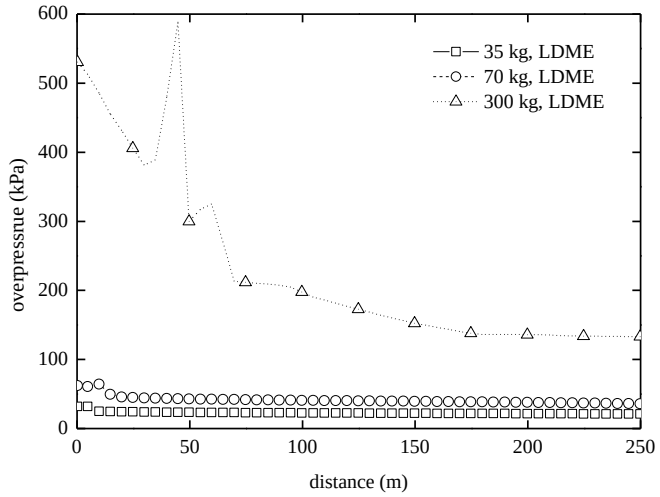

Figure 57 The overpressure vs. distance for LDME tanks of various quantities.

9.3.3 Battery in a tunnel

Figure 58 shows the peak overpressure as a function of distance for cloud explosion of batteries of various quantities in a tunnel.

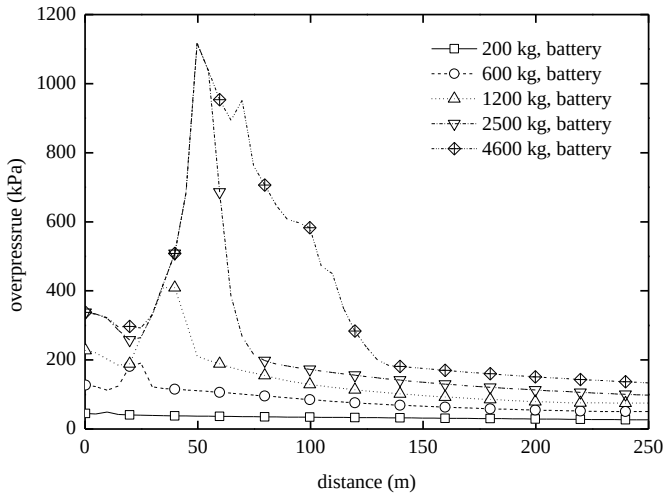

Figure 58 The overpressure vs. distance for batteries of various quantities.

9.3.4 Comparison for gas cloud explosion

A summary of the peak overpressures and explosion energies for gas cloud explosion with various fuels in existing vehicles is summarized in Table 18. The explosion energy is in a range of 0.2 – 23 GJ. The peak overpressure is in a range of 0.15 – 11.2 bar at 50 m, and 0.15-18.5 bar at 100 m from the ignition center. The consequences of such incidents are mostly not tolerable, compared to the criteria shown in Appendix C. The overpressures for GH2 and LH2 are relatively low as the fuel mass or the explosion energy is small in comparison to others. This

does not mean that they are safer than the others. It only means that the hydrogen tank sizes presently used in vehicles are relatively small.

Table 18 Comparison of energy and peak overpressure for gas cloud explosion with various fuel types.

Vehicle type	Energy	Overpressure at 50 m	Overpressure at 100 m
	GJ	kPa	kPa
CNG	0.5 - 20	15-780	15-830
GH2	0.2 - 0.7	19-38	18-36
LNG	5.5 - 23	136-850	120-1850
LH2	0.2 - 1	19-84	18-73
LPG	1.4 - 11	30-600	30-223
LDME	1.4 - 11	23-300	22-200
Battery	0.4 - 9	37-1120	34-582

9.4 Blast wave transportation along a tunnel

The pressure distribution along the distance from the tank in the open is very different to that in a tunnel. An example showing the difference in pressure distribution along the distance is given in Figure 59 where a 10 kg CNG tank experiences a rupture in a tunnel and in the open, respectively. Clearly, the overpressure decreases much more slowly in a tunnel. The only exception is that during the first several meters the overpressure in the tunnel is lower, but this should be attributed to the fact that within this range the one-dimensional assumption is not valid.

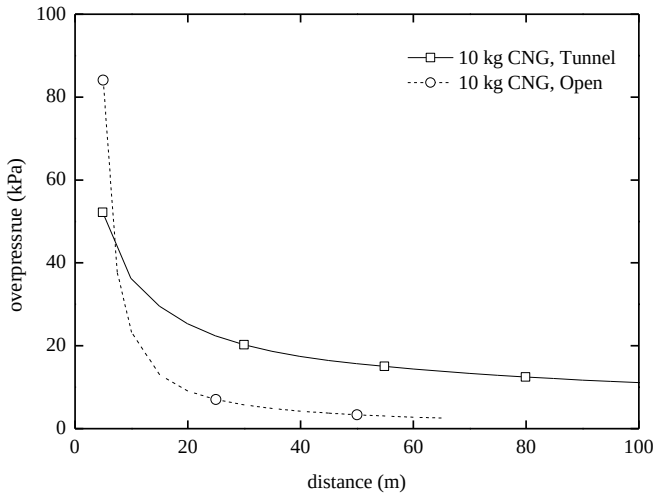

Figure 59 Example showing the difference in pressure distribution along the distance.

However, for a gas cloud explosion in a tunnel, the distribution of overpressure along the tunnel is very different. Generally, the decay of overpressure is much lower. The main reason for this is that the explosion energy in case of a gas cloud explosion releases within a certain period and thus the overpressure sustains for a longer period. In contrast, for a gas tank rupture or a BLEVE, the explosion energy is released instantaneously, and therefore the peak overpressure only exists for a very short period. Especially within the combustion region, the overpressure

normally maintains at a high level and even increases with distance from the ignition point. Only if a detonation immediately initiated by a large ignition source, it may be reasonable to assume an instantaneous release of the explosion energy and the scenarios may be similar. However, this is a rather rare case in a vehicle tunnel incident. Therefore, the decay of overpressure for gas cloud explosion in a tunnel is completely different from that for a tank rupture or BLEVE.

Note that in this chapter, the tunnel cross sectional area is assumed to be 50 m^2. If the tunnel area is smaller, the overpressure will be slightly higher and vice versa.

10 Practical considerations

10.1 Use of various alternative fuels

Liquid fuels such as methanol and ethanol are similar to gasoline and diesel, but their flames are generally hard to observe and thus can pose thermal hazards for users and fire fighters.

Liquid fuels such as gasoline or methanol also pose a risk of BLEVE. The main difference between such liquid fuels and liquefied fuels such as LPG and LNG is that before the rupture of the tank, significant amount of heat needs to be provided to heat up the liquid fuels before a possible BLEVE for liquid fuels tanks, while it is unnecessary for liquefied fuel tanks. As a consequence, before a BLEVE for a liquid fuel tank, there should be plenty of time to evacuate from the site. In contrast, in case of a BLEVE for a liquefied fuel tank, there may be no response time. Further, quality of fuel tanks also play an important role as it determines under which pressure the tank may probably fail. As the amount of fuels in a tank is approximately the same for most hydrocarbon fuels due to similar values for heat of combustion, the main difference in explosion energy depends on the tank rupture pressure. Regular tanks for gasoline and diesel are normally not designed to resist high pressures, and therefore fail at much lower pressures compared to LNG and LPG. For composite tanks, the risk of existence of high tank pressure appears to be low due to its characteristic of infiltration while being exposed to a fire. But for steel tanks, a certain pressure can be maintained before it ruptures although it is mostly much lower than liquefied fuel tanks. Therefore, the explosion energy for regular fuel tanks is generally much lower, and so is the strength of the blast wave. It is worthwhile to mention that pressure relief devices should be installed to ease the problem while using steel tanks.

By comparing the numbers of fuel tanks for compressed gas vehicles and liquefied fuel vehicles, it is known that the number of liquefied fuel tanks is mostly 1 or 2 but can be up to 10 for compressed gas tanks in a vehicle. This may be attributed to the fact that liquefied fuel tanks such as LNG tanks are under cryogenic conditions, which requires significant space for the thermal insulation. In comparison, the number of compressed fuel tanks in a vehicle appears to be more flexible. Note that in case of an incident the probability that all compressed gas tanks fail simultaneously is extremely low, and instead the highest probability is failure of one tank in the incident or failure of several tanks at various times. Therefore, the fire and explosion hazards can reduce significantly by increasing the number of fuels for a given total amount of fuel. The disadvantage of compressed gas tanks is that the tank pressure is significantly higher than that for a liquefied fuel tank. Therefore, a gas tank rupture occurs immediately after a failure of a tank, while a BLEVE for a liquefied fuel tank generally needs some time for heating the liquid to its superheat temperature. Further, the explosion energy per unit mass in case of a tank rupture is also significantly higher than that for a BLEVE. Concerning explosion hazards, due to the low probability of simultaneous failure of all compressed gas tanks, the explosion energy may also be low. To reduce the hazards, using a large number of small fuel tanks instead of one or several fuel tanks is preferred for a given total amount of fuel for a vehicle, although the risk of fuel leakage may rise accordingly.

The explosion energies for electric vehicles and internal combustion engine vehicles are roughly estimated and presented in Table 19. The energy efficiency of electric vehicles is about 59 % - 62 % of the electrical energy from the grid to power at the wheels, and conventional gasoline vehicles convert about 17 % - 21 % of the energy stored in the fuels [84]. The energy efficiencies of CNG and H2 are assumed to be the same as gasoline. The energy stored in battery, energy at wheel and explosion energy are calculated in sequence, and then the values for internal combustion engines are estimated based on the same energy at wheel. The equivalent masses of CNG and H2 are also given, for comparison with the mass of battery. Clearly, the potential explosion energy of a battery is several times the energy stored in the

battery, and it is even slightly higher than the explosion energy for an internal combustion engine that produces the same energy at the wheel. The masses of batteries are also much higher than gasoline or hydrogen due to the low energy density.

Therefore, from the perspective of possible gas cloud explosion energy, the electric vehicles are at a slightly higher or equivalent level compared to internal combustion engine vehicles. However, it should be noted that the gas tanks in a gas vehicle, such as CNG and GH2, may have low risk of leaking gases from all tanks simultaneously and accumulating in a tunnel before any possible ignition. It should also be noted that venting of battery cells in a module takes some time even after a thermal runaway, and the fire spread between modules may not occur or take a longer period. The majority of the venting gases from one module may be ignited or diluted before the other module starts to vent. Therefore, the explosion hazards may be much lower than considered in this work. Despite this, the toxic gas release may cause major problems for tunnel users. The use of LiPF6 as solvent in batteries needs to be reconsidered.

For internal combustion engine vehicles with various fuels, the possible gas cloud explosion energy is approximately the same. Therefore, from the perspective of gas cloud explosion, there is no significant difference between these vehicles of various fuels. However, the consequences can be different for fuels with high reactivity such as hydrogen which corresponds to shorter DDT distances.

Table 19 Comparison of gas cloud explosion energy between electric vehicles and vehicles of internal combustion engines.

Type	Mass of battery	Energy at wheel (MJ)	Energy contained in fuels (MJ) [a]		Explosion energy (MJ) [b]		Equivalent mass (kg) [c]	
			Battery	Internal combustion engine	Battery	Internal combustion engine	CNG	H2
Car	200	54	90	270	384	270	8	3
	600	162	270	810	1152	810	23	9
Bus	1200	324	540	1620	2304	1620	46	18
	2500	675	1125	3375	4800	3375	96	38
Truck	600	162	270	810	1152	810	23	9
	4600	1242	2070	6210	8832	6210	177	71

[a] The input energy that is required to produce the amount of energy at wheel. It is estimated by use of energy efficiencies of battery and internal combustion engine. [b] It refers to the energy that can contribute to a possible explosion. [c] The mass of the fuel that produce the same energy at wheel, assuming the same energy efficiency as gasoline.

There is no recommendation here on use of which is the best. As far, it is known that all types of vehicles have similar amounts of gas cloud explosion energy, but concerning fire and other explosion hazards, their hazards are of different severities. On open roads, the vehicles with pressurized tanks pose high hazard of primary fragment projection. In comparison, in tunnels, this hazard related to primary fragments is not so severe but the secondary fragments such as vehicle glasses and tunnel equipment are more severe. The electric battery vehicles cause no primary fragments, however, they may produce significant amounts of toxic gases during a fire or a thermal runaway.

10.2 Vehicle and fuel storage design

Concerning compressed gas and liquefied fuel vehicles, fuel tank arrangement and the positioning of PRDs are also important. As mentioned previously, less amount of fuel in one single tank corresponds to lower hazard while a larger number of tanks indicates a higher risk of leakage. An optimum fuel tank size may exist by balancing the both effects. The outlet direction

of a PRD may be upwards, downwards or sideward etc. As the jet flame is generally very long, impingement onto floor, ceiling or wall will mostly occur. The deflected flame will be extended along floor, ceiling and walls. Fire spread by directly flame touching or radiation needs to be carefully investigated in key scenarios. On open roads, the side flame may impinge on nearby vehicles, trees and buildings, causing fire spread to others. In tunnels, the impingement of flame on ceiling may be a good option as vehicles and tunnel users are at the floor level. Further researches are in urgent need.

The probability of the primary fragments directly thrown towards a vehicle far behind without hitting the tunnel structure is rather low. Instead, the secondary fragments, e.g. pieces of windows broken by a blast wave can be a problem. To reduce the possible damage caused by primary fragments in case of an explosion, the tanks are not recommended to be placed on top the vehicle. However, if they are placed on top, some physical barriers are recommended to be placed around the tanks to avoid the tank fragments directly being thrown towards the surroundings. These physical barriers should resist its integrity with the vehicle after such an explosion. Concerning the possible damage caused by secondary fragments in case of an explosion, the quality of the glass windows used in vehicles may need to be improved to avoid breakage. For example, normally a smaller and thicker glass can sustain a much higher blast load.

For electric battery vehicles, fire barriers between modules are recommended to prevent fire spread from one to another module. Inside the battery cell, Golubkov et al. [36] proposed to (1) increase the temperature endurance and heat absorption capability of used materials; (2) minimize heat propagation to neighbouring burnable elements; (3) minimize gas ignition probability (e.g. mechanical separation of electric components from the gas release position). Further, as mentioned previously, the use of LiPF6 as solvent in batteries needs to be reconsidered.

10.3 Tunnel design and operation

The design of easing the explosion hazards in tunnels can be learnt from the railway design to ease the pressure wave problem arising from high speed train running in the tunnel. Explosion hazards in a tunnel can be eased by use of venting shafts. Venting of explosion gases is a standard method to deal with the overpressure in confined space. One example is the service tunnel of the Channel tunnel, which was designed mainly due to the very small tunnel cross-section. Note that recently much attention has been paid to the natural ventilation systems with short shafts, see for example Figure 60 where the shafts are connected the top of the two tunnels. This system has been used for both road and subway tunnels. Note that the shaft outlets can be placed in the middle of a road. In case of an explosion, the strength of a blast wave can be reduced significantly. The hazard to external personnel and structure may need to be estimated but it should be lower than as would occur on the road. During the transportation stage, use of some obstacles may also help, but they can cause adverse effect nearby the cloud region where cloud explosion occurs by increasing the turbulence and thus reducing the DDT distance. After an explosion, the doors between tunnels and/or the doors between tunnel and the path for evacuation or fire service may fail after an explosion incident. Therefore, the design of the doors connecting tunnels to other accesses needs to consider the influence of such explosions.

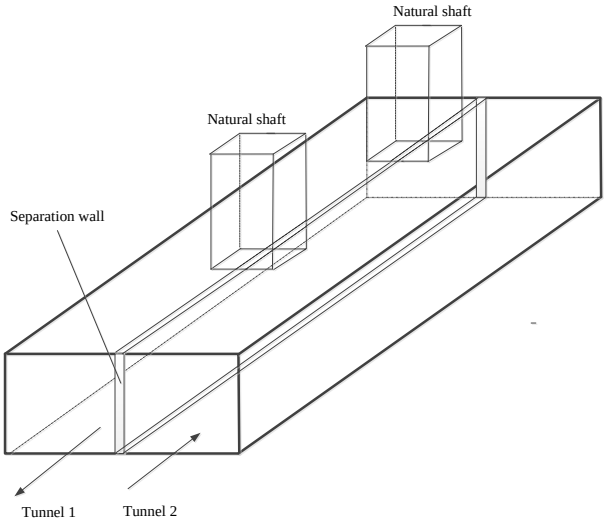

Figure 60 Natural ventilation system with short shafts

The pool fire hazards can be reduced by appropriate design of the tunnel slopes and the tunnel drainage system. For compressed gas tanks and liquefied tanks, the jet fire hazards in tunnels can be reduced by appropriate design of fuel tank arrangement, the number and size of PRDs and the positioning of PRDs. More detailed researches on these fire behaviors are required.

In case of a battery fire, toxic gases will be released, and thus tunnel ventilation is important to either blow away or exhaust the toxic gases. When a battery starts venting or a gas tank starts releasing gases, strong tunnel ventilation may also be recommended to dilute the fuel concentration.

It may be recommended that vehicles over a certain amount of fuels should be prohibited to enter some important tunnels.

10.4 Vehicle users

In the following, an example to handle alternative fuel vehicle incidents is given. According to the information sheet in the driver's manual from Scania, the following safety procedure should be followed after an incident:

- In the event of fire: switch off the engine and immediately notify the fire brigade that the vehicle contains vehicle gas and what type of gas it is.

- Damaged gas bottle: Stop the vehicle as soon as possible and apply the parking brake. Switch off the engine and evacuate the vehicle. Call the local emergency number.

- Gas odour: Immediately switch off engine. Close the manual tap. Tow the vehicle to workshop to have the leak rectified. Park the vehicle outdoors as long as there is leakage.

The contents presented above are relatively limited and more information is needed.

It is clear that when a tank rupture or BLEVE occurs due to a physical failure, there is no response time. The consequence would depend on how many vehicles are beside the incident

vehicle. Such a tank failure is a case that may occur with a high probability. Therefore, as mentioned previously, the amount of fuel of one single tank has to be limited.

In case that an incident starts with a fire but it has potential explosion hazards, the driver should try to extinguish the fire. If the extinguishment is not successful, after switching off the engine, the driver should run away from the vehicle and warn the others behind with the triangle sign, which should be placed at a certain distance (e.g. 50 - 100 m) behind the incident vehicle in a unidirectional tunnel. Then the drivers should use cross-passages to evacuate. The existing knowledge is that the overpressure decreases rapidly with the distance from the tank in a tunnel in case of a compressed gas tank rupture or BLEVE.

A special training to drivers with these alternative fuel vehicles may be needed, concerning the fire and explosion hazards. This may be added as one part of risk education for a driving license. The qualitative analysis and the event trees presented in Chapter 5 can be used as reference.

10.5 Fire and rescue service

The event trees presented in Chapter 5 can be used as a guide for fire and rescue service.

Methanol and ethanol flames are generally hard to observe and thus can pose hazard of thermal hazards for users and fire fighters. In such fire incidents, thermal cameras may be good tools for fire fighters. As mentioned previously, a hydrogen flame has similar problem for visual observation, while it may be more noticeable due to the noises affiliated with the high-speed hydrogen jet releases.

Cooling may cause problem in activation of thermally activated PRDs, such as a CNG tank. This may mean that in design of the fuel tanks and arrangement of the fuel tanks in vehicles, measures should be taken to facilitate the cooling and treatment of the fuel tanks.

Battery fires are hard to extinguish as the thermal runaway occurs inside the batteries. After extinguish a battery fire, it may restart it later. Measures to easy displacement of these batteries should be considered in design. In a battery fire, fire fighters should also notice the toxicity of the combustion products and the venting gases.

In a scenario with possible failure of pressurized tanks, the fire fighters may be equipped with some special equipment, e.g. a movable shield that can protect them from flying fragments.

11 Conclusions

Different types of alternative fuel vehicles are investigated and detailed parameters are obtained. According to the different fuels used, they could be divided into four types: liquid fuels, liquefied fuels, compressed gases, and electricity.

Qualitatively analysis of the hazards and consequences for each type of alternative fuel vehicles in tunnels are presented. It is concluded that a flash fire and a gas explosion may occur in an incident with any type of the fuels. Besides, an incident may also be a pool fire for liquid fuels, a jet fire, a pool fire or a BLEVE for liquefied fuels, a jet fire or a rupture for compressed gas vehicles, and a jet fire for electric battery vehicles. It can be expected that the most severe hazards are the rupture and gas explosion. If the fuels are releasing (or leaking) but not burning, it may indicate there may be a vapor cloud that can potentially cause an explosion. If the fuels in tanks are not releasing (or leaking), it may indicate a tank rupture may occur.

From the perspective of fire size, the liquid fuels may pose equivalent or even much lower fire hazards compared to the traditionally used fuels, but the liquefied fuels may pose higher hazards. The pool fire hazards are related to the spillage area, which however highly depends on the slopes of the floor and the outflow holes. The gas release rates from the compressed gas tanks are highly transient. For hydrogen vehicles, the heat release rates are significantly higher than those for the CNG tanks, while the flame lengths are only slighter higher. The flame length increases with the increasing diameter of the PRDs. The flame length can be as long as 40 m. The heat flux can be up to 14 kW/m^2 for CNG and 45 kW/m^2 for GH2 at 10 m from the fire. This indicates that the possibility for fire spread is high.

Investigation of the peak overpressure in case of an explosion in a tunnel was also carried out. The results showed that, for the vehicles investigated, the peak overpressure of tank rupture and BLEVE are mostly in a range of 0.1 to 0.36 bar at 50 m away. The situations in case of cloud explosion are mostly much more severe and intolerable.

These hazards need to be carefully considered in both vehicle safety design and tunnel fire safety design, e.g. limiting the fuels and stringent prevention of such incidents. Further researches on these hazards, especially large scale experiments, are in urgent need.

References

1. Lönnermark, A. *New Energy Carriers in Tunnels*. in *Proceedings from the Fourth International Symposium on Tunnel Safety and Security*. 2010. Frankfurt am Main, Germany: SP Technical Research Institute of Sweden.
2. Ingason, H., Y.Z. Li, and A. Lönnermark, *Tunnel Fire Dynamics*. 2015, New York: Springer.
3. Weerheijm, J. *Explosion risks and consequences for tunnels*. in *ISTSS 6th International Symposium on Tunnel Safety and Security*. 2014. Marseille: SP Technical Research Institute of Sweden.
4. Groethe, M., et al., *Large-scale hydrogen deflagrations and detonations.* International Journal of Hydrogen Energy, 2007. **32** p. 2125 – 2133.
5. Baraldi, D., et al., *An inter-comparison exercise on CFD model capabilities to simulate hydrogen deflagrations in a tunnel.* International Journal of Hydrogen Energy, 2009. **34**: p. 7862-7872.
6. Malmtorp, J., et al. *Safety in road tunnels – Safety target proposal*. in *ISTSS 7th International Symposium on Tunnel Safety and Security*. 2016. Montreal: SP Technical Research Institute of Sweden.
7. Hurley, M.J., *SFPE Handbook of Fire Protection Engineering*. 2016, New York: Springer.
8. Ingason, H. and Y.Z. Li, *Spilled Liquid Fires in Tunnels.* Fire Safety Journal, 2017, In Publication.
9. Lowesmith, B.J., et al., *An overview of the nature of hydrocarbon jet fire hazards in the oil and gas industry and a simplified approach to assessing the hazards.* Trans IChemE, Part B, 2007.
10. Heskestad, G., *Turbulent Jet Diffusion Flames: Consolidation of Flame Height Data.* Combustion and Flame, 1999. **118**(1-2): p. 51-60.
11. Delichatsios, M.A., *Transition from momentum to buoyancy-controlled turbuelnt jet diffusion flames and flame height relationships.* Combustion and Flame, 1993. **92**: p. 349-364.
12. Virk, A.S., *Heat Transfer Characterization in Jet Flames Impinging on Flat Plates*. 2015, Virginia Polytechnic Institute and State University.
13. Wu, Y., *Assessment of the impact of jet flame hazard from hydrogen cars in road tunnels.* Transportation Research Part C, 2008. **16** p. 246–254.
14. *Natural Gas Systems: Suggested Changes to Truck & Motorcoach Regulations & Inspection Procedures*. 2013, U.S. Department of Transportation (FMCSA), Report No. FMCSA-RRT-13-044.
15. *Additional information for ECE/TRANS/WP.15/2015/6e – Use of Liquefied Petroleum Gas (LPG) and Compressed Natural Gas (CNG) as fuel for vehicles carrying dangerous goods: Focus on CNG safety*. 2015, Economic Commission for Europe, Inland Transport Committee, Working Party on the Transport of Dangerous Goods.
16. *Guidelines for Vapor Cloud Explosion, Pressure Vessel Burst, BLEVE, and Flash Fire Hazards*. 2010, Hoboken, New Jersey: John Wiley & Sons Inc.
17. Zipf Jr., R.K., et al., *Deflagration-to-detonation transition in natural gas–air mixtures.* Combustion and Flame 161, 2014. **161**: p. 2165–2176.
18. Groethea, M., et al., *Large-scale hydrogen deflagrations and detonations.* International Journal of Hydrogen Energy, 2007. **32** p. 2125 – 2133.
19. Venetsanos, A.G., et al., *CFD modelling of hydrogen release, dispersion and combustion for automotive scenarios.* Journal of Loss Prevention in the Process Industries, 2008. **21**(2): p. 162-184.
20. Middha, P. and O.R. Hansen, *CFD simulation study to investigate the risk from hydrogen vehicles in tunnels.* International Journal of Hydrogen Energy, 2009. **34**: p. 5875-5886.

21. Zalosh, R. and N. Weyandt, *Hydrogen Fuel Tank Fire Exposure Burst Test*. SAE Technical Paper 2005-01-1886, 2005.
22. Schoor, F.V.d., P. Middha, and E.V.d. Bulck, *Risk analysis of LPG (liquefied petroleum gas) vehicles in enclosed car parks.* Fire Safety Journal, 2013. **57**: p. 58-68.
23. Smith, P.D., et al., *Blast wave transmission along rough-walled tunnels.* International Journal of Impact Engineering, 1998. **21**(6): p. 419-432.
24. Pavan Kumar, C.V.L.C.S., et al., *Attenuation of Shock Waves using Perforated Plates.* IOP Conference Series: Materials Science and Engineering, 2017. **225**.
25. Silvestrini, M., B. Genova, and F.J.L. Trujillo, *Energy concentration factor. A simple concept for the prediction of blast propagation in partially confined geometries.* Journal of Loss Prevention in the Process Industries, 2009. **22**: p. 449–454.
26. Truchot, B., F. Fouillen, and S. Collet. *An Experimental Evaluation of the Toxic Gas Emission in Case of Vehicle Fires*. in *ISTSS 7th International Symposium on Tunnel Safety and Security*. 2016. Montreal: SP Technical Research Institute of Sweden.
27. Colella, F., et al. *Electric Vehicle Fires*. in *ISTSS 7th International Symposium on Tunnel Safety and Security*. 2016. Montreal: SP Technical Research Institute of Sweden.
28. Andersson, P., et al., *Using Fourier transform infrared spectroscopy to determine toxic gases in fires with lithium-ion batteries.* Fire and Materials, 2016. **40**: p. 999-1015.
29. Zalosh, R. *CNG and Hydrogen Vehicle Fuel Tank Failure Incidents, Testing, and Preventive Measures*. in *42nd Annual Loss Prevention Symposium*. 2008.
30. Board, D.S., *Fire in a CNG bus, Wassenaar, 29 Oktober 2012*. 2013: The Hague.
31. Hagberg, M., J. Lindström, and P. Backlund, *Olycksutredning - Brand i gasbuss Gnistängstunneln, Göteborg 12 juli 2016*. 2016, Räddningstjänsten Storgöteborg.
32. *Interventions marquantes 1901 - 2015*. 2016, SERVICE DÉPARTEMENTAL-MÉTROPOLITAIN D'INCENDIE ET DE SECOURS: Lyon.
33. Agility fuel systems, *First Responder Guide: CNG and LNG vehicle fuel systems*, in *ENP-084 Rev. B.* . 2015, Agility Fuel Systems Product Support Group: Santa Ana.
34. Sturk, D. and L. Hoffmann, *E-fordons Potentiella Riskfaktorer vid Trafikskadehändelse*. 2013, SP Report 2013:58, SP Technical Research Institute of Sweden: Borås.
35. *Corvus Battery Pack Risk Analysis*. 2015, RPT10038.
36. Golubkov, A., Fuchs, D., Wagner, J., Wiltsche, H., Stangl, C., Fauler, G., Voitic, G., Thaler A., Hacker, V., *Thermal-runaway experiments on consumer Li-ion batteries with metal-oxide and olivin-type cathodes.* Royal society of chemistry Adv., 2014. **4**: p. 3633-3642.
37. RECHARGE, *Safety of lithium-ion batteries*. 2013, The European Association for Advanced Rechargeable Batteries.
38. *Buyers guide for electric and plug-in hybrid cars*. 2013, Green Highway.
39. Qin, X. and Y. Ju, *Measurements of burning velocities of dimethyl ether and air premixed flames at elevated pressures.* Proceedings of the Combustion Institute, 2005. **30**: p. 233–240.
40. Capp, B. and J. Seebold, *Detonation experiments in an 18 inch pipe*, in *AIChE Annual Meeting*. 1991: Los Angeles.
41. Reid, R.C., *Superheated liquids.* Amer. Scientist, 1976. **64**: p. 146- 156.
42. Stock, M., W. Geiger, and H. Giesbrecht, *Scaling of Vapor Cloud Explosions After Turbulent Jet Release*, in *Dynamics of Detonations and Explosions: Explosion Phenomena, Progress in Astronautics and Aeronautics*, W.A.S. A. A. Borisov, A. L. Kuhl, and J.-C. Leye, Editor. 1989, American Institute fo Aeronautics and Astronautics: Washington. p. 3-20.
43. Bhatti MS and Shah RK, eds. *Turbulent and transition convective heat transfer in ducts*. Handbook of Single-phase Convective Heat Transfer, ed. S.R.K. Kakaç S., Aung W. 1987, John Wiley: New York.

44. Tien CL, Lee KY, and Stretton AJ, *Radiation heat transfer*, in *SFPE Handbook of Fire Protection Engineering*, P.J. DiNenno, Editor. 2002, National Fire Protection Association: Quincy, MA, USA. p. 1-73 -- 1-89.
45. van den Berg, A.C., *''BLAST'': A compilation of codes for the numerical simulation of the gas dynamics of explosions.* Journal of Loss Prevention in the Process Industries, 2009. **22** p. 271–278.
46. UPTUN, *Workpackage 2 Fire development and mitigation measures - D212*, in *Explosion effects in traffic tunnels*. 2008.
47. Lowesmith, B.J., G. Hankinson, and D.M. Johnson, *Vapour cloud explosions in a long congested region involving methane/hydrogen mixtures.* Process Safety and Environmental Protection, 2011. **89**: p. 234-247.
48. Thomas, G., G. Oakley, and R. Bambrey, *An experimental study of flame acceleration and deflagration to detonation transition in representative process piping.* Process Safety and Environmental Protection, 2010. **88**: p. 75-90.
49. CATLIN, C.A. and D.M. JOHNSON, *Experimental Scaling of the Flame Acceleration Phase of an Explosion by Changing Fuel Gas Reactivity.* COMBUSTION AND FLAME, 1992. **88**: p. 15-27.
50. Ciccarelli, G. and S. Dorofeev, *Flame acceleration and transition to detonation in ducts.* Progress in Energy and Combustion Science, 2008. **34**: p. 499–550.
51. Hendersen, E., Proceedings of the Pacific Coast Gas Association, 1941. **32**: p. 98-106.
52. Steen, H. and H. Schampel, *Experimental investigations on the run up distance of gaseous detonations in large pipe.* 4th Int. Symp. on Loss Prevention in the Process Industries Series, 1986. **82**(E23).
53. Ginsburgh, I. and W.L. Bulkley, *Hydrocarbon–air detonations, industrial aspects.* Chemical Engineering Progress, 1963. **59**: p. 82–86.
54. Bollinger, L.E., *Experimental detonation velocities and induction distances in hydrogen–air mixtures.* AIAA Journal, 1964. **2**: p. 131-133.
55. Lowesmith, B.J., et al., *Vented confined explosions involving methane/hydrogen mixtures.* International Joural of hydrogen energy, 2011. **36**: p. 2337-2343.
56. M.M. van der Voort, et al., *Blast from explosive evaporation of carbon dioxide: experiment, modeling and physics.* Shock Waves, 2012. **22**: p. 129-140.
57. Sato, Y., et al., *Hydrogen release deflagrations in a sub-scale vehicle tunnel*, in *WHEC 16*. 2006: Lyon, France.
58. Babrauskas, V., *Heat Release Rates*, in *The SFPE Handbook of Fire Protection Engineering*, P.J. DiNenno, et al., Editors. 2002, National Fire Protection Association: Quincy, MA, USA. p. 3-1 -- 3-37.
59. Energy, U.S.D.o., *Liquefied Natural Gas Safety Research*. 2012: Washington.
60. Ingason, H. and Y.Z. Li, *Spilled Liquid Fires in Tunnels* Fire Safety Journal, IAFSS special issue, In publication, 2017. **91**: p. 399-406.
61. Gottuk, D.T. and D.A. White, *Liquid Fuel Fires*, in *The SFPE Handbook of Fire Protection Engineering*, P. DiNenno, Editor. 2008, Quincy: National Fire Protection Association. p. 2-337 -- 2-357.
62. Ingason, H. *Small Scale Test of a Road Tanker Fire*. in *International Conference on Fires in Tunnels*. 1994. Borås, Sweden: SP Swedish National Testing and Research Institute.
63. Beyler, C., *Fire Hazard Calculations for Large, Open Hydrocarbon Fires*, in *In third Edition SFPE Handbook of Fire Protection Engineering*. 2002. p. p.3-268 - 3-314.
64. DiNenno, P.J., *SFPE Handbook of Fire Protection Engineering*. 2002, Quincy, MA, USA: National Fire Protection Association.
65. Ingason, H., K. Nireus, and P. Werling, *Fire Tests in a Blasted Rock Tunnel*. 1997, FOA: Sweden.
66. Steinert, C. *Smoke and Heat Production in Tunnel Fires*. in *The International Conference on Fires in Tunnels*. 1994. Borås, Sweden: SP Swedish National Testing and Research Institute.

67. Steinert, C., *Experimentelle Untersuchhungen zum Abbrand-und Feuerubersprungsverhalten von Personenkraftwagen.* vfdb-Zeitschrift, Forschung, Technik und Management im Brandschutz, 2000. **4**: p. 163-172.
68. Shipp, M. and M. Spearpoint, *Measurements of the Severity of Fires Involving Private Motor Vehicles*. Fire and Materials, 1995. **Vol. 19**: p. 143-151.
69. Mangs, J. and O. Keski-Rahkonen, *Characterization of the Fire Behavior of a Burning Passenger Car. Part I: Car Fire Experiments.* Fire Safety Journal, 1994. **23**: p. 17-35.
70. Mangs, J. and O. Keski-Rahkonen, *Characterization of the Fire Behavior of a Burning Passenger Car. Part II: Parametrization of Measured Rate of Heat Release Curves.* Fire Safety Journal, 1994. **23**: p. 37-49.
71. Lecocq, A., et al., *Comparison of the fire consequences of an electric vehicle and an internal combustion engine vehicle*, in *2nd International Conference on Fires In Vehicles - FIVE 2012*. 2012, SP Technical Research Institute of Sweden: Chicago. p. 183-194.
72. Ingason, H., S. Gustavsson, and M. Dahlberg, *Heat Release Rate Measurements in Tunnel Fires*, in *SP Report 1994:08*. 1994, SP Swedish National Testing and Research Institute: Borås, Sweden.
73. Axelsson, J., et al., *Bus Fire Safety*. 2008, SP Technical Research Institute of Sweden: Borås, Sweden.
74. Kunikane, Y., et al. *Thermal Fumes and Smoke Induced by Bus Fire Accident in Large Cross Sectional Tunnel*. in *The fifth JSME-KSME Fluids Engineering Conference*. 2002. Nagoya, Japan.
75. Li, Y.Z., H. Ingason, and A. Lönnermark, *Correlations between different scales of metro carriage fire tests*. 2013, SP Report 2013:13, SP Technical Research Institute of Sweden: Borås.
76. Li, Y.Z., H. Ingason, and A. Lönnermark, *Fire development in different scales of train carriages*, in *11th International Symposium on Fire Safety Science*. 2014: Christchurch, New Zealand. p. 302-315.
77. *Fires in Transport Tunnels: Report on Full-Scale Tests*. 1995, edited by Studiensgesellschaft Stahlanwendung e. V.: Düsseldorf, Germany.
78. Ingason, H., Y.Z. Li, and A. Lönnermark, *Runehamar Tunnel Fire Tests.* Fire Safety Journal, 2015. **71**: p. 134–149.
79. Cheong, M.K., et al., *Heat Release Rates of Heavy Goods Vehicle Fire in Tunnels with Fire Suppression System.* Fire Technology, 2013.
80. Cheong, M.K., et al. *Heat release rates of heavy goods vehicle fires in tunnels*. in *15th International Symposium on Aerodynamics, Ventilation & Fire in Tunnels*. 2013. Barcelona, Spain: BHR Group.
81. Tang, M.J., C.Y. Cao, and Q.A. Baker, *Blast Effects From Vapor Cloud Explosions*, in *International Loss Prevention Symposium,*. 1996: Bergen, Norway.
82. Brode, H.L., *Blast wave from a spherical charge.* Physics of Fluids, 1959. **2**(2): p. 217-229.
83. Prugh, R.W., *Quantitative Evaluation of "Bleve" Hazards.* Journal of Fire Protection Engineering, 1991. **3**(1): p. 9-24.
84. Energy, U.D.o.E.-O.o.E.e.R. *All-Electric Vehicles*. 2017 [cited 2017 20 Dec]; Available from: https://www.fueleconomy.gov/feg/evtech.shtml.
85. Center for Chemical Process Safety, A., *AICHE Guidelines for Evaluating the Characteristics of Vapor Cloud Explosions, Flash Fires, and BLEVEs*. 1998.
86. TNO, *Methods for the determination of possible damage - CPR 16E*. 1989, Voorburg: TNO.
87. Baraldi Daniele, et al., *Gap Analysis of CFD Modelling of Accidental Hydrogen Release and Combustion*, in *JRC Scientific and Technical Reports*. 2010, Joint Research Centre.
88. Jeffries, R.M., S.J. Hunt, and L. Gould, *Derivation of Fatality of Probability Function for Occupant Buildings Subject to Blast Loads*. 1997, Health & Safety Executive.

Appendix A – Fuel properties for various vehicles

Table A- 1 A summary of tank properties for vehicles with CNG tank.

Vehicle type	Vehicle's name	CNG mass*	No. of tanks
		kg	
	Audi A3 Sportback g-tron	14.4	2
Passenger cars	Audi A4 Avant g-tron	19	1
	Fiat Qubo Natural Power	13	
	Fiat Panda Natural Power	12	
	Fiat Punto Natural Power	13	
	Fiat 500 L Natural Power	14	
	Fiat 500 L Living Natural Power	14	
	Lancia Ypsilon Ecochic CNG	12	
	Mercedes-Benz B-Class B 200 NGD	21	1
	Opel Zafira Tourer 1.6 CNG Turbo	25	1 (70%) +2(30%)
	Seat Mii Ecofuel	11	
	Seat Leon TGI	15	
	Seat Leon ST TGI	15	
	Skoda Citigo G-TEC	11	
	Skoda Octavia G-TEC (6 g.m. / 7 g.a.)	15	
	Skoda Octavia Combi G-TEC (6 g.m. / 7 g.a.)	15	
	Volkswagen eco up	11	
	Volkswagen load up	12	
	Volkswagen Golf TGI	15	
	Volkswagen Golf TGI Variant	15	2
	Volkswagen Caddy Passenger TGI manual & DSG	26	4
	Volkswagen Caddy Passenger Maxi TGI manual & DSG	37	5
	Volvo V60 Bi-fuel (delayed OEM)	16	
Light commercial vehicles	Fiat Panda Van	12	
	Fiat Fiorino Natural Power	13	
	Fiat Doblò Natural Power	16	
	Fiat Doblò Cargo Natural Power	16	
	Opel Combo 1.4 CNG Turbo	16.15	
	Opel Combo Cargo 1.4 CNG Turbo	22.1	
	Volkswagen Caddy Panel TGI & Automatic	25	
	Volkswagen Caddy Panel Maxi TGI & Automatic	36/32	
	Fiat Ducato Cargo Natural Power	36	5
	Fiat Ducato Panorama	36	
	Iveco Daily Natural Power	39	
	Iveco Daily Cabinato Natural Power	39	

	Mercedes-Benz Sprinter NGT Panel/Group Van (2-9 seats)	19-32	
	Mercedes-Benz Sprinter NGT Pickup Van (w/double cabin)	19-45	3-6
Trucks	Iveco Eurocargo Natural Power 12 - 16 Ton	81	2
	Iveco Stralis NP C-LNG	195	4
	Iveco Stralis Hi Road CNG	198	
	Iveco Stralis NP CNG	390	8
	Mercedes-Benz Econic NGT	90/105	
	Mercedes-Benz Econic 2630 NGT	90	8
	Renault D Wide CNG	90/120	6/8
	Scania P/G 280/340 CNG	100/130	
	General information for Scania trucks	90-135	8
	Volvo FE CNG	90/120	6 or 8
Buses	Iveco Bus Daily Citys CNG (10 seats)	42	
	Iveco Bus Urbanway CNG	200/230	4/10
	MAN Lion's city CNG	188-289	8-10
	Mercedes Citaro (G) NGT	160-320	
	Scania Citywide LE/LF CNG	200-290	
	Scania Interlink LD CNG	200	
	Solaris Urbino 12/15/18 CNG	205-274	7**
	Solbus Solcity CNG	365	
	Van Hool A 330 / A 360 CNG	NA	
	Vectia Veris.12.CNG *	NA	

*Data from survey and references (Vehicle catalogue June 2016, Natural & Bio Gas Vehicle Association. NGVA Europe for sustainable mobility. 2016., and Vehicle catalogue June 2017, Natural & Bio Gas Vehicle Association. NGVA Europe for sustainable mobility. 2017). **For Solaris Urbino 15E CNG, the number of tank is 7. The bus is 15 m long.

Table A- 2 A summary of tank properties for vehicles with LNG tanks.

Vehicle type	Vehicle/tank	mass	volume	Size L×D	No. of tanks
		kg	Liter	m×m	
Trucks	Iveco Stralis Hi Road LNG	185	438*		
	Iveco Stralis NP C-LNG	225*	540		1
	Iveco Stralis NP LNG	450	1080		2
	Scania P/G 280/340 LNG	190/310	450/735*		1/2
	Volvo truck – small	112	315	1.4×0.71	1
	Volvo truck – medium	160	445	1.8×0.71	1
	Volvo truck – large	202	565	2.2×0.71	1
Buses	Solbus Solcity LNG	150-214*	356-508		
	Solbus Solcity 18 LNG	150-214*	356-508		

*estimated based on fuel density.

Table A- 3 A summary of tank properties for vehicles with CH_2 tank.

Vehicle type	Vehicle's name	Pressure	Mass	No. of tanks	Tank volume	Gasoline tank
		bar	kg		Liter	Liter
Fuel cell vehicles	Hyundai ix35 FCEV	700	5.63	1	152	
	Toyota Mirai*	700	5	2	122.4	
	Toyota FCHV	700	6	4	156	
	Honda FCX Clarity	350	4.1			
	Mercedes-Benz F-Cell	350/700	4	2		
Internal combustion engine	Mazda RX-8 hydrogen rotary	350	2.4		110	61
	Mazda Premacy Hydrogen RE Hybrid	350	2.4		110	60

* Carbon fiber high-pressure tanks. http://insideevs.com/toyota-mirai-fuel-cell-sedan-priced-at-57500-specs-videos/ accessed on 5 Oct 2016.
**https://en.wikipedia.org/wiki/Toyota_FCHV accessed on 5 Oct 2016.
http://www.netinform.net/h2/h2mobility/Detail.aspx?ID=241

Table A- 4 A summary of tank properties for vehicles with LH_2 tank.

Vehicle	Mass	Pressure	Gasoline tank
	kg	bar	liter
BMW Hydrogen7	8	*	73.8
Mazda RX-8 hydrogen rotary	2.4	NA	61
BMW H2R	NA	NA	NA
Musashi 9 Liquid hydrogen truck**	NA	NA	NA

* The pressure inside should be only several bar. https://en.wikipedia.org/wiki/BMW_Hydrogen_7 . accessed on 6 Oct 2016.
**Concept vehicle in 1990s.

Table A- 5 Properties of batteries in electric passenger cars.

Vehicle/Source	Battery type	mass	Capacity	No. of modules	No. of cells per module
		kg	kWh		
Data by China Taxation Administration [a]		120-450	15-62		
Chevy Volt 2011[b]	LiMn2O4/NMC	197	16	9	32
Mitsubishi iMiEV[c]	LiMn2O4	200	16	22	4
Smart Fortwo ED[c]	LiMn2O4		16.5		
BMW i3[c]	LiMn2O4/NMC	204	22		
Nissan Leaf[c]	LiMn2O4	218 (272)	24(30)	48	4

Tesla S [d]	LiNiCoAlO2	540	90 (60-100)	16	444(6*74)
BYD e6 [e]	LiFePO4		61.4		

[a] http://www.chinatax.gov.cn/n810341/n810755/c2813460/content.html, data for 50 cars.
[b] https://en.wikipedia.org/wiki/Chevrolet_Volt
[c] http://batteryuniversity.com/learn/article/electric_vehicle_ev;
[d] https://en.wikipedia.org/wiki/Tesla_Model_S. The fuel mass of 540 kg is for S85.
[e] http://www.byd.com/la/auto/e6.html

Table A- 6 Properties of batteries in electric buses.

Vehicle	Battery type	mass	Capacity	No. of modules	No. of cells per module
		kg	kWh		
Data by China Taxation Administration [a]	Li-Ion	800-2770	90-330		
Solaris Urbino 12[b]	Li-Ion		210		
Cobus 2500e[c]			150	7	
SOR EBN 10.5					180
Proterra Catalyst 40 Foot Bus[d]	Li4Ti5O12		79-660		
Proterra Catalyst 35 Foot Bus[d]	Li4Ti5O12		79-440		
BYD K9[e]	LiFePO4		324		

[a] http://www.chinatax.gov.cn/n810341/n810755/c2813460/content.html, data for 211 buses.
[b] https://en.wikipedia.org/wiki/Solaris_Urbino_12;
[c] https://de.wikipedia.org/wiki/Cobus_2500e
[d] https://www.proterra.com/wp-content/uploads/2016/08/Proterra-Catalyst-Vehicle-Specs.pdf
[e] http://www.byd.com/la/auto/ebus.html

Table A- 7 Properties of batteries in electric trucks.

Vehicle	Battery type	mass	Capacity	No. of modules	No. of cells per module
		kg	kWh		
Newton[a]	LiFePO4		80(120)		
Coop E-Force One[a]	LiFePO4	1300	120	7	
Emoss[a]	LiFePO4		160(200)		180
Volvo FL/FE [b]	Li-Ion	1605	150	90	12
Volvo FL/FE [b]	Li-Ion	2140	200	120	12
Volvo FL/FE [b]	Li-Ion	2675	250	150	12
Volvo FL/FE [b]	Li-Ion	3210	300	180	12
BYD111017GBEV1[c]	Li-Ion	1600	175		
BYD4180D8DBEV[d]	Li-Ion	3355	350		
CGC4180BEV1AAEJNALD[d]	Li-Ion	1820	151		

[a] https://en.wikipedia.org/wiki/Electric_truck
[b] data from Volvo.
[c] http://www.chinatax.gov.cn/n810341/n810755/c2813460/content.html
[d] http://www.chinatax.gov.cn//n810341/n810755/c2425201/content.html

Appendix B – Calculation of nozzle flows

The safety devices, i.e. pressure relief devices (PRDs), pressure relief valves (PRVs) or other nozzles, commence to open after a predetermined pressure or temperature is achieved. The high pressure inside the tank pushes the fuel flowing out through the nozzles. As the pressure difference between the inlet and outlet of the nozzle is normally very large, the resulting flow velocity is also high. This process can be assumed to be isentropic. Therefore the flow velocity can be simply estimated. It is assumed that the tank pressure is p (bar) and the ambient pressure is p_o (bar).

At first, the critical pressure, p_c (bar) , is defined:

$$p_c = p(\frac{2}{k+1})^{\frac{k}{k-1}} \tag{68}$$

where k is specific heat ratio.

For critical flows, i.e. $p_o < p_c$, the flow velocity is:

$$u = \sqrt{\frac{2k}{k+1}\frac{\bar{R}T}{M}} \tag{69}$$

and the density is:

$$\rho = \frac{p}{ZRT}(\frac{2}{k+1})^{\frac{1}{k-1}} \tag{70}$$

For subcritical flows, i.e. $p_o > p_c$, the flow velocity is:

$$u = \sqrt{\frac{2k}{k-1}\frac{\bar{R}T}{M}[1-(\frac{p_o}{p})^{\frac{k-1}{k}}]} \tag{71}$$

and the density is:

$$\rho = \frac{p}{ZRT}(\frac{p_o}{p})^{\frac{1}{k}} \tag{72}$$

The mass flow velocity can be calculated by:

$$\dot{m} = C_d \frac{\pi d^2}{4}\rho u \tag{73}$$

where C_d is flow discharge coefficient of the nozzle. The parameter d is the nominal nozzle diameter (DN), which can be estimated based on equivalent flow area as follows:

$$d = \sqrt{\frac{4A}{\pi}} \tag{74}$$

The discharge density is:

$$\rho = \frac{P}{ZRT}\left(\frac{p_c}{p}\right)^{\frac{1}{k}} \tag{75}$$

To consider the discharge coefficient, the average discharge velocity needs to be corrected by the following:

$$u_{corr} = C_d u \tag{76}$$

As the tank pressure is very high, the flow is mostly critical.

Appendix C –Damage criteria

The consequence of a blast wave is generally expressed using the Probit functions. Several probit equations for death due to lung hemorrhage exist. AICHE [85] proposed the following correlation:

$$Y = -77.1 + 6.91\ln(\Delta P) \tag{77}$$

while TNO [86] proposed the following correlation:

$$Y = 5 - 5.54\ln(4.2\frac{P_o}{P_{ef}}) + \frac{1.3}{i_{sc}}) \tag{78}$$

where

$$P_{ef} = \Delta P + \frac{5\Delta P^2}{2\Delta P + 1.4\times 10^6}$$

$$i_{sc} = \frac{I}{P_o^{1/2} m^{1/3}}$$

For eardrum rupture, the probit equation is expressed as follows [86]:

$$Y = -12.6 + 1.524\ln(\Delta P) \tag{79}$$

For death due to head impact, the probit equation can be expressed as follows [86]:

$$Y = 5 - 8.49\ln(\frac{2430}{\Delta P} + \frac{4\times 10^8}{I\Delta P}) \tag{80}$$

For death due to whole body impact, the probit equation can be expressed as follows [86]:

$$Y = 5 - 2.44\ln(\frac{7380}{\Delta P} + \frac{1.3\times 10^9}{I\Delta P}) \tag{81}$$

For death due to whole body impact, the probit equation can be expressed as follows [86]:

$$Y = \begin{cases} -13.19 + 10.54\ln(u_{project}), & \text{for } 4.5 \text{ kg} < m_{\text{fragement}} \\ -17.56 + 5.3\ln(S_1), & \text{for } 0.1 \text{ kg} < m_{\text{fragement}} < 4.5 \text{ kg} \\ -29.15 + 2.1\ln(S_2), & \text{for } 0.001 \text{ kg} < m_{\text{fragement}} < 0.1 \text{ kg} \end{cases} \tag{82}$$

where $u_{project}$ is the velocity of projectile and

$$S_1 = m_{project} u_{project}^2, \quad S_2 = m_{project} u_{project}^{5.115}$$

In the above equation, m is mass of person (kg), ΔP is overpressure (Pa) and I is impulsle (Pa·s). A table is presented in the green book [86] to correlate the calculated values with the probabilties.

The probabilities as a function of pressure for damage to eardrum [86] and lung [85] are shown in Figure 61. Clearly, the probability of eardrum rupture increases significantly with the overpressure for an overpressure over a value around 20 kPa, and the probability of death due to lung hemorrhage increases significantly with the overpressure for an overpressure over a value around 100 kPa.

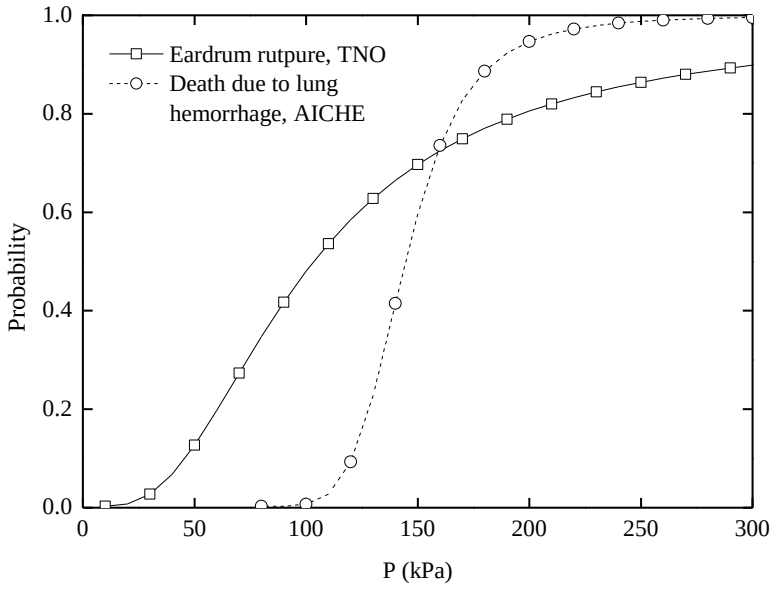

Figure 61 The probabilities as a function of pressure for damage to lung and eardrum.

The damage criteria were summarized by Bradldi et al [87]. Some damage criteria proposed by Jeffries [88] and the guideline [85] are presented in Table 20, Table 21, and Table 22.

Table 20 Direct effects on people [88].

Overpressure (kPa)	**Description of Damage**
13.8	Threshold for eardrum rupture
34.5 – 48.3	50% probability of eardrum rupture
68.9 – 103.4	90% probability of eardrum rupture
82.7 – 103.4	Threshold for lung hemorrhage
137.9 – 172.4	50% probability of fatality from lung hemorrhage
206.8 – 241.3	90% probability of fatality from lung hemorrhage
48.3	Threshold of internal injuries by blast
482.6 – 1379	Immediate blast fatalities

The data in Table 20 show that the blast wave affects the personnel after the overpressure is above around 10 kPa. For an overpressure of 34.5 kPa to 48.3 kPa, the probability of eardrum rupture is 50 %, and it beocmes 90 % for an overpressure of 68.9 kPa to 103.4 kPa. These values are slightly higher than those shown in Figure 61. The corresponding overpressure is slightly higher for lung hemorrhage, within a range of 82.7 kPa to 241.3 kPa. The threshold for internal injuries by last is 48.3 kPa.

Vehicles normally have tempered-glasses as windows. Accroding to TM5-1300 , the peak blast pressrue that the tempered glass panes can withistand varies between 4 kPa to 69 kPa for a pane with an area of 0.1 to 2.3 m^2 and a thickness of 5.1 mm. For windows of cars with an area between 0.5 m^2 and 1.2 m^2 and the same thickness, the failure pressure varies between 10 kPa

and 20 kPa. Similar values are given by Jeffries [88]. They also showed that for thick glasses the failure pressures can be much higher. Note that the desgin values in literature are mostly for a blast duration of 100 ms. The failure pressure can be higher for a shorter duration and vice versa.

From the results, it appears that the maixmum tolerable overpressure for personnel and strcture is around 10 kPa – 20 kPa.

Table 21 Indirect effects on people [88].

Overpressure (kPa)	**Description of Damage**
10.3 – 20	Personnel knocked down or thrown to the ground
13.8	Possible fatality by being projected against obstacles
55.2 – 110.3	People standing up will be thrown a distance
6.9 – 13.8	Threshold of skin lacerations by missiles
27.6 – 34.5	50 % probability of fatality from missile wounds
48.3 – 68.9	100 % probability of fatality from missile wounds

Table 22 Effects on Structures and Equipment [85].

Overpressure (kPa)	**Description of Damage**
15-20	Collapse of unreinforced concrete or cinderblock walls
20 to 30	Collapse of industrial steel frame structure
35 to 40	Displacement of pipe bridge, breakage of piping
70	Total destruction of buildings; heavy machinery damaged
50 to 100	Displacement of cylindrical storage tank, failure of pipes

Through our international collaboration programmes with academia, industry, and the public sector, we ensure the competitiveness of the Swedish business community on an international level and contribute to a sustainable society. Our 2,200 employees support and promote all manner of innovative processes, and our roughly 100 testbeds and demonstration facilities are instrumental in developing the future-proofing of products, technologies, and services. RISE Research Institutes of Sweden is fully owned by the Swedish state.

I internationell samverkan med akademi, näringsliv och offentlig sektor bidrar vi till ett konkurrenskraftigt näringsliv och ett hållbart samhälle. RISE 2 200 medarbetare driver och stöder alla typer av innovationsprocesser. Vi erbjuder ett 100-tal test- och demonstrationsmiljöer för framtidssäkra produkter, tekniker och tjänster. RISE Research Institutes of Sweden ägs av svenska staten.

RISE Research Institutes of Sweden
Box 857, 501 15 BORÅS
Telefon: 010-516 50 00
E-post: info@ri.se, Internet: www.sp.se / www.ri.se

Safety and Transport –
Fire Research
RISE Rapport 2018:20
ISBN 978-91-88695-55-0
ISSN 0284-5172

RISE Research Institutes of Sweden
P.O. Box 857, 501 15 BORÅS, SWEDEN
PHONE: 0046-10-516 50 00
E-post: info@ri.se,
Internet: www.ri.se

OUR SPONSORS & PARTNERS:

Brandforsk

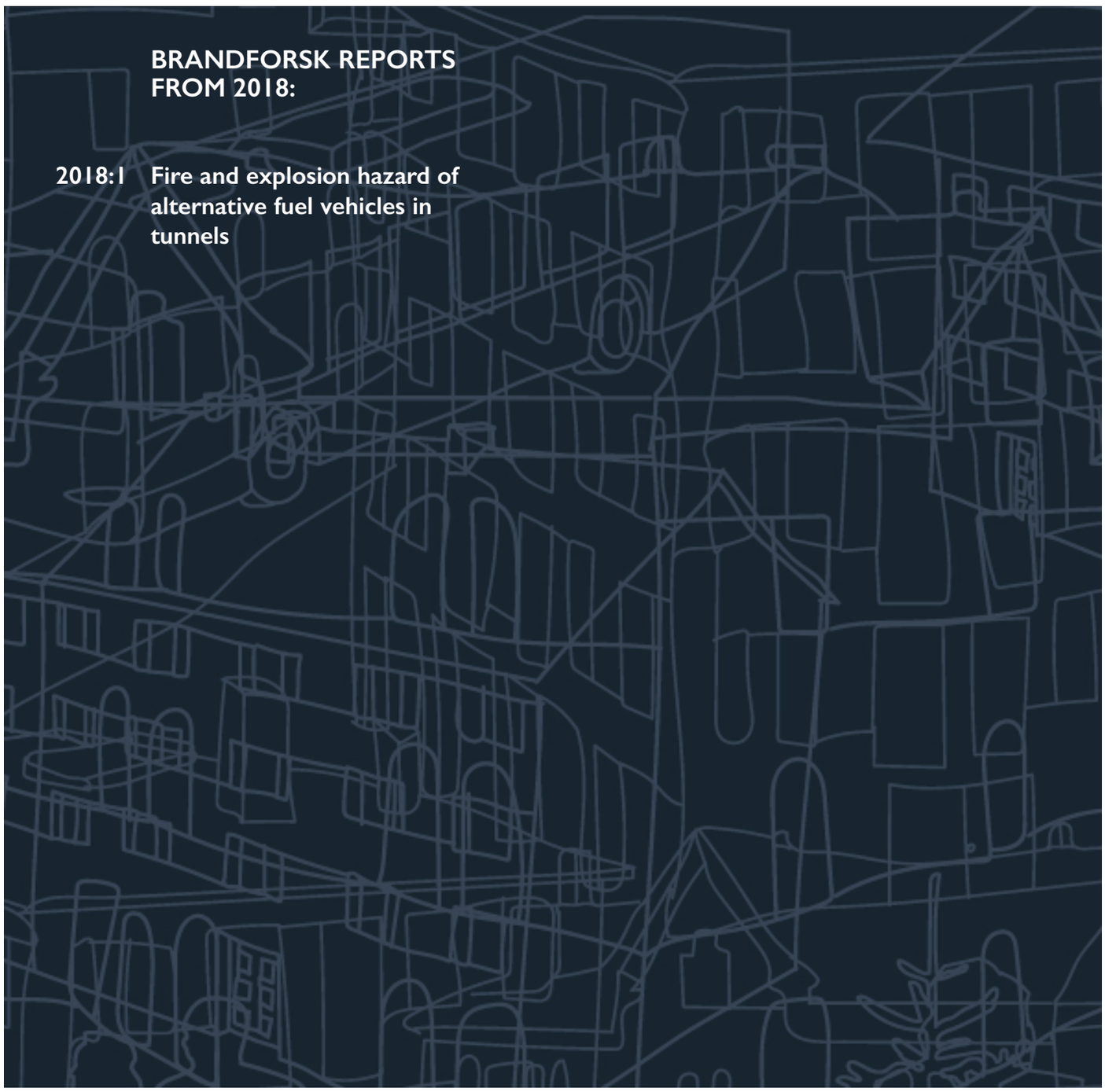

BRANDFORSK REPORTS FROM 2018:

2018:1 Fire and explosion hazard of alternative fuel vehicles in tunnels

The Swedish Fire Research Board, Brandforsk, is a non-profit body, formed in collaboration between insurance companies, industry, associations, government agencies and local municipalities.
The purpose of Brandforsk is to initiate and fund research and knowledge development within the field of fire safety in order to reduce the negative social and economic impact of fire.

The work is under the leadership of the board of directors and is undertaken in the form of projects at universities, institutes of technology, research organisations, government agencies and industrial enterprises. The Secretariat of Brandforsk shares the pre¬mises of the Swedish Fire Protection Association, SFPA, which is also the principal organization.

Brandforsk

Årstaängsvägen 21 c
P.O. Box 472 44, SE-100 74 Stockholm, Sweden
Phone: 0046-8-588 474 14
brandforsk@brandskyddsforeningen.se
www.brandforsk.se